Master's thesis

NTNU
Norwegian University of Science and Technology
Faculty of Information Technology and Electrical Engineering
Department of Engineering Cybernetics

Tord Saghaug Solberg

Nonlinear Model Predictive Control of Offshore Hybrid Power Systems

Master's thesis in Cybernetics and Robotics
Supervisor: Lars Struen Imsland
Co-supervisor: Kiet Tuan Hoang
June 2021

NTNU
Norwegian University of
Science and Technology

Tord Saghaug Solberg

Nonlinear Model Predictive Control of Offshore Hybrid Power Systems

Master's thesis in Cybernetics and Robotics
Supervisor: Lars Struen Imsland
Co-supervisor: Kiet Tuan Hoang
June 2021

Norwegian University of Science and Technology
Faculty of Information Technology and Electrical Engineering
Department of Engineering Cybernetics

NTNU
Norwegian University of
Science and Technology

Preface

This master's thesis is about nonlinear model predictive control of an offshore hybrid power system. The work is carried out during the spring semester of 2021 and accounts for 30 credits. The thesis is written as a part of the study program Cybernetics and Robotics, under the Department of Engineering Cybernetics at the Norwegian University of Science and Technology. The reader of this thesis is assumed to have knowledge of control systems and mathematical modeling.

Trondheim, 15.06.2021

Tord Saghaug Solberg

Acknowledgements

First, I want to thank my supervisor Lars Struen Imsland, which has guided me through this master's project. His unique ideas for the project, together with solid guidance, have been of great utility. The next person to thank is my co-supervisor Kiet Tuan Hoang, who has shown a special interest throughout the entire master's project. The knowledge gained from conversations with him has certainly helped me on the way.

I also want to thank Otávio Fonseca Ivo for providing me with relevant modeling theory from his work.

A big thank you goes to my family for all the support I have gotten throughout the time of my study. At last, I want to thank my classmates for the study motivation, social events, and sharing of experience.

Abstract

Oil and gas production on offshore platforms is a crucial industry for several countries worldwide. Unfortunately, production currently suffers from high emissions of greenhouse gasses. An approach already set in motion to deal with these offshore emissions is integrating offshore wind power production into the current power systems on the offshore platforms, resulting in hybrid power systems. This thesis aims to make a controller for an offshore hybrid power system to exploit the potential energy in the wind. More specifically, this thesis investigates the use of a model predictive controller for such a power system. A model predictive controller is a controller that is based on a mathematical model of the plant.

A mathematical plant model is firstly derived to test the performance of a model predictive controller in a hybrid power system. The plant model is then used as a test plant and design basis for the model predictive controller. Several test cases under different realistic conditions are simulated to analyze the behavior of the controlled hybrid power system plant model. The resulting simulations show that the model predictive controller manages to utilize a large proportion of the potential wind power. Additionally, the overall power in the hybrid power system is appropriately distributed between components.

The findings from this thesis show the potential of model predictive control for offshore hybrid power systems.

Contents

List of Figures xi

List of Tables xiii

Nomenclature xv

1 Introduction 1
1.1 Potential for a Sustainable Future in Offshore Oil and Gas Production 1
1.2 Problem Specification, Objectives, and Contributions 2
1.3 Limitations 3
1.4 Outline 4

2 Offshore Hybrid Power System 5
2.1 Pump 6
2.1.1 QH Model 7
2.1.2 QP Model 8
2.1.3 Qη Model 9
2.1.4 Head PI Control 9
2.2 Gas Turbine Generator 10
2.2.1 Gas Turbine Generator Model 10
2.2.2 Efficiency Function 11
2.3 Wind Turbine Generator 12
2.3.1 Turbine Model 12
2.3.2 Drive Train Model 13
2.3.3 Generator Model 13
2.4 Battery 14
2.5 Connection 14

3 Optimal Control 17
3.1 System Classification 17
3.2 Optimal Control Problems 19
3.2.1 Continuous Time Optimal Control Problem Formulation 19
3.2.2 Optimal Control Problem Classes 20
3.3 Numerical Approaches 21
3.3.1 State-Space Approach 22
3.3.2 Indirect Approach 22
3.3.3 Direct Approach 22

3.4 Differential Equation Solvers . . . 26
3.4.1 Explicit Runge-Kutta Method . . . 27
3.4.2 Implicit Runge-Kutta Method . . . 27
3.5 Optimization Methods . . . 28
3.5.1 Karush–Kuhn–Tucker Conditions . . . 28
3.5.2 Newton's Method . . . 29
3.5.3 Step Length Methods . . . 29
3.5.4 Interior-Point Method . . . 30
3.5.5 Sequential Quadratic Programming . . . 31
3.6 Model Predictive Control . . . 31
3.6.1 Objective Function . . . 33

4 Nonlinear Model Predictive Control Design **35**
4.1 Lookup Table Approximations . . . 36
4.1.1 Generator Torque Lookup Table Approximation . . . 36
4.1.2 Turbine Lookup Table Approximation . . . 37
4.2 Prediction Model State-Space Formulation . . . 39
4.2.1 Original State-Space Formulation . . . 39
4.2.2 Augmented State-Space Formulation . . . 41
4.3 Controller Constraints . . . 41
4.3.1 State Constraints . . . 41
4.3.2 Input Constraints . . . 42
4.4 Objectives . . . 43
4.5 Controller Tuning . . . 44
4.5.1 Tuning Guideline . . . 44
4.5.2 Parameter Tuning . . . 45
4.6 Software and Implementation . . . 46

5 Simulations, Results, and Analysis **49**
5.1 Simulation Setup and Conditions . . . 49
5.1.1 Hardware and Software . . . 50
5.1.2 Analytic Focus and Test Cases . . . 50
5.1.3 Simulation Times . . . 51
5.1.4 Initial Conditions . . . 51
5.1.5 Environmental Conditions and Reference Values . . . 52
5.2 Stationary Wind and Pump Flow Rate Reference . . . 53
5.2.1 Gentle Breeze . . . 53
5.2.2 Fresh Breeze . . . 54
5.2.3 Strong Breeze . . . 55
5.2.4 Gale . . . 56
5.3 Varying Wind and Pump Flow Rate Reference . . . 58
5.3.1 Varying Wind Speed and Constant Flow Rate Reference . . . 58
5.3.2 Constant Wind Speed and Varying Flow Rate Reference . . . 59
5.3.3 Varying Wind Speed and Flow Rate Reference . . . 60

5.4 Feedback Measurement Noise Robustness . . . 61
5.4.1 Dynamic Measurement Noise . . . 62
5.4.2 Static Measurement Noise . . . 63

6 Discussion 65
6.1 Nonlinear Model Predictive Controller Performance . . . 65
6.1.1 Power Distribution and Reference Tracking . . . 65
6.1.2 External Disturbances . . . 67
6.2 Control Design Complexity and Model Assumptions . . . 68
6.3 Computational Resources for Implementation . . . 69

7 Conclusion and Further Work 71
7.1 Conclusion . . . 71
7.2 Further Work . . . 72
7.2.1 Stochastic Model Predictive Control . . . 72
7.2.2 Disturbance Estimation . . . 72
7.2.3 Mixed Integer Program Formulation . . . 73
7.2.4 Electrodynamic Extension . . . 73
7.2.5 Moving Horizon Estimation . . . 73

Bibliography 75

Acronyms 79

Appendix 81
A Model Parameters . . . 81
B Control Parameters . . . 82
C Extra Simulation Plots and Values . . . 83

List of Figures

2.1 Offshore HPS in connection with a control unit . . . 5
2.2 Pump model in a closed-loop connection with a PI controller . . . 10
2.3 Connected HPS model with inputs and outputs . . . 16

3.1 Visualization of an OCP with two states, a control variable, and constraints . . . 20
3.2 Direct single shooting approach . . . 23
3.3 Direct multiple shooting approach . . . 25
3.4 Overview of a model predictive controller with a feedback connection to a plant through an output measurement unit . . . 32
3.5 History and prediction from a receding horizon strategy . . . 33

4.1 Design elements for the NMPC . . . 35
4.2 Generator torque lookup table and approximation of generator torque for a varying rotational speed . . . 36
4.3 Curve fitted 3-dimensional plane for the turbine lookup table approximation . . . 38
4.4 Numerical methods for the NMPC design . . . 47

5.1 Feedback connection between the implemented NMPC and HPS plant model . . . 49
5.2 Measured battery energy, pump flow rate, and powers during a gentle breeze . . . 53
5.3 Measured battery energy, pump flow rate, and powers during a fresh breeze . . . 55
5.4 Measured battery energy, pump flow rate, and powers during a strong breeze . . . 56
5.5 Measured battery energy, pump flow rate, and powers during a gale . . . 57
5.6 Inputs during a gale . . . 58
5.7 Measured battery energy, pump flow rate, and powers during a varying wind and constant flow rate reference . . . 59
5.8 Measured battery energy, pump flow rate, and powers during a constant wind and varying flow rate reference . . . 60
5.9 Measured battery energy, pump flow rate, and powers during a varying wind and flow rate reference . . . 61
5.10 Measured battery energy, pump flow rate, and powers during a fresh breeze with dynamic noise in the feedback measurements . . . 62
5.11 Measured battery energy, pump flow rate, and powers during a fresh breeze with static noise in the feedback measurements . . . 63

C.1 Measured battery energy, pump flow rate, and powers during a gentle breeze with a high GTG throttle weighting . . . 84
C.2 Measured battery energy, pump flow rate, and powers during a gale with an adjusted initial pitch . . . 84

C.3 Rotational speed of the wind turbine; comparing the plant and prediction model . 85
C.4 Measured battery energy, pump flow rate, and powers during a gale with an adjusted initial pitch and physical WTG power saturation 85
C.5 Measured battery energy, pump flow rate, and powers during a fresh breeze with a high flow acceleration weighting and dynamic noise in the feedback measurements 86
C.6 Measured battery energy, pump flow rate, and powers during a fresh breeze with a negative static noise in the feedback measurements 86

List of Tables

2.1 HPS model variables 15

4.1 Test of polynomial approximations of the turbine lookup table 38

5.1 Initial conditions for simulation cases 51
5.2 Environmental conditions and reference values for simulation cases 52

A.1 GTG parameters 81
A.2 WTG parameters 81
A.3 Battery parameters 82
A.4 WTG lookup table approximation parameters 82
A.5 Input constraints for augmented state-space 82
B.1 PI controller parameters 82
B.2 NMPC time periods 83
B.3 NMPC objective scaling factors 83
B.4 NMPC objective weights 83
C.1 Extended simulation case values 83

Nomenclature

Physical Quantities

Symbol	Meaning	Unit
A	Area	m^2
C	Lookup table	
D	Approximated lookup table function	
E	Energy	kW h
H	Head	m
I	Inertia	kg m^2
M	Torque	N m
N	Gear ratio	
P	Power	kW
Q	Flow Rate	m^3 s^{-1}
R	Radius	m
SoC	State of charge	%
t	Time	s
T	Time period	s
v	Wind	m s^{-1}
V	Fuel flow	pu
β	Blade pitch	deg
γ	Throttle	pu
ϵ	Power conversion factor	
η	Efficiency	
κ	Energy conversion factor	
τ	Time constant	s
ϕ	Tip speed ratio	
ω	Rotational speed	rad s^{-1} | rpm

Physical Constants

Symbol	Meaning	Value	Unit
g	Average gravity at earth's surface	9.807	$\mathrm{m\,s^{-2}}$
ρ_{air}	Density of dry air at sea level	1.225	$\mathrm{kg\,m^{-3}}$
ρ_{wat}	Density of water used in the pump	1014.946	$\mathrm{kg\,m^{-3}}$

Mathematical Quantities

Symbol	Meaning
e	Error
$\mathbf{f}$	Function
$\mathbf{K}$	Runge-Kutta increment
n	Dimension of
$\mathbb{N}$	Set of natural numbers
p	Polynomial coefficient
$\mathbf{p}$	Parameter vector
$\mathbb{R}$	Set of real numbers
$\mathbf{r}$	Reference vector
$\mathbf{u}$	Control vector
$\mathbb{U}$	Control set
$\mathbf{w}$	White unit noise vector
$\mathbf{v}$	Measurement noise vector
$\mathbf{x}$	State vector
$\mathbb{X}$	State space set
$\mathbf{y}$	Measurement vector
$\mathbb{Z}$	Set of integer numbers
δ	Reference extension
Δ	Change in
μ	Normalization factor
σ	Normalization factor
∇	Gradient
∇^2	Hessian

Optimization Quantities

Symbol	Meaning
$\mathbf{B}$	Modified Hessian
$\mathbf{f}$	State transition function
$\mathbf{g}$	Equality constraints
$\mathbf{h}$	Inequality constraints
$\mathbf{J}$	Objective function
$\mathbf{L}$	Lagrangian term
$\mathcal{L}$	Lagrangian function
N	Number of optimization instances
q	Control variable weight
$\mathbf{Q}$	Control variable weight matrix
r	Manipulation variable weight
$\mathbf{R}$	Manipulation variable weight matrix
s	Slacking variable
$\mathbf{w}$	Vector of optimization variables
λ	Lagrange multiplier for equality constraint
μ	Lagrange multiplier for inequality constraint
τ	Smoothing constant

Subscripts and Superscripts

Symbol	Meaning
0	Initial
al	Allowable lower
air	Air
aug	Augmented
b	Battery
ch	Control horizon
d	Desired
dy	Dynamic
fb	Fresh breeze
g	Gas turbine generator
gen	Generator
ga	Gale
gb	Gentle breeze
h	Inequality constraint
i	Numbering
j	Numbering
k	Discrete time instance

Subscripts and Superscripts

Symbol	Meaning
l	Lossless
max	Maximum
mid	Middle
min	Minimum
n	Nominal
new	New variable for simulation
p	Pump
ph	Prediction horizon
pl	Preferable lower
pu	Preferable upper
s	Number of stages
sat	Saturated
sb	Strong breeze
st	Stationary
tur	Turbine
u	Input
va	Varying
w	Wind turbine generator
wat	Water
x	State
¯	Normalized
*	Optimal value
'	Piecewise
"	Relative to start of timeline

1 Introduction

1.1 Potential for a Sustainable Future in Offshore Oil and Gas Production

Gas and oil production on offshore platforms is an important industry for many countries, Norway included [1]. A large quantity of power is required to extract the oil and gas from the bottom of the sea. These offshore platforms most commonly utilize gas turbine generators (GTGs) in order to produce power [2]. GTGs runs on gas which releases greenhouse gases (GHG), such as carbon dioxide (CO_2), as a byproduct [3]. High amounts of GHG significantly contribute to nationwide emission [4], and can additionally be costly due to taxes [5].

A future worldwide goal is to reduce the emission of GHG drastically. The goal of emission reduction is represented through the Paris Agreement, where Norway is one of the many participants [6]. For offshore facilities, a feasible solution can be found in the use of wind turbine generators (WTGs) [7]. Studies show that the average wind speed of the coast of Norway and the United Kingdom is about $7.5\ \mathrm{m\,s^{-1}}$, which gives a high potential for producing large quantities of renewable wind power [8]. This implies that GTGs are less needed for power production, resulting in reduced emissions of GHG offshore.

A challenge with WTGs is that the power production is unreliable due to varying winds [9]. As many platforms already have installed efficient GTGs, an ongoing approach is to, in the first round, integrate new WTGs with the existing power systems to increase the share of renewable energy. In addition, to obtain a stable grid with offshore wind power production, a battery solution is necessary unless the grid is connected to the mainland. A battery solution can also help to utilize more wind power as this gives the possibility of fast storage and delivery without the costs of a mainland transfer cable [10]. This integration of wind energy and batteries results in an offshore hybrid power system (HPS). The HPS combined with the goal of minimizing GHG emission from the GTGs means that new ways of controlling the power on the offshore platforms might be profitable.

A control method that has gotten popular in power systems in the last years is model predictive control (MPC) [11]. This type of control is based on a model of the plant, which in turn is used to predict the future behavior of the plant and control the outcome [12]. Using MPC to control offshore HPSs can therefore be a huge advantage as the power flow can be allocated optimally concerning the utilization of potential wind energy.

In [13] it is shown that the use of MPC to control offshore WTGs offers the advantage of a significantly increased power utilization compared to a standard approach of using proportional-integral (PI) control. A maritime hybrid energy system is controlled with the use of MPC in [14], and the results show that the power is distributed quite well in the system. If the stated effects of a highly utilized WTG power production and reliable power distribution can be transferred to the offshore HPS with the use of MPC, there is a high potential for reducing offshore GHG emissions.

Solutions for sustainable offshore power productions in the future are something that appeals to a large number of people and companies. The research institution SINTEF has introduced the concept LowEmission to speed up the technological development regarding offshore energy production. The major energy company Equinor is also highly interested in the production of renewable energy offshore as a large proportion of their activities are located offshore. Two statements from the interested parties mentioned are further provided.

"LowEmission develops new technology and concepts for offshore energy systems and integration with renewable power production technologies. LowEmission is a platform for innovation, and strong interaction within the Centre will generate spin-off projects and technology transfer possibilities for the industry." - SINTEF [15]

"The next decisive phase in the global transition to low carbon and renewable energy is happening now, with offshore wind at the centre of the revolution." - Equinor [16]

1.2 Problem Specification, Objectives, and Contributions

Now that the potential for a sustainable future in offshore oil and gas production with offshore HPSs is defined, it is time to formally establish the problem specifications, objectives, and contributions of this thesis. The overall goal is to produce a model-based controller (specifically MPC) which can handle the power distribution in a system like an offshore HPS. Additionally, it is desired for the MPC to be able to utilize all the potential energy in the wind, thus lowering the emission of GHG to a full extent.

First off, a mathematical HPS model to use for testing and control design is required. For that, a HPS model derived in an earlier specialization project [17] is to be utilized. However, some modifications are wanted for this model. The overall goal of the modifications is to make the model less computational costly for simulations. Additionally, the model is desired a bit more intuitive and realistic.

To design a MPC, an amount of background theory is necessary. A review and collection of relevant theory concerning MPC are therefore of importance in this thesis.

With the essential background theory in place, a MPC is wanted designed. Additionally, the design is required implemented on a digital computer for simulation purposes.

Lastly, to observe how well the designed MPC performs, a series of test cases based on realistic scenarios is called for. The tests are to be executed using a HPS plant model connected to the implemented MPC.

As a list, the objectives in this master's thesis are to:

- Modify an existing offshore HPS model to make it more intuitive, accurate, and decrease the required computational power
- Review and collect background theory on MPC
- Design and implement a MPC digitally
- Create realistic simulation cases to test the performance of the MPC connected to the HPS plant model

With all the objectives met, the main contributions from this master's thesis are:

- A computationally cheap offshore HPS plant model
- A prototype MPC for control of an offshore HPS
- Case studies on control of a HPS plant model using MPC

1.3 Limitations

This master's thesis is subject to several limitations. The two most significant limitations are mentioned in this section, but more specific cases are found in the relevant sections.

Model Assumptions

The model focus in this thesis is on the larger power producing and consuming components in the HPS. The electrical grid is assumed to be stable and in steady-state, and the electrodynamics are removed under this assumption. The models are also scaled in their powers for adjustments of the overall power distribution. Real components are not necessarily scaleable.

Computational Resources

A noteworthy limitation in this master's thesis is the limited computational power. To use the MPC, a sizable amount of computational power is required. The results of the computational power shortcoming are shorter simulation periods and larger controller time steps than initially desired. However, great results for analysis are still produced.

1.4 Outline

This thesis is divided into seven chapters and three appendices. Chapter 2 is partwise method and partwise background theory as this is a modeling continuation originating from [17]. The main background theory is found in chapter 3. Chapter 4 represents the central method in this thesis. In the chapters 5, 6, and 7, the results, discussion, and conclusion are represented. More information about the particular chapters is found in the following listing:

- **Chapter 2:** Introduces a mathematical plant model of an offshore HPS, containing algebraic and differential equations together with constraints.
- **Chapter 3:** Expounds relevant theory of model-based control and optimization. An analysis of the HPS's properties is also provided.
- **Chapter 4:** Imparts the design method and choices for the MPC. Tuning of the controller is also a subject here.
- **Chapter 5:** Presents different simulation cases to test the HPS plant model with the MPC. Further, an analysis of the obtained results from the simulation is performed here.
- **Chapter 6:** Brings forth a discussion based on the methods carried out in this thesis.
- **Chapter 7:** Puts forward a conclusion of the work executed in this thesis. A suggestion for further work is also included.
- **Appendix A:** Provides the values of the parameters used for the HPS model described in chapter 2.
- **Appendix B:** Contains all the tuning parameter values from the control designs in chapter 2 and 4.
- **Appendix C:** Shows off excessive plots resulting from simulations in chapter 5.

2 Offshore Hybrid Power System

In reality, the power systems on offshore platforms are complex due to the composition and connections of complex subsystems [18]. Adding components such as WTGs and batteries even complicates things further. In order to work with a manageable HPS model, only the most impactful components regarding power production and consumption are concerned in this thesis. These components are a pump used for oil and gas extraction, a GTG for power production, a WTG for renewable power production, and a battery for storage and delivery of power from/to the other components.

Figure 2.1 shows how the offshore HPS model is connected. The pump needs a power supply to function. This power is distributed from the GTG and WTG through the battery. Additionally, a control unit is illustrated here. This control unit is used to control the power distribution in the HPS based on observations made through measurements. Eventually, the control unit is to be replaced by a MPC in this thesis.

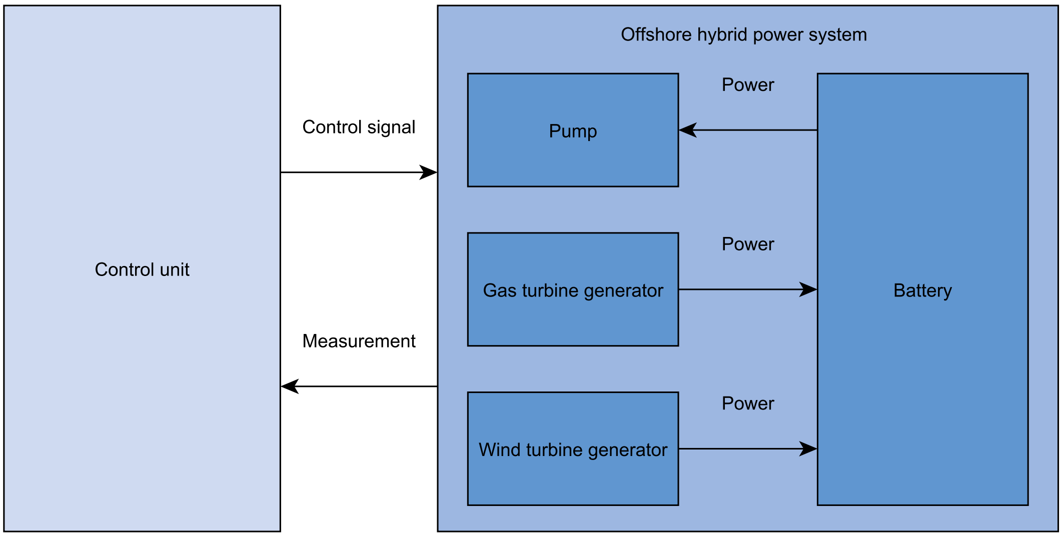

Figure 2.1: Offshore HPS in connection with a control unit

This chapter further presents a plant model of the offshore HPS. Section 2.1 introduces a pump model along with a simple pump controller. In section 2.2 a GTG model is put forward. Following are section 2.3, containing a WTG model. Then comes section 2.4, describing a battery model. Lastly, each individual component are connected as a HPS in section 2.5. The content in this chapter is taken from [17], where the HPS model is assembled and scaled. However, the following model changes are made:

- **Pump model:** Previously, the pump model has been arranged differently. The inverse of the equations 2.1a-2.1f had to be solved to obtain the desired solution. This yielded the necessity for a nonlinear equation solver, which resulted in too much computational power needed for longer simulations. To get a faster model to simulate, the need for a nonlinear equation solver is removed through the change of inputs and outputs. For this, a PI controller is connected to the pump model. The PI controller is further implemented digitally and tuned for a desired response.

- **GTG model:** A curve fitted efficiency function for the GTG is added and used for the output power. This efficiency function creates a more realistic GTG model in terms of power delivery. Instead of using a power reference as input, a throttle together with a gain is now used. This change is made to get a unit input, which linearly corresponds to the fuel usage of the GTG, making it more intuitive to observe the overall fuel usage.

- **WTG model**: In this model, one of two control inputs is removed to simplify the model. The removed input belongs to a simplified generator model, and removing it does not extensively reduce the overall model realism. To compensate for the missing control input, a mathematical coupling is used as a direct replacement.

- **Battery model**: A state of charge (SoC) attribute, which measures the battery energy relative to its maximum, is added for a more intuitive energy storage monitoring.

2.1 Pump

The pump is used in an offshore water pumping station which distributes water to ocean disposal, well injection, and recycling [19]. Multiple designs of pumps for different applications exist. In this thesis, a centrifugal pump is in the scope. The overall build of the pump consists of a casing, bearing house, impeller, and shaft. The shaft is connected to the impeller through the bearing house. When the shaft is applied a mechanical rotational force, the impeller creates a pressure difference on the liquid, which is then sucked in on one side of the casing and pushed out on the other side, resulting in a liquid flow through the pump. The mechanical force needed to drive the pump can be applied to the shaft with the help of, for example, an electric motor or a gas turbine [20].

The pump model used, which is stationary, originally comes from [19] and consists of three submodels. The submodels are head-flow-rate (QH), power-flow-rate (QP), and efficiency-flow-rate (Qη), which are described in subsections 2.1.1, 2.1.2, and 2.1.3 respectively. The pump model does not have a specific power source, but it is assumed to be a lossless motor that can utilize power from the other components in the HPS. Note that all the parameters for the pump model are excluded from this thesis due to confidentiality. In subsection 2.1.4 a PI controller is assembled and connected to the pump model in order to make it computational efficient for simulations.

2.1.1 QH Model

The QH model is given by equations 2.1a-2.1f and is found from regression in [19]. The purpose of this submodel is to calculate the pump head from a given flow rate and rotational speed. The variables Q_p, ω_p and H_p are the flow rate through the pump (m^3 s^{-1}), rotational speed of the pump (rpm), and head (m) which is the height the pump can lift a liquid. The overline notation $\overline{i}$ means that the variable is normalized.

$$\overline{Q_p} = \frac{Q_p - \mu_{Q_p}}{\sigma_{Q_p}} \tag{2.1a}$$

$$\overline{\omega_p Q_p} = \frac{\omega_p Q_p - \mu_{\omega_p Q_p}}{\sigma_{\omega_p Q_p}} \tag{2.1b}$$

$$\overline{\omega_p^2} = \frac{\omega_p^2 - \mu_{\omega_p^2}}{\sigma_{\omega_p^2}} \tag{2.1c}$$

$$\overline{Q_p^2} = \frac{Q_p^2 - \mu_{Q_p^2}}{\sigma_{Q_p^2}} \tag{2.1d}$$

$$\overline{Q_p^3} = \frac{Q_p^3 - \mu_{Q_p^3}}{\sigma_{Q_p^3}} \tag{2.1e}$$

$$H_p = b_{p0} + b_{p_1}\overline{Q_p} + b_{p_2}\overline{\omega_p Q_p} + b_{p3}\overline{\omega_p^2} + b_{p_4}\overline{Q_p^2} + b_{p_5}\overline{Q_p^3} \tag{2.1f}$$

The constraints on the QH model are given in equations 2.2-2.4 and split the pump's operable area into two regions, an allowable and a preferable region. The preferable region gives constraints on where the pump's efficiency η_p is at its highest values, and the allowable lower constraint ensures that the model stays in its valid region. Note that the allowable region is not upper constrained.

Allowable lower constraint:

$$\overline{Q_{p_{al}}^2} = \frac{Q_{p_{al}}^2 - \mu_{Q_{p_{al}}^2}}{\sigma_{Q_{p_{al}}^2}} \tag{2.2a}$$

$$H_p = d_{p_0} + d_{p_1}\overline{Q_{p_{al}}^2} \tag{2.2b}$$

$$Q_{p_{al}} \leq Q_p \tag{2.2c}$$

Preferable lower constraint:

$$\overline{Q^2_{p_{pl}}} = \frac{Q^2_{p_{pl}} - \mu_{Q^2_{p_{pl}}}}{\sigma_{Q^2_{p_{pl}}}} \tag{2.3a}$$

$$H_p = e_{p_0} + e_{p_1}\overline{Q^2_{p_{pl}}} \tag{2.3b}$$

$$Q_{p_{pl}} \leq Q_p \tag{2.3c}$$

Preferable upper constraint:

$$\overline{Q^2_{p_{pu}}} = \frac{Q^2_{p_{pu}} - \mu_{Q^2_{p_{pu}}}}{\sigma_{Q^2_{p_{pu}}}} \tag{2.4a}$$

$$H_p = f_{p_0} + f_{p_1}\overline{Q^2_{p_{pu}}} \tag{2.4b}$$

$$Q_p \leq Q_{p_{pu}} \tag{2.4c}$$

2.1.2 QP Model

The QP model is linear in its parameters and is found with the use of affinity laws in [19] with the nominal rotational speed ω_{p_n} as a basis. The affinity laws use a known characteristic curve of the pump at a known speed to predict the pump's characteristic curves at other speeds [21]. This model provides the power consumption of the pump P_p (kW) for a given Q_p and ω_p. The QP model is described through equations 2.5a-2.5e.

$$Q_{p_n} = (\frac{\omega_{p_n}}{\omega_p})Q_p \tag{2.5a}$$

$$\overline{Q_{p_n}} = \frac{Q_{p_n} - \mu_{Q_{p_n}}}{\sigma_{Q_{p_n}}} \tag{2.5b}$$

$$P_{p_n} = c_{p_0} + c_{p_1}\overline{Q_{p_n}} \tag{2.5c}$$

$$P_p = (\frac{\omega_p}{\omega_{p_n}})^3 P_{p_n} \tag{2.5d}$$

$$\omega_{p_{min}} \leq \omega_p \leq \omega_{p_{max}} \tag{2.5e}$$

2.1.3 Qη Model

The Qη model is used to find the efficiency η_p for the pump. It is expressed with equation 2.6, where g is gravity ($\mathrm{m\,s^{-2}}$), ρ_{wat} is the density of the water used in the pump ($\mathrm{kg\,m^{-3}}$), and ϵ is an unit conversion factor.

$$\eta_p = \frac{gH_p\rho_{wat}Q_p}{P_p}\epsilon \tag{2.6}$$

2.1.4 Head PI Control

To simplify the simulation of the pump model, a PI controller is introduced. This controller also institutes dynamics into the stationary pump model expressed in the previous subsections. The PI controller is used to control the pump model to reach a stationary head value equal to a chosen desired head value H_{p_d}, given an arbitrary flow rate input value. By using this PI controller, the need for solving the inverse of equations 2.1a-2.1f is eliminated, and the simulation time for the pump model is drastically decreased.

From the QH model, it is observed that both the flow rate and the rotational speed can be used to control the head. The flow rate is assumed to be given externally, leaving the rotational speed to be controlled. The rotational speed is then controlled with the PI controller such that the head value converges to the desired head value. For the PI control design, the flow rate is assumed to be a disturbance and decoupled from the head. In this way, the controlled pump model is treated as a single-input single-output (SISO) system even though it originally is a multiple-input singel-output system (MISO). The error in head value e_p and the pump's rotational speed closed-loop function with the PI controller are given in equations 2.7a and 2.7b.

$$e_p = H_{p_d} - H_p \tag{2.7a}$$

$$\omega_p = K_{P_p}e_p + K_{I_p}\int e_p \tag{2.7b}$$

The PI controller is further tuned to mimic the response of a realistic pump system as in [22]. The gains K_{P_p} and K_{I_p} belonging to the PI controller are found in table B.1. Figure 2.2 shows the connection of the pump model and PI controller, where the flow rate Q_p is modeled as a disturbance.

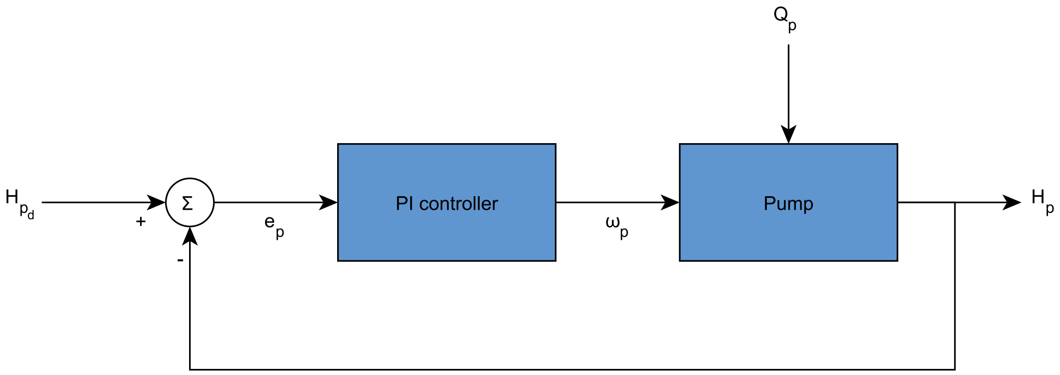

Figure 2.2: Pump model in a closed-loop connection with a PI controller

2.2 Gas Turbine Generator

A gas turbine mainly consists of three parts; a compressor, a combustion chamber, and a turbine. The compressor draws in air for compression. The compressed high-pressure air is then delivered to the combustion chamber, where it is mixed with fuel. The mixture combusts and is released as hot steam into the turbine. The hot steam has a high pressure which creates a pressure difference on the turbine. This pressure difference makes the turbine start spinning. In this way, the chemical energy in the fuel is transformed into mechanical energy. The mechanical energy is so transformed into electrical energy with the use of an electrical generator connected to the turbine with a shaft and potentially a gear exchange. The combination of the gas turbine and the electrical generator makes up the GTG [23].

Further in this section, a mathematical model of a GTG is described. Firstly, subsection 2.2.1 expresses a simple GTG model. To find an efficiency for the GTG model, an efficiency function is produced with curve fitting of an existing efficiency curve. Subsection 2.2.2 explains the process of and results from the curve fitting.

2.2.1 Gas Turbine Generator Model

The GTG model used comes from a simplification of a GAST model [24]. This model consists of two first-order systems in series. The first system represents the fuel valve to control the fuel input and the second system represents the fuel system that converts the fuel into mechanical power. Note that the fuel system here is equivalent to a simplified version of the compressor, combustion chamber, and turbine. The GAST model is originally equipped with a temperature control loop and a loss due to mechanical factors. To simplify the model further, the temperature in the gas turbine is assumed to be low, and the moving components are assumed to be frictionless. Under these assumptions, the temperature control and mechanical loss are removed from the model. Additionally, the gas turbine is not connected to an electrical generator in the GAST model, but the gas turbine is assumed to be connected to a lossless generator with no dynamics, thus forming a GTG.

The GTG model is described with equations 2.8a-2.8e where the variables V_g and γ_g represent the fuel flow (pu) and GTG throttle (pu), both referred to the maximum lossless power $P_{g_{l_{max}}}$ (kW). P_{g_l}, η_g, and P_g are the lossless power (kW), efficiency, and power output (kW) respectfully.

$$\dot{V}_g = \frac{\gamma_g - V_g}{\tau_{g1}} \tag{2.8a}$$

$$\dot{P}_{g_l} = \frac{V_g P_{g_{l_{max}}} - P_{g_l}}{\tau_{g2}} \tag{2.8b}$$

$$P_g = \eta_g P_{g_l} \tag{2.8c}$$

$$P_{g_{l_{min}}} \leq P_{g_l} \leq P_{g_{l_{max}}} \tag{2.8d}$$

$$\gamma_{g_{min}} \leq \gamma_g \leq \gamma_{g_{max}} \tag{2.8e}$$

The parameters belonging to the model are found in table A.1. The time constants τ_{g_1} and τ_{g2} (s) are adjusted a bit from the ones in [24] due to simulation efficiency. The maximum lossless power $P_{g_{l_{max}}}$ is scaled to fit the potential pump power requirement and the minimum power $P_{g_{l_{min}}}$ is set as a limit, so that the GTG cannot consume power.

2.2.2 Efficiency Function

The GTG has a varying efficiency dependent on the load, where the load is given as a percentage of the maximum power output $P_{g_{l_{max}}}$. The efficiency η_g is modeled as a second-order polynomial using the curve fitting tool [25] in MATLAB on the efficiency-load curve from [26]. The resulting efficiency function is expressed in equation 2.9, and the belonging coefficients a_{g_i} are found in table A.1.

$$\eta_g = a_{g1}(\frac{P_{g_l}}{P_{g_{l_{max}}}})^2 + a_{g2}\frac{P_{g_l}}{P_{l_{g_{max}}}} + a_{g3} \tag{2.9}$$

The curve fit gives an approximation of the efficiency-load curve and a fit with an R-square value (goodness of fit measurement between 0 and 1, where 1 is a perfect fit) of 0.9839 is chosen as a trade-off between complexity and accuracy. For load values under 20%, the curve is non-existing. The curve fit, however, gives an estimate of the efficiency for loads under 20%. This estimate is used in the model but with the uncertainty factor in mind.

2.3 Wind Turbine Generator

Wind is something that occurs naturally and in "unlimited" amounts on earth, and it is considered to be a renewable resource. A WTG converts the kinetic energy in the wind into electrical energy. The WTG is roughly built of; a rotor part, gear exchange, and electrical generator. The rotor part contains a number of blades attached to it, which are either fixed or can be pitched. When the wind hits the rotor blades, it starts spinning and converts the wind energy into rotational mechanical energy. The amount of energy transferred from the wind to the rotor is dependent on the design and pitch of the blades. The gear exchange is used to speed up the rotational speed provided by the turbine. The electrical generator is connected to the gear exchange on the high-speed side (opposite of the turbine), where the speed is at a magnitude desirable for the electrical generator. Finally, the electrical generator converts the rotational mechanical energy into electrical energy [27].

The WTG model is based on a realistic model found in [28] and the lookup tables and parameters are taken from the digital model of this WTG [29]. However, the generator time constant τ_w and efficiency η_w are altered. τ_w is edited to obtain more efficient simulations, and η_w is used as a power scaling variable. The parameters can be found in table A.2. The WTG model mainly consists of three submodels, which is the turbine (rotor with blades), drive train, and generator described in subsections 2.3.1, 2.3.2, and 2.3.3. As a side note, the lookup tables in the WTG model use interpolation and "act continuous" in the model simulation.

2.3.1 Turbine Model

The turbine's dynamic is based on aerodynamics, and the wind is assumed to blow perpendicular to the turbine. A tower model originally belongs to the WTG, but it is removed under the assumption that the wind does not twist the WTG. The equations for the turbine torque, tip speed ratio, and pitch constraints are given in equations 2.10a-2.10c.

$$M_{w_{tur}} = \frac{\frac{1}{2} v_w^3 \rho_{air} A_w C_{w_{tur}}}{\omega_{w_{tur}}} \tag{2.10a}$$

$$\phi_w = \frac{R_w \omega_{w_{tur}}}{v_w} \tag{2.10b}$$

$$\beta_{w_{min}} \leq \beta_w \leq \beta_{w_{max}} \tag{2.10c}$$

The variable v_w is the average rotor wind speed (m s^{-1}), ρ_{air} is the air density (kg m^{-3}), A_w is the rotor disc area (m^2), R_w represents the rotor radius (m), and $\omega_{w_{tur}}$ is the turbine rotational speed (rad s^{-1}). $C_{w_{tur}}$ is a lookup table that approximates the aerodynamics of the turbine. This lookup table is dependent on the pitch of the turbine blades β_w (deg) and the tip speed ratio ϕ_w.

2.3.2 Drive Train Model

The drive train model is originally based on a spring, damper, and gear ratio. The spring and damper behaviors are removed under the assumption that the drive train is rigid and free of friction. This assumption removes some of the oscillations in the WTG model without changing the overall power production significantly. This result is a constant relationship between the turbine and generator rotational speed. Due to this constant relationship, the rotational speeds can be calculated using the same reference frame. The equations for angular acceleration of the turbine and rotational speed of the generator are given in equations 2.11a and 2.11b. Equation 2.11c makes sure that the rotational speed $\omega_{w_{tur}}$ is in a strictly positive direction, avoiding a singularity in the torque equation 2.10a.

$$\dot{\omega}_{w_{tur}} = \frac{M_{w_{tur}} - M_{w_{gen}} N_w}{I_{w_{tur}} + I_{w_{gen}} N_w^2} \tag{2.11a}$$

$$\omega_{w_{gen}} = \omega_{w_{tur}} N_w \tag{2.11b}$$

$$\omega_{w_{tur_{min}}} < \omega_{w_{tur}} \tag{2.11c}$$

The inertia (kg m^2) of the turbine and generator in their respective frames are $I_{w_{tur}}$ and $I_{w_{gen}}$. The torque (N m) of the generator (which is defined to be positive for power generation) is $M_{w_{gen}}$ and the generator rotational speed (rad s^{-1}) is $\omega_{w_{gen}}$. The gear ratio between the generator and turbine is given by N_w, and it is used to transform rotational speed, inertia, and torque between the reference frames.

2.3.3 Generator Model

The generator is modeled with the use of a lookup table. The lookup table $C_{w_{gen}}$ provides a generator reference torque $M_{w_{gen}}$ (N m) given by the generators rotational speed $\omega_{w_{gen}}$ (rad s^{-1}). Originally, the generator torque reference is given by a controller. The torque control of the generator is now removed to reduce the number of inputs in the WTG model. However, the generator torque is indirectly controlled through the pitch of the turbine with this new formulation. Equations 2.12a-2.12c provides the generator torque, power output, and power constraints.

$$\dot{M}_{w_{gen}} = \frac{C_{w_{gen}} - M_{w_{gen}}}{\tau_w} \tag{2.12a}$$

$$P_w = \frac{M_{w_{gen}} \omega_{w_{gen}} \eta_w}{1000} \tag{2.12b}$$

$$P_{w_{min}} \leq P_w \leq P_{w_{max}} \tag{2.12c}$$

The generator torque also depends on a time constant τ_w (s) which is used to model a delay. P_w is the power output (kW) of the WTG and it is dependent on the efficiency η_w. The maximum power output possible is $P_{w_{max}}$. Additionally, the WTG cannot consume power, which is ensured by $P_{w_{min}}$.

2.4 Battery

A battery is an element that can store electrical energy in the form of chemical energy. The electrical energy entering the battery is transformed into chemical energy through electrochemical processes. The battery can also deliver the stored chemical energy in the form of electrical energy through a reversed process. Batteries can be made of different materials, and how well the energy is stored and delivered can differ for the different battery types, and the use of them [30].

The battery is modeled as a simple integrator, which summarizes the total power flow in the HPS. The electrical and chemical properties in this model are absent, and the battery's efficiency is therefore assumed to be 100% at all times. Equations 2.13a-2.13d express the mathematical battery model and its constraints. The unit conversion constant κ together with the constraint values are derived in [17] and can be found in table A.3.

$$P_b = P_g + P_w - P_p \tag{2.13a}$$

$$\dot{E}_b = \frac{P_b}{\kappa} \tag{2.13b}$$

$$SoC_b = 100\frac{E_b}{E_{b_{max}}} \tag{2.13c}$$

$$E_{b_{min}} \leq E_b \leq E_{b_{max}} \tag{2.13d}$$

The variables P_b and E_b represent the battery power (kW) and stored battery energy (kW h). The unit kW h is used instead of kJ as this is the normal measure for battery capacity [31]. SoC_b is the SoC of the battery (%). The energy storage of the battery is upper constrained by a maximum energy $E_{b_{max}}$ and lower constrained by $E_{b_{min}}$. As a result of the way the battery is modeled, it becomes a subject to indirect control through the pump power P_p, GTG power P_g, and WTG power P_w. A positive battery power P_b means that the battery is charging, and a negative power means that the battery delivers energy.

2.5 Connection

The individual models are connected through their power flow. Instead of consuming power, the pump model delivers "negative" power. The battery model consumes "negative" power while it is delivering power and consumes positive power while it is charging. The GTG model and WTG model are only able to deliver positive power. In table 2.1 the model variables along with their attributes are found. A diagram of the HPS model connection is shown in figure 2.3.

Model	Symbol	Variable name	Unit	Input/Output
PI controller	H_{p_d}	Desired head	m	Input
	ω_p	Rotational speed	rpm	Output
Pump	ω_p	Rotational speed	rpm	Input
	Q_p	Flow rate	$\mathrm{m^{3}\,s^{-1}}$	Input
	H_p	Head	m	Output
	P_p	Power consumption	kW	Output
	η_p	Efficiency		Output
	$Q_{p_{al}}$	Lower allowable flow rate	$\mathrm{m^{3}\,s^{-1}}$	Output
	$Q_{p_{pl}}$	Lower preferable flow rate	$\mathrm{m^{3}\,s^{-1}}$	Output
	$Q_{p_{pu}}$	Upper preferable flow rate	$\mathrm{m^{3}\,s^{-1}}$	Output
GTG	γ_g	Throttle	pu	Input
	V_{g_0}	Initial fuel flow	pu	Input
	P_{g_0}	Initial lossless power	kW	Input
	V_g	Fuel flow	pu	Output
	P_{g_l}	Lossless power	kW	Output
	P_g	Power delivery	kW	Output
	η_g	Efficiency		Output
WTG	v_w	Average rotor wind	$\mathrm{m\,s^{-1}}$	Input
	β_w	Blade pitch	deg	Input
	$M_{w_{gen_0}}$	Initial generator torque	N m	Input
	$\omega_{w_{tur_0}}$	Initial turbine speed	$\mathrm{rad\,s^{-1}}$	Input
	$M_{w_{tur}}$	Turbine torque	N m	Output
	$\omega_{w_{tur}}$	Turbine rotational speed	$\mathrm{rad\,s^{-1}}$	Output
	$M_{w_{gen}}$	Generator torque	N m	Output
	$\omega_{w_{gen}}$	Generator rotational speed	$\mathrm{rad\,s^{-1}}$	Output
	ϕ_w	Tip speed ratio		Output
Battery	P_b	Power flow	kW	Input
	E_{b_0}	Initial stored energy	kW h	Input
	E_b	Energy stored	kW h	Output
	SoC_b	State of charge	%	Output

Table 2.1: HPS model variables

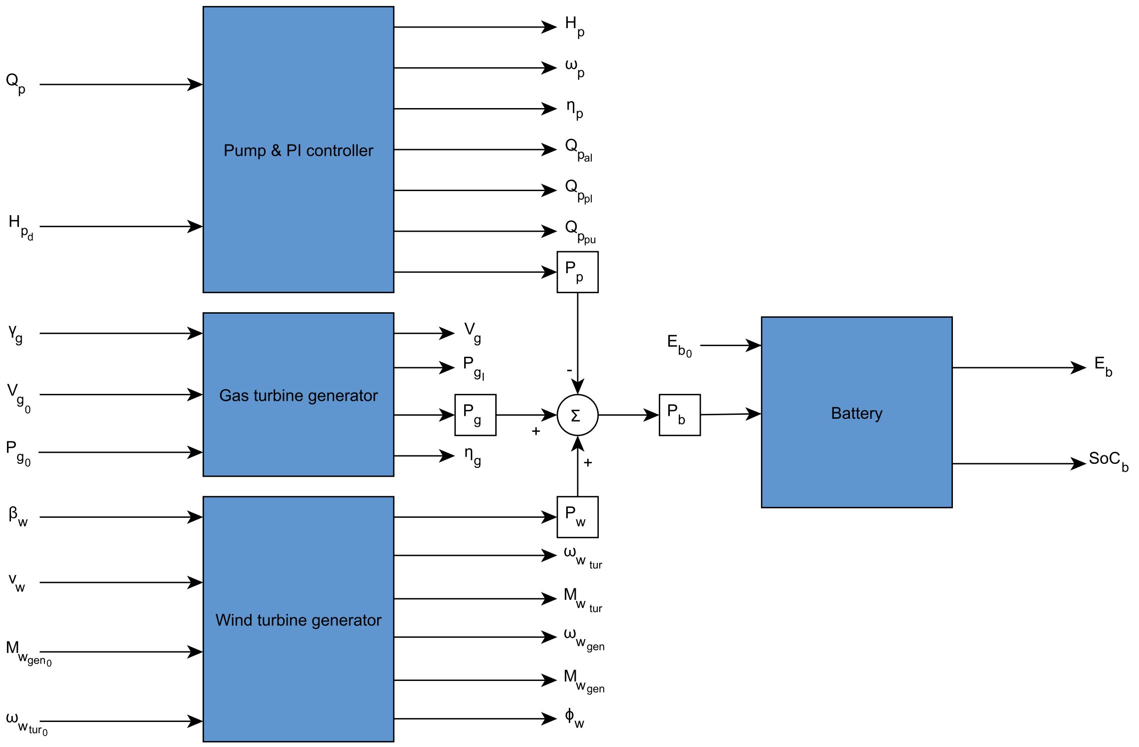

Figure 2.3: Connected HPS model with inputs and outputs

3 Optimal Control

In this chapter, the theory of optimal control, which is essential for MPC, is described. The chapter gradually changes its focus from basic control theory and optimization to nonlinear optimal control used in nonlinear model predictive control (NMPC). Section 3.1 starts with a classification of the HPS to capture its properties, which further is used for the design of a NMPC. In section 3.2 a continuous time optimal control problem (OCP) is defined along with a description of different classes of OCPs. The OCP for this thesis is also classified in order to consider the right control design approaches. Some numerical approaches used to solve OCPs on digital computers are explained in section 3.3. Section 3.4 provides information about differential equation solvers used in the numerical approach. The next section, 3.5, focuses on methods for finding optimal solutions. At last, to set it all together, MPC and NMPC are explained in section 3.6.

3.1 System Classification

To classify the HPS, the theory found in [32] is used in this section. The classification is important for choosing the right control scheme later on.

A dynamical system can be of two variants, either continuous or discrete. Continuous time systems evolve with a time t consisting of all real numbers $\mathbb{R}$ in an interval, opposed to discrete time systems, which evolve with a time t_k of natural numbers $\mathbb{N}$. The system in scope, the HPS is a continuous time system as it exists in the real world. However, the plant model is discrete as it is built on a digital computer.

The state-space of a dynamical system can also contain continuous or discrete properties. For a continuous state-space, the state vector $\mathbf{x}$ can take on any values in $\mathbb{X} \subset \mathbb{R}$. A discrete state-space, on the other hand, is when $\mathbb{X}$ is a finite set. Since the HPS fits with the first case, the system is in a continuous state-space. As a note, combinations between continuous and discrete state-spaces also exist.

Another property of the continuous system is if the state-space is of finite or infinite dimension. For a finite dimension state-space, the states are defined by a set of real numbers, and the system dynamics are often described by ordinary differential equations (ODEs) or differential algebraic equations (DAEs). Infinite state-spaces have a state-space that is a subset of a function space. To describe these systems, partial differential equations (PDEs) are usually used. The HPS is expressed by ODEs, and the state vector $\mathbf{x}$ takes on real values, meaning that it is in a finite state-space.

The control set $\mathbb{U}$, which consists of the values that the control input $\mathbf{u}$ can have, is also of continuous or discrete form. Hybrid forms of control sets, such as integer control sets, also exist. For the HPS, all control inputs are of continuous values.

The system dynamics can depend on time. This property is called time-variant as opposed to a system independent of time, called a time-invariant system. Since the dynamic of the HPS is the same for all time, this system is time-invariant.

For a system to be linear, it must be linearly dependent on its initial values and inputs. If this is not the case, the system is said to be nonlinear. The HPS consists of both linear and nonlinear components, which makes the overall system nonlinear.

The system can either be controlled or uncontrolled. An uncontrolled system means that the control set is empty. In the case of the HPS, the system is controlled as the control set is nonempty. If the system is controlled, it can also have the property of being controllable. Controllability implies that all the states in $\mathbf{x}$ can be controlled to desired values given the initial values. The pump head H_p is controlled through the input flow rate Q_p and the pump rotational speed ω_p. The GTG's states are being controlled in cascade, meaning that the input throttle γ_g makes the GTG controllable. The pitch β_w of the WTG is steering the torque of the turbine $M_{w_{tur}}$, which again controls the generator speed $\omega_{w_{gen}}$, making this component controllable as well. Lastly, the battery input is a function of controllable states. Since the battery only integrates its input, it is also controllable. In conclusion, the entire HPS system is controllable.

The system can be deterministic or stochastic, meaning that it is either possible to predict the evolutions of state trajectories or that the trajectories behave randomly. The HPS is deterministic as it does not have any random behavior (its wind input, however, can appear to behave randomly).

Lastly, the system can be open-loop or closed-loop controlled. In open-loop control, the control inputs are predetermined and only dependent on time. Closed-loop control uses the information about the current states, gained by measurements or estimation, in such a way that the inputs are dependent on the states. Practical MPC acts as closed-loop control with the current system states used as initial states for the prediction (thoroughly described in section 3.6). In this thesis, the HPS model is therefore mainly closed-loop controlled.

The properties of the controlled HPS are summarized as:

- Continuous time
- Continuous state-space
- Finite state-space
- Continuous control set
- Time-invariant
- Nonlinear
- Deterministic

- Closed-loop controlled

3.2 Optimal Control Problems

In this section, general OCPs are introduced. In subsection 3.2.1 the formulation of a continuous time OCP is formulated and described. Subsection 3.2.2 goes through different classes of OCPs in addition to classify the OCP for use in this thesis. The theory found here is mainly based on [32].

3.2.1 Continuous Time Optimal Control Problem Formulation

A type of control problem for systems existing in continuous time is a continuous time OCP. The continuous time OCP for a system of ODEs can be formulated as an objective function, modeled dynamics, and constraints as in equations 3.1a-3.1e.

$$\min_{\mathbf{x}(t),\mathbf{u}(t)} \mathbf{J}(\mathbf{x}(t),\mathbf{u}(t)) = \min_{\mathbf{x}(t),\mathbf{u}(t)} \int_0^T \mathbf{L}(\mathbf{x}(t),\mathbf{u}(t))\ dt \tag{3.1a}$$

$$\text{subject to} \qquad \mathbf{f}(\mathbf{x}(t),\mathbf{u}(t)) = \dot{\mathbf{x}}(t) \tag{3.1b}$$

$$\mathbf{h}(\mathbf{x}(t),\mathbf{u}(t)) \leq \mathbf{0} \tag{3.1c}$$

$$\mathbf{g}(\mathbf{x}(t),\mathbf{u}(t)) = \mathbf{0} \tag{3.1d}$$

$$\mathbf{x}(0) = \mathbf{x}_0 \tag{3.1e}$$

In the OCP (equation 3.1a), the goal is to minimize the objective function $\mathbf{J}$ by optimizing with respect to the system states $\mathbf{x}$ and inputs $\mathbf{u}$ as decision variables. The term $\mathbf{L}$ is called the Lagrangian term and contains the states and inputs to be optimized in time $t \in [0,T]$. As a side note, the Mayer term, which is the terminal cost at $t = T$, is often used in stability proofs and has a low practical impact. This term is therefore not included in the objective function.

The dynamics for the OCP is given by the state transition function $\mathbf{f}$ in equation 3.1b, and it consists of a mathematical model of the system to be controlled. The dynamical model is typically simplified to have a trade-off between model-system accuracy and computational efficiency.

The terms $\mathbf{h}$ and $\mathbf{g}$ from equation 3.1c and 3.1d are the problem's inequality and equality constraints. These constraints describe physical limitations for the system, or they can be chosen to form the OCP according to specifications. The trajectories are typically only bounded by inequality constraints.

The last equation 3.1e gives equality constraints on the initial values. It ensures that at time $t = 0$, the state vector $\mathbf{x}$ is bounded at the initial values $\mathbf{x}_0$.

The OCP is illustrated in figure 3.1, where the problem contains an input u and two states x_1 and x_2. The states are constrained by the initial value at $t = 0$. Furthermore, the state x_1 is constrained by the inequality constraint h and the state x_2 is bounded by the equality constraint g. The important aspect here is to find the optimal value of the objective function by controlling $\mathbf{x}$ trough $\mathbf{u}$.

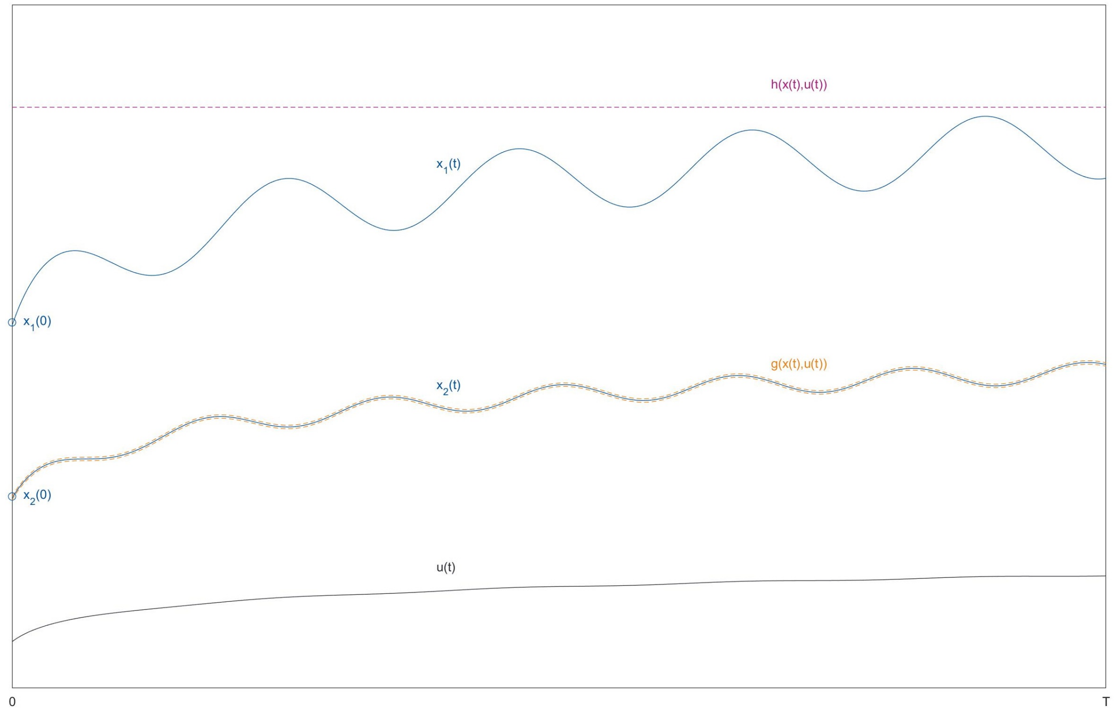

Figure 3.1: Visualization of an OCP with two states, a control variable, and constraints (based on [32])

3.2.2 Optimal Control Problem Classes

In this subsection, the different properties that can be found in continuous time OCPs are briefly discussed. Additionally, the OCP at hand is classified by analyzing the formulation in subsection 3.2.1 together with the HPS's properties from section 3.1. An important feature for the design of the OCP is that it can be formulated to have different properties than the system (e.g. continuous inputs can be optimized as integers).

First off, the OCP can be of a constrained or unconstrained nature. If the equality and inequality sets are empty (i.e. no constraints exist), the problem is said to be unconstrained. If this is not the case, the problem is constrained. Since the physical system possesses limitations (hard constraints), the OCP has to be formulated as a constrained problem to be practically useful. The HPS is naturally constrained by physics, and the HPS plant model is further constrained by valid model regions. Constrained problems can, however, be infeasible, meaning that no solution exists inside the constrained set [33].

Another important property of the OCP is if it is convex or non-convex. The problem is convex if the objective function $\mathbf{J}$ is convex and the feasible set (set given $\mathbf{f}$, $\mathbf{h}$, $\mathbf{g}$, and $\mathbf{x}_0$) is convex. Convex means that a line can be created between two arbitrary points on the function and that the line always lays above the function. For convex problems, the local minimum is also the global minimum. Non-convex problems, on the other hand, can have multiple local minimums, making it NP-hard (not solvable in polynomial time) to find the global minimum [34]. Unfortunately, the nonlinear system dynamics of the HPS makes the feasible set of the OCP non-convex, and therefore making the OCP itself non-convex.

The OCP can be classified as continuous, meaning that the optimization variables are continuous. For continuous OCPs, linear programs (LPs) and nonlinear programs (NLPs) are the main categories. LPs are problems where all of the constraints together with the objective function is linear. This also implies that all LPs are convex. As a special case of NLPs, a class of quadratic programs (QPs) exist. These programs have quadratic objective functions with linear constraints. If the quadratic form is positive (semi)definite, the problem is convex. Other NLPs either have a nonlinear objective function, constraints, or both. This means that NLPs are generally non-convex, except for the special cases [12]. Due to the system dynamics $\mathbf{f}$ (constraint) being nonlinear, the OCP in this thesis is also nonlinear.

There also exist discrete OCPs. If all of the variables in the problem are integers laying in the set $\mathbb{Z}$, the problem is called an integer program (IP). If only some of the variables are integers, the problem is called a mixed integer program (MIP). In addition, these programs can be categorized as linear or nonlinear [12]. However, since the feasible set contains discrete values, these problems are all non-convex. On the upside, IPs and MIPs can model many realistic systems [35]. In this thesis, integer variables are out of the scope, making the OCP continuous.

The OCP properties for the HPS are summarized as:

- Continuous time
- Constrained
- Non-convex
- Nonlinear
- Continuous

3.3 Numerical Approaches

There are multiple approaches to approximate the solution of the continuous time OCP of a finite horizon numerically. These approaches are categorized into state-space approach described in subsection 3.3.1, indirect approach in subsection 3.3.2, and direct approach found in subsection 3.3.3. As the control system is implemented on a digital computer, the continuous time OCP has to be transformed into discrete time. The numerical approaches account for this by the process of discretization. Most of the theory used in this section is gathered from [32] and [36].

3.3.1 State-Space Approach

The state-space approach is based on solving the OCP with the use of the Hamilton-Jacobi-Bellman (HJB) equation. The HJB equation constitute a PDE, which is solved numerically. This continuous approach relies on that all the optimal subarcs of a trajectory provide an optimal trajectory. The use of the HJB equation in continuous time can be connected to the use of dynamical programming (DP) in discrete time. By discretizing the OCP, the HJB equation becomes an algebraic DP type of equation. This equation can then be solved numerically using an iterative minimization routine.

A good reason for using the state-space approach is that an approximation of a feedback law is provided directly. The approach works well for many kinds of special problems. It is, however, restricted to problems of a lower state-space dimension n_x as the number of nodes needed for accuracy grows exponentially with n_x and thus increasing computational time drastically. This is known as the "curse of dimensionality". As the state-space of the HPS model is of a higher dimension, this approach is not preferred.

3.3.2 Indirect Approach

The indirect approach for control is based on using Pontryagin's Maximum Principle, which is the optimality conditions in continuous time. The approach is based on solving a boundary value problem (BVP) for the system of ODEs. This method is often called: "first optimize, then discretize" as the discretization happens after the derivation of the optimality conditions.

The indirect approach offers a quite exact approximation, even better than the direct approach, but it has some major drawbacks. The drawbacks are problems connected to complex algebraic manipulation, non-smooth ODEs, and nonlinear/unstable behavior. Due to its many issues, the indirect approach is usually not chosen as a preferred method, and it is therefore not utilized in this thesis either.

3.3.3 Direct Approach

The direct approach uses the principle; "first discretize, then optimize", as opposed to the indirect method where the order is turned. When the OCP is discretized, the problem to be solved is a finite dimensional NLP, which is an approximation of the original problem. This approach makes it easy to deal with the problem's constraints, and several efficient solvers for NLPs exist. The direct approach is, therefore, the simplest and most popular approach of the ones mentioned.

The direct approach is chosen as the method for approximating the solution of the OCP at hand, but there are several variants. These variants are different in the way that they transcribe the original problem into a NLP. The direct methods mainly consist of single shooting, multiple shooting, and collocation. The methods are based on parametrizing the continuous time input $\mathbf{u}(t)$ into a discrete time input $\mathbf{u}_k$. A trait of the shooting methods is that they use external equation solvers to eliminate the continuous time dynamics.

Direct Single Shooting

The direct single shooting method uses a sequential approach, meaning that the optimization and simulation run sequentially. The states $\mathbf{x}(\mathrm{t})$ are calculated by integrating over $\dot{\mathbf{x}}(\mathrm{t})$ for the full time horizon $[0,T]$. First, a discrete time grid is chosen as in equation 3.2a. The new discrete inputs are set as $\mathbf{u}_k$ in equation 3.2b for the discrete time grid, where n_u is the input dimension. The inputs are then held constant between the points in the time grid as in equation 3.2c. The path constraints $\mathbf{h}$ and $\mathbf{g}$ are also discretized, typically at the same time grid as the inputs.

$$0 < t_0 < t_1 ... < t_N = T \tag{3.2a}$$

$$\mathbf{u}_k \in \mathbb{R}^{n_u}, \; k = 0, ..., N-1 \tag{3.2b}$$

$$\mathbf{u}(t) = \mathbf{u}_k, \; t \in [t_k, t_{k+1}] \tag{3.2c}$$

In short, the single shooting method suffers from large amounts of non-linearity during longer simulations. This method is, therefore, generally not preferred. Figure 3.2 shows an illustration of the direct single shooting approach.

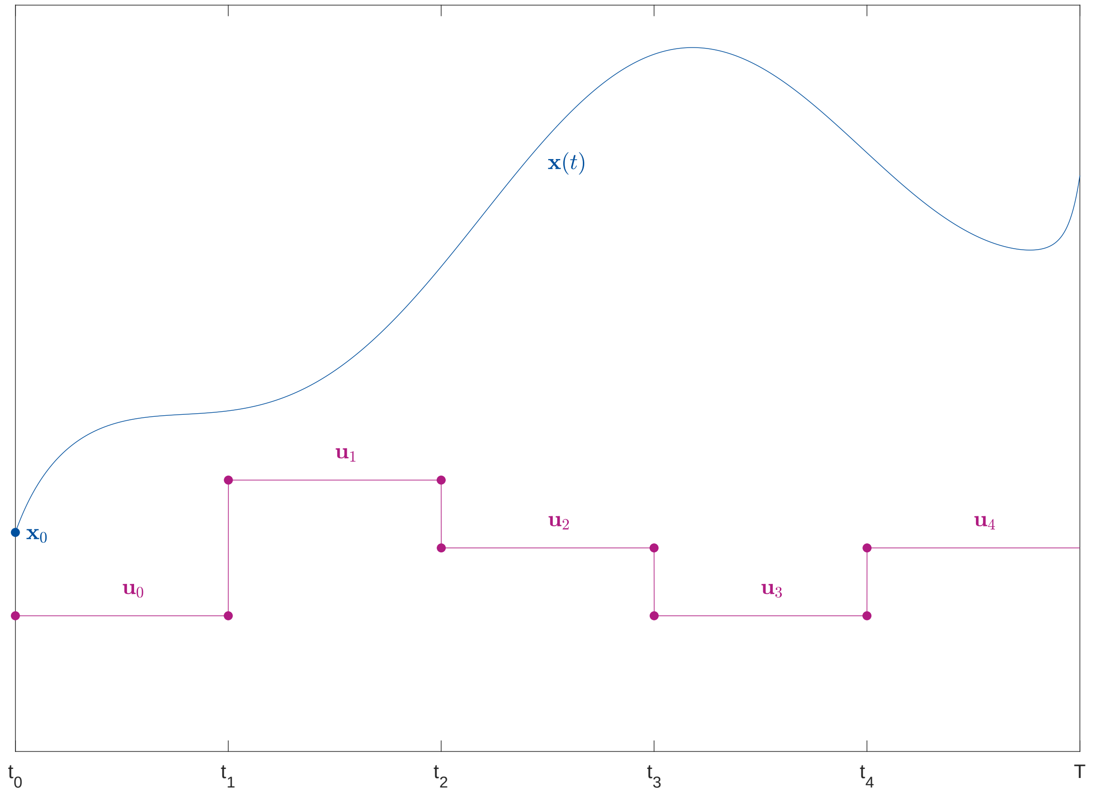

Figure 3.2: Direct single shooting approach (based on [32])

Direct Multiple Shooting

The direct multiple shooting method is based on solving the ODEs at each time interval $t \in [t_k, t_{k+1}]$, instead of the entire horizon as the direct single shooting method does. The trajectories are calculated piecewise, and a new set of initial values $\mathbf{x}_k$ are defined at each time interval. $\mathbf{x}'_k$ is used as the notation for the piecewise trajectories. The input vector $\mathbf{u}$ is discretized the same way as for the single shooting method.

Equation 3.3a provides the dimension of the initial state vector and the number of calculations of the trajectories. The splitting of the dynamic and new initial values are given by equations 3.3b and 3.3c. The method ensures continuity for the trajectories by adding the additional shooting constraint as in equation 3.3d. The constraints $\mathbf{h}$ and $\mathbf{g}$ are also discretized in a time grid, often the same as for the input, but a denser time grid is also possible. The constraints are checked for in every discrete time t_k.

$$\mathbf{x}_k \in \mathbb{R}^{n_x}, \;\; k = 0, ..., N \tag{3.3a}$$

$$\dot{\mathbf{x}}'_k(t, \mathbf{x}_k, \mathbf{u}_k) = \mathbf{f}(\mathbf{x}'_k(t, \mathbf{x}_k, \mathbf{u}_k), \mathbf{u}_k), \;\; t \in [t_k, t_{k+1}] \tag{3.3b}$$

$$\mathbf{x}'_k(t_k, \mathbf{x}_k, \mathbf{u}_k) = \mathbf{x}_k \tag{3.3c}$$

$$\mathbf{x}'_k(t_{k+1}, \mathbf{x}_k, \mathbf{u}_k) = \mathbf{x}_{k+1} \tag{3.3d}$$

Multiple shooting acts as a series of single shootings, but the discrete NLP is now easier to solve. The reason for this is that the short intervals reduce the non-linearity. The downside of this method is the increased number of optimization variables. Figure 3.3 shows an example of direct multiple shooting.

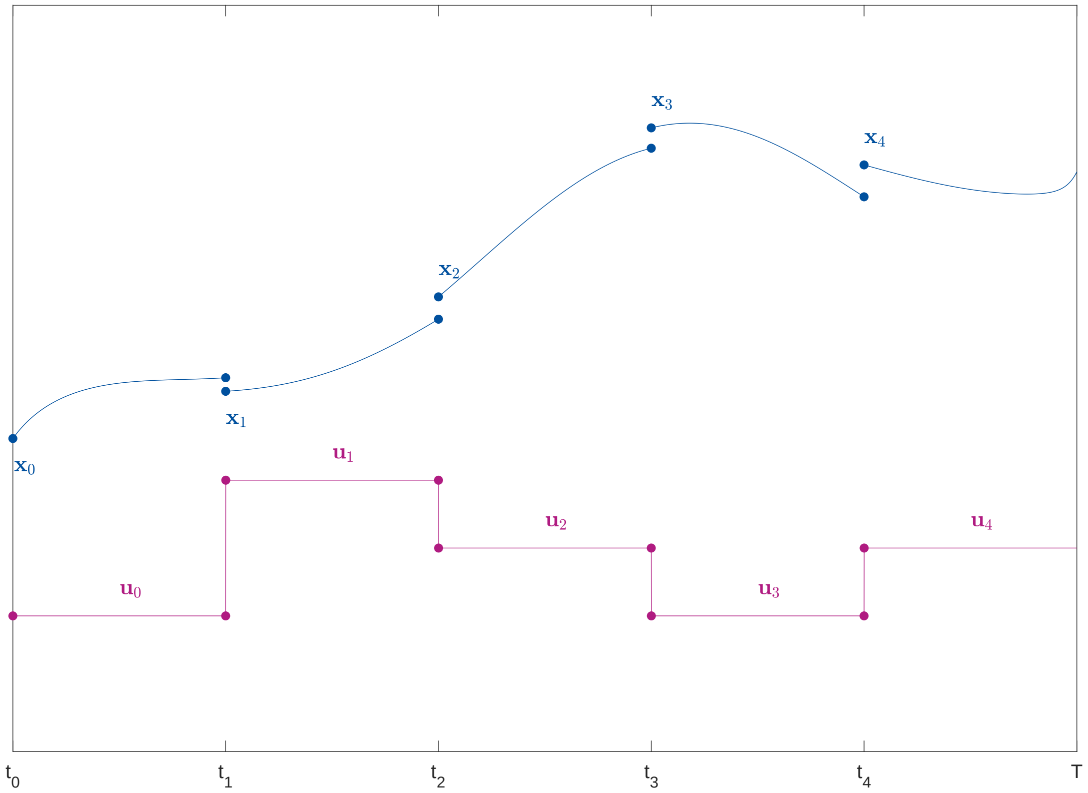

Figure 3.3: Direct multiple shooting approach (based on [32])

The multiple shooting approach uses a simultaneous procedure, meaning that both the optimization and simulation are performed at the same time. This approach is based on a sparse structure of the OCP and provides an efficient solution method. Therefore, direct multiple shooting is the preferred method in most cases, and it is utilized in this thesis as well.

To get a sparse structure of the OCP, the optimization variables are collected in a vector $\mathbf{w}$ in a specific order as in equation 3.4a. The constraints $\mathbf{h}$ and $\mathbf{g}$ are also arranged in a particular structure as in equations 3.4b and 3.4c for the same purpose [37]. The constraints are, in this case, discretized in the same time grid as the rest of the OCP.

$$\mathbf{w} = \begin{bmatrix} \mathbf{x}_0^\top & \mathbf{u}_0^\top & \dots & \mathbf{u}_{N-1}^\top & \mathbf{x}_N^\top \end{bmatrix} \tag{3.4a}$$

$$\mathbf{h}(\mathbf{w}) = \begin{bmatrix} \mathbf{h}(\mathbf{x}_0, \mathbf{u}_0) \\ \vdots \\ \mathbf{h}(\mathbf{x}_{N-1}, \mathbf{u}_{N-1}) \\ \mathbf{h}(\mathbf{x}_N) \end{bmatrix} \tag{3.4b}$$

$$\mathbf{g}(\mathbf{w}) = \begin{bmatrix} \mathbf{x}(0) - \mathbf{x}_0 \\ \mathbf{f}(\mathbf{x}_0, \mathbf{u}_0) - \mathbf{x}_1 \\ \vdots \\ \mathbf{f}(\mathbf{x}_{N-1}, \mathbf{u}_{N-1}) - \mathbf{x}_N \end{bmatrix} \tag{3.4c}$$

The OCP in discrete time is expressed with equations 3.5a-3.5c, where $\mathbf{L}_k$ represents the discrete time Lagrangian term. Note that the Mayer term is also removed in the discrete time OCP.

$$\min_{\mathbf{w}} \ \mathbf{J}(\mathbf{w}) = \min_{\mathbf{x},\mathbf{u}} \sum_{k=0}^{N-1} \mathbf{L}_k(\mathbf{x}_k, \mathbf{u}_k) \tag{3.5a}$$

$$\text{subject to} \qquad \mathbf{h}(\mathbf{w}) \leq \mathbf{0} \tag{3.5b}$$

$$\mathbf{g}(\mathbf{w}) = \mathbf{0} \tag{3.5c}$$

Direct Collocation

Collocation is based on discretizing the inputs and states on a higher resolution time grid. On each interval $[t_k, t_{k+1}]$, the trajectories are approximated with the use of polynomials. The NLP is then made by direct collocation of the obtained equations. The collocation method is much similar to the multiple shooting method, but unlike multiple shooting, the variables in the solution algorithm also act as optimization variables.

3.4 Differential Equation Solvers

The shooting methods require an external differential equation solver. Since all of the equations of the HPS model are ODEs, an ODE solver for this type of equations is needed. The popular integration methods (solving methods) briefly discussed in this thesis are the explicit (subsection 3.4.1) and implicit (subsection 3.4.2) Runge-Kutta (RK) methods. These methods iteratively integrate the differential equations. The following content is based on the theory found in [38].

First off, the generalized RK method of s stages is expressed as in equations 3.6a-3.6c. The number of stages corresponds to the number of times the function $\mathbf{f}$ is evaluated. The constants a, b, and c are given by butcher tableaus, which are value tables containing values depending on the method. Δt is the time step, set by the time grid for the integrator. If the next $\mathbf{K}$ can explicitly be calculated by the previous $\mathbf{K}$, the discrete state vector $\mathbf{x}_k$, and input $\mathbf{u}$, the method is said to be explicit. If this is not the case, the method is implicit, and both the diagonal and the upper diagonal of the butcher tableau are nonzero.

$$\mathbf{K}_1 = \mathbf{f}(\mathbf{x}_k + \Delta t \sum_{j=1}^{s} a_{1j}\mathbf{K}_j, \mathbf{u}(t_k + c_1 \Delta t)) \tag{3.6a}$$

$$\vdots$$

$$\mathbf{K}_s = \mathbf{f}(\mathbf{x}_k + \Delta t \sum_{j=1}^{s} a_{sj}\mathbf{K}_j, \mathbf{u}(t_k + c_s \Delta t)) \tag{3.6b}$$

$$\mathbf{x}_{k+1} = \mathbf{x}_k + \Delta t \sum_{i=1}^{s} b_i \mathbf{K}_i \tag{3.6c}$$

3.4.1 Explicit Runge-Kutta Method

The simplest form of explicit RK method is the Euler method: Runge-Kutta of first order (RK1). This method is easy to implement, but it neglects the trajectory curvature. Increasing the order of the method makes it possible to capture the trajectory characteristics but at the cost of more computational time. In general, reducing the approximation error can be obtained by increasing the order of the method or decreasing the time step Δt. Increasing the time step also results in increased computational time.

For orders up to and including Runge-Kutta of fourth order (RK4), the computational power needed is proportional to the order. This does not, however, hold for higher-order explicit RK methods, where an increase in order requires a larger increase in computational power due to multiple extra stages needed. On the bright side, the number of stages gives an exponential increase in accuracy. In this thesis, the RK4 method is chosen as this method generally gives the best trade-off between computational time and accuracy.

The explicit RK methods suffer from potential instability. The stability region increase with an increase in order or decrease in time step value. The stability region, however, is still limited to a certain degree. The RK4 method has a decent stability region with a reasonable choice of the time step Δt.

3.4.2 Implicit Runge-Kutta Method

The reason for choosing an explicit RK method is the advantage of a lower computational cost. That being said, the implicit method has its advantages. The stability of this integration method is independent of the time step Δt, but this is, as mentioned, not the case for explicit methods. The number of stages required for higher orders is also lower for implicit RK methods, but this does not necessarily make them more efficient for solving differential equations. The last advantage of the implicit method mentioned here is that it handles DAEs smoothly. This property is, however, irrelevant in this thesis since all model equations to be solved are ODEs.

3.5 Optimization Methods

To solve the NLP arising from the direct multiple shooting approach, an optimization method is used to find a set of optimal trajectories and inputs $\mathbf{w}^*$. The optimization methods for NLPs are divided into two classes; the nonlinear interior point (IP) method and sequential quadratic programming (SQP). These methods are based on solving the Karush-Kuhn-Tucker (KKT) conditions (subsection 3.5.1), which are the necessary conditions for optimality in NLPs. Newton's method (subsection 3.5.2) together with step length methods (subsection 3.5.3) make up the basis of both IP (subsection 3.5.4) and SQP (subsection 3.5.5) methods. These methods differ as IP uses the barrier functions while SQP uses linearization. The optimization theory is reached from [32] and [33].

3.5.1 Karush–Kuhn–Tucker Conditions

The KKT conditions are given in equations 3.7a-3.7e. $\mathcal{L}$ is called the Lagrangian function and is a function of the optimization variables in $\mathbf{w}$ and Lagrange multipliers λ and μ (multipliers for equality and inequality constraints respectfully). The $*$ notation implies that the variable is a local minimizer (i.e. a variable belonging to a local minimum). The parameter n_h represents the number of inequality constraints.

$$\nabla\mathcal{L}(\mathbf{w}^*, \lambda^*, \mu^*) = \nabla\mathbf{J}(\mathbf{w}^*) + \lambda^*\nabla\mathbf{g}(\mathbf{w}^*) + \mu^*\nabla\mathbf{h}(\mathbf{w}^*) = \mathbf{0} \tag{3.7a}$$

$$\mathbf{g}(\mathbf{w}^*) = \mathbf{0} \tag{3.7b}$$

$$\mathbf{h}(\mathbf{w}^*) \leq \mathbf{0} \tag{3.7c}$$

$$\mu^* \geq \mathbf{0} \tag{3.7d}$$

$$\mu_i^*\mathbf{h}_i^*(\mathbf{w}^*) = \mathbf{0},\ i = 1, ..., n_h \tag{3.7e}$$

A subset of the KKT conditions (equations 3.7c-3.7e) goes by the name complementary conditions. If $\mu_i^* = \mathbf{h}_i(\mathbf{w}^*) = \mathbf{0}$ the conditions form a set that is non-smooth (not differentiable at the origin), and the constraint is said to be weakly active. The constraint is strictly active if $\mu_i^* > \mathbf{0}$. If all of the constraints are strictly active, the property of strict complementary is obtained.

3.5.2 Newton's Method

Both the SQP and nonlinear IP methods are based on solving the nonlinear KKT conditions using Newton's method. The idea of this method is to iteratively find the roots of the function $\mathbf{f}(\mathbf{x})$ by using its gradient $\nabla\mathbf{f}$ and Hessian $\nabla^2\mathbf{f}$. The method starts with an initial guess for the solution.

Equation 3.8a shows one iteration j of Newton's method. This equation uses the exact Hessian $\nabla^2\mathbf{f}$ of the function $\mathbf{f}$, and it is not guaranteed to provide a descent step close to the solution. A modified Hessian $\mathbf{B}_j$ is, therefore, an alternative to ensure convergence. The equation using the modified Hessian is given in 3.8b. The Quasi-Newton method, which uses a modified Hessian, makes sure that $\mathbf{B}_j$ is positive definite by updating it with a given formula every iteration. Other modifications also exist, such as adding positive values to the original Hessian.

The variable $\alpha_j \in (0,1]$ represents the step length for the iteration. The step can be scaled to ensure progress to the root-finding, as a full step ($\alpha_j = 1$) might skip solutions in some regions (e.g. a large step from the edge of a steep hill can miss the local minimum at the bottom of the hill).

$$\mathbf{x}_{j+1} = \mathbf{x}_j - \alpha_j \nabla^2\mathbf{f}(\mathbf{x}_j)^{-1}\nabla\mathbf{f}(\mathbf{x}_j) \tag{3.8a}$$

$$\mathbf{x}_{j+1} = \mathbf{x}_j - \alpha_j \mathbf{B}_j(\mathbf{x}_j)^{-1}\nabla\mathbf{f}(\mathbf{x}_j) \tag{3.8b}$$

3.5.3 Step Length Methods

The performance of the step length can be checked through a merit function that measures the solution's progress. The merit function works as a somehow scaled version of the NLP where it combines the objective value and constraint violations. It accepts steps if it produces a lower merit function in the next iteration. Using a merit function can cause a slow convergence of the algorithm as it tends to throw away numerous step suggestions. It is also possible to use filter methods where a decrease in either objective value or constraint violation makes the step acceptable. The filter stores the best combinations of objective values and constraint violations and uses them as comparisons. The filter methods often result in full steps.

To find appropriate steps, a line search or trust region algorithm is used. The line search method uses some chosen conditions (for example, Wolfe conditions), and with the help of the merit function or a filter, it reduces the step length from a full step length until the conditions are met. The trust region method adds an extra constraint to make a small region close to the last iteration. This is to get a decrease in the merit function. The region size can be adjusted to ensure progress towards the solutions. Using both these methods does, in theory, result in global convergence, meaning that a local solution is always found using an arbitrary initial starting point.

3.5.4 Interior-Point Method

The IP method approximates the non-smooth set from the complimentary conditions as a smooth set. A hyperbola function is commonly used for this. A strictly positive constant τ is used for the smoothing in this approximation. This constant starts out large and is gradually reduced during the iterations of solving the nonlinear equations. Equation 3.9 shows how the complimentary conditions in equations 3.7c-3.7e are smoothed to obtain a smooth system of equations. The equation solving is then executed by using Newton's method. This method is called the primal-dual method.

$$\mu_i^* \mathbf{h}_i^*(\mathbf{w}^*) + \tau = \mathbf{0}, \;\; i = 1, ..., n_h \tag{3.9}$$

Another IP method, is the primal method, where equation 3.9 is inserted into equation 3.7a. This results in the so called barrier problem as expressed in equations 3.10a and 3.10b.

$$\min_{\mathbf{w}} \;\; \mathbf{J}(\mathbf{w}) - \tau \sum_{i=1}^{n_h} log(-\mathbf{h}_i(\mathbf{w})) \tag{3.10a}$$

$$\text{subject to} \quad \mathbf{g}(\mathbf{w}) = \mathbf{0} \tag{3.10b}$$

The primal and primal-dual methods provide the same solution to the problem, but the primal method suffers from ill-conditioned matrices when τ becomes small. A small solution error is desired, and the error linearly decreases with τ. The primal-dual method is, therefore, the preferred method when it comes to numerical implementation.

The primal-dual formulation can be extended to include slack variables s. The complimentary conditions then end up as in equations 3.11a and 3.11b. Even though this yields the same solution as with equation 3.9, the slack variables provide some benefits. With slack variables, the initial guess can be infeasible. Through the iterations of Newton's method, equation 3.11b makes sure that the solutions are feasible. Another advantage of using slack variables is that backtracking (step size reduction), which can be computationally expensive, is not required.

$$\mu_i^* \mathbf{s}_i^* - \tau = \mathbf{0}, \;\; i = 1, ..., n_h \tag{3.11a}$$

$$\mathbf{h}_i(\mathbf{w}^*) + \mathbf{s}_i^* = \mathbf{0}, \;\; i = 1, ..., n_h \tag{3.11b}$$

In this thesis, the nonlinear IP (primal-dual) method is chosen for optimization as it offers a great open-source code solver called interior-point optimizer (IPOPT). This solver is based on using a linear solver as its subroutine to compute the roots of the KKT conditions. The solver also uses the line search and filter method to progress [39].

3.5.5 Sequential Quadratic Programming

The SQP methods iteratively transform the NLP into a QP by linearizing the objectives and constraints. The resulting inequality constrained QP is then solved by using an IP method for QPs or an active set method. The active set method solves the optimization problem directly by computing active sets. The SQP method is advantageous for both large and small problems. However, the IP method proves better performance in this thesis.

3.6 Model Predictive Control

The main goal of MPC is to compute the optimal inputs $\mathbf{u}$, resulting in an optimal evolution of $\mathbf{x}$. To do this, the OCP (section 3.2) is solved by using a numerical approach (section 3.3). The prediction model $\mathbf{f}$ together with $\mathbf{u}$ are used to predict the future trajectories $\mathbf{x}$ with the use of a differential equation solver (section 3.4). The predicted trajectories are used in the optimization method (section 3.5) to find the optimal inputs $\mathbf{u}_k$. A regular type of objective function to specify the control goals of the MPC is further described in subsection 3.6.1. The content here stems from [32] and [12].

There are two ways of using the MPC, either in open-loop or closed-loop. The open-loop method solves the finite horizon OCP once and applies the calculated inputs $\mathbf{u}_k$ to the plant at every discrete time t_k. This is called open-loop optimization. The closed-loop optimization method recomputes the finite horizon OCP at every discrete time step t_k and applies the first optimal input $\mathbf{u_k}$ of the solution to the plant. As the solution is recomputed, the initial conditions $\mathbf{x}_0$ are replaced by the current plant measurements $\mathbf{y}_k$, which are the discrete time measurements at time t_k. This technique is also called a receding horizon.

A significant issue with the open-loop approach is that the predictions drift away from the real system dynamics due to model imperfections. The closed-loop optimization compensates for the modeling imperfections by introducing the receding horizon as described in the previous paragraph. This approach provides a correction at every discrete time step, yielding a more accurate control. The focus of this thesis is on a receding horizon MPC.

In this thesis, all plant states are measurable as they are outputs from the HPS plant model. In reality, where measurements are impossible or hard, a Kalman filter (KF) or moving horizon estimator (MHE) can be used to estimate the states.

Figure 3.4 shows the MPC in a closed-loop connection to a plant with a measurement unit. The measurement unit measures the plant outputs $\mathbf{y}$ at discrete times t_k. A reference $\mathbf{r}$ is included as the objective typically is to track a reference. In this thesis, the plant is replaced with a plant model. The plant model is commonly more complex than the prediction model due to less power needed for simulation than optimization.

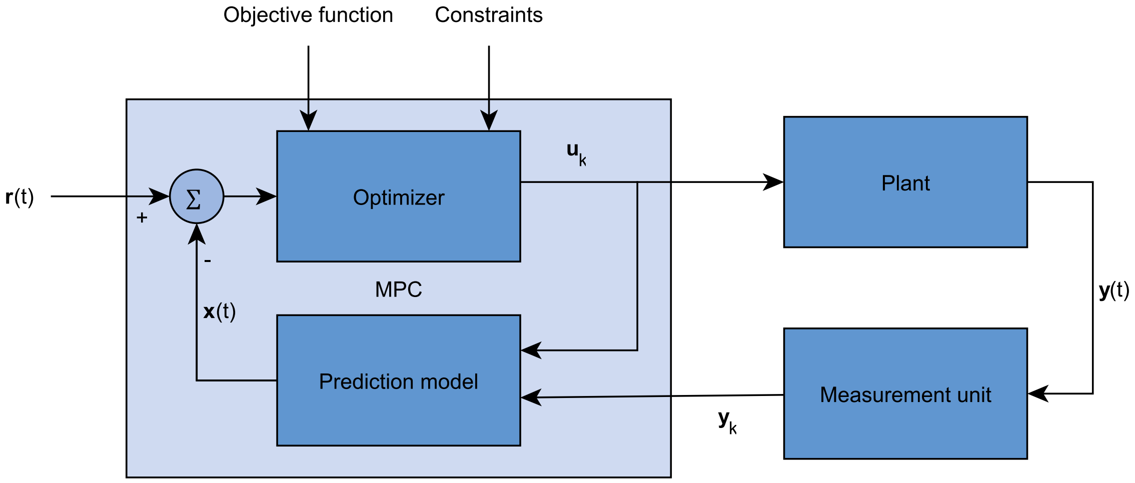

Figure 3.4: Overview of a model predictive controller with a feedback connection to a plant through an output measurement unit (based on [40])

The evolution of the model trajectories $\mathbf{x}$ is predicted for the finite horizon T_{ph}, called the prediction horizon. The prediction of optimal inputs $\mathbf{u}_k$ can be chosen to lay in a shorter interval T_{ch}, which is called the control horizon. The control inputs are then held constant for $t \in [T_{ch}, T_{ph}]$. A reason for using a reduced control horizon is to decrease the number of optimization variables, bringing down the needed computational power. The inputs are typically less necessary at the end of the prediction horizon. In addition, a plant with a large delay needs some adjustment time.

Equations 3.12a-3.12c show modifications to the discrete time OCP when using different horizons. N_{ch} and N_{ph} are the number of discrete time steps for the control and prediction variables, where $N_{ch} \leq N_{ph}$. Moreover, the constraints $\mathbf{h}$ and $\mathbf{g}$ are accounted for lesser variables if $N_{ch} \neq N_{ph}$.

$$\min_{\mathbf{w}} \ \mathbf{J}(\mathbf{w}) = \sum_{k=0}^{N_{ph}-1} \mathbf{L}_k(\mathbf{x}_k) + \sum_{k=0}^{N_{ch}-1} \mathbf{L}_k(\mathbf{u}_k) \tag{3.12a}$$

$$\mathbf{u}_k \in \mathbb{R}^{n_u}, \ k = 0, ..., N_{ch} - 1, \ 0 < t_0 < t_1 ... < t_{N_{ch}} = T_{ch} \tag{3.12b}$$

$$\mathbf{x}_k \in \mathbb{R}^{n_x}, \ k = 0, ..., N_{ph} - 1, \ 0 < t_0 < t_1 ... < t_{N_{ph}} = T_{ph} \tag{3.12c}$$

As the horizon moves for every time step Δt, a notation for the time given the current placement of the horizon is essential. The discrete time inputs, states, measurements, and references are redefined as $\mathbf{u}_{k,k"}$, $\mathbf{x}_{k,k"}$, $\mathbf{y}_{k,k"}$, and $\mathbf{r}_{k,k"}$, where k denotes the position relative to the horizon and $k"$ gives the position of the horizon start relative to the global timeline. Using this notation, the inputs to be applied at each time step are $\mathbf{u}_{0,k"}$.

Figure 3.5 shows an example of a receding horizon strategy. The figure is divided into the past, where the control inputs already have been applied, and the future, which is the prediction of the

MPC. The dots represent measurements, predictions, and input appliances in discrete time. The shaded plot in the past area of the figure shows the history of inputs $\mathbf{u}$ applied to the plant, the actual measured outputs $\mathbf{y}$, and the past references $\mathbf{r}$. In the future region, the predicted optimal open-loop trajectories $\mathbf{x}$ and inputs $\mathbf{u}$ are calculated to follow the reference $\mathbf{r}$ in the future. This example also includes a shorter control horizon compared to the prediction horizon.

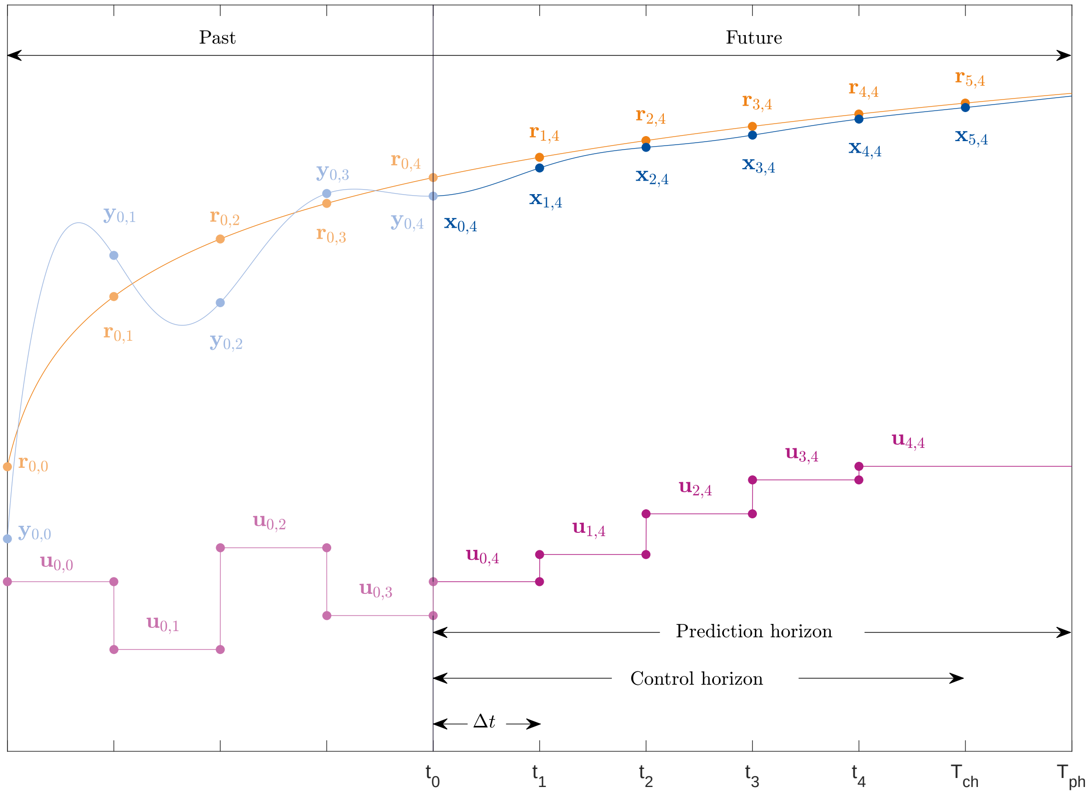

Figure 3.5: History and prediction from a receding horizon strategy (based on [12] and [41])

NMPC is a special form of MPC where the dynamical model is nonlinear. The NMPC approaches usually end in non-convex OCPs. This is also the case in this thesis, as analyzed in section 3.2.

3.6.1 Objective Function

The objective function is designed in order to reach desired objectives. The standard approach for MPC is to use reference tracking, where the controlled variables (CVs) track the references $\mathbf{r}$ which is time-varying or stationary. The manipulation variables (MVs) are also included in the objective function [42]. Figure 3.5 shows an example of a time-varying reference tracking.

Both the terms containing the reference tracking of CVs and the MVs are weighted by the diagonal matrices $\mathbf{Q}_k$ and $\mathbf{R}_k$ respectfully. These weight matrices can be time-varying or constant. Time-varying matrices yield a more complex tuning due to an increased number of tuning parameters.

A higher weight value on the CVs means a higher priority in tracking the reference, and a higher weight value on the MVs makes the inputs more costly to use. The Lagrangian term for typical reference tracking is shown in equation 3.13 [42], [43].

$$\mathbf{L}_k(\mathbf{x}_k, \mathbf{u}_k) = \mathbf{Q}_k(\mathbf{r}_k - \mathbf{x}_k)^2 + \mathbf{R}_k\mathbf{u}_k^2 \tag{3.13}$$

The terms in the objective function are often chosen to be quadratic. This makes the objectives convex and the derivatives easier to analyze. In addition, one extreme point is ensured. Other forms of formulations also exist, for example, robust MPC, which is designed to handle disturbances.

4 Nonlinear Model Predictive Control Design

This chapter describes the details around the design of the NMPC. It is required that the NMPC handles the power distribution in the HPS under different wind conditions, with a high focus on utilizing potential wind power. Additionally, the controller should be concerned with rapid movements to decrease wear and tear. Figure 4.1 shows how the design aspects of the NMPC are put together.

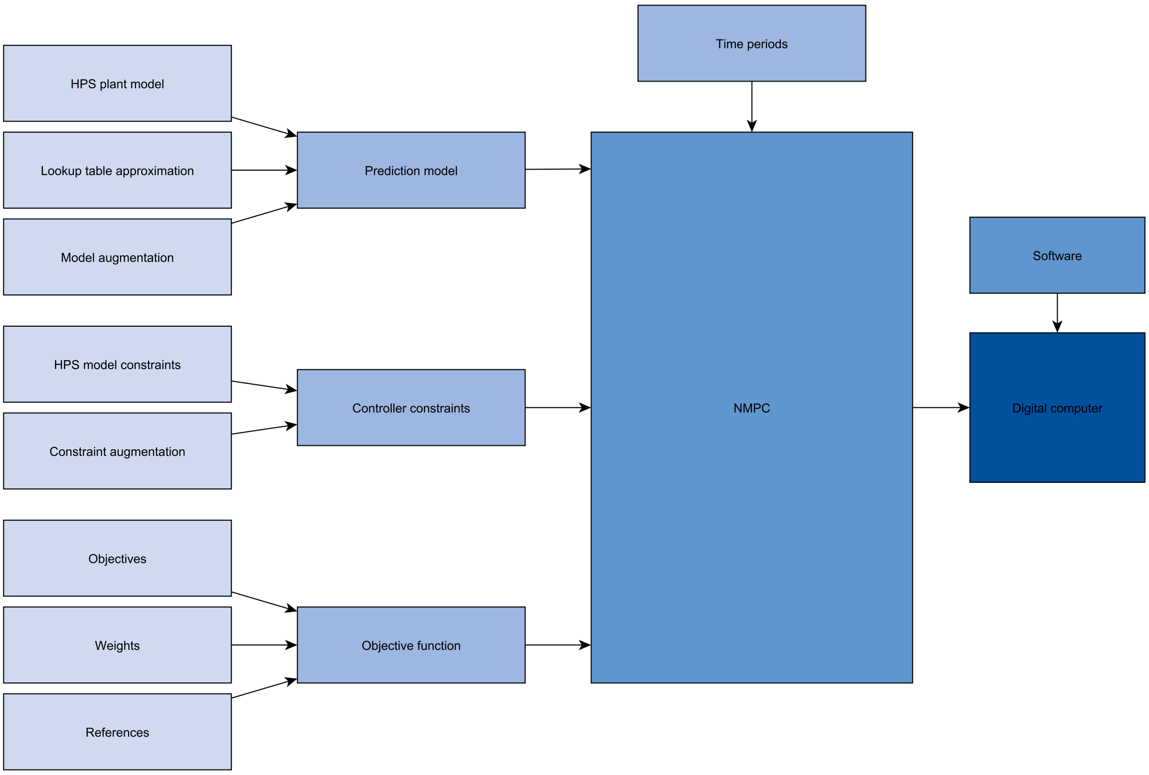

Figure 4.1: Design elements for the NMPC

Firstly, section 4.1 describes approximations of the HPS model's lookup tables, which are used in the HPS prediction model. Section 4.2 arranges the prediction model equations into a state-space form and augments the system to include input dynamics. The NMPC constraints are found in section 4.3. In section 4.4, the controller objectives needed to gain a desired control response are expressed. A guideline for general MPC tuning and the specific tuning for the NMPC are described in section 4.5. Lastly, the software choice and implementation method for the NMPC are represented in section 4.6.

4.1 Lookup Table Approximations

As the lookup tables used in the WTG model (section 2.3) consist of a limited number of values, this makes the OCP a mixed integer nonlinear program (MINLP), where a subset of the states lay in discrete state-space. To formulate the OCP as a NLP, which are generally less complex to solve, the lookup tables are approximated as continuous functions. In subsection 4.1.1 the generator torque lookup table is approximated and the turbine lookup table is approximated in subsection 4.1.2. To that end, the curve fitting tool [25] from MATLAB is utilized. The resulting parameters are given in table A.4.

4.1.1 Generator Torque Lookup Table Approximation

The characteristics of the generator torque $M_{w_{gen}}$ as a function of rotational speed $\omega_{w_{gen}}$ resemble the characteristics of a sigmoid function. Therefore, this type of function, and more specifically a logistic function, is used to approximate $M_{w_{gen}}$. The function has a flat region at the start and end, with a steep slope in between. Figure 4.2 shows the generator torque lookup table and the approximated generator torque function for a varying rotational speed.

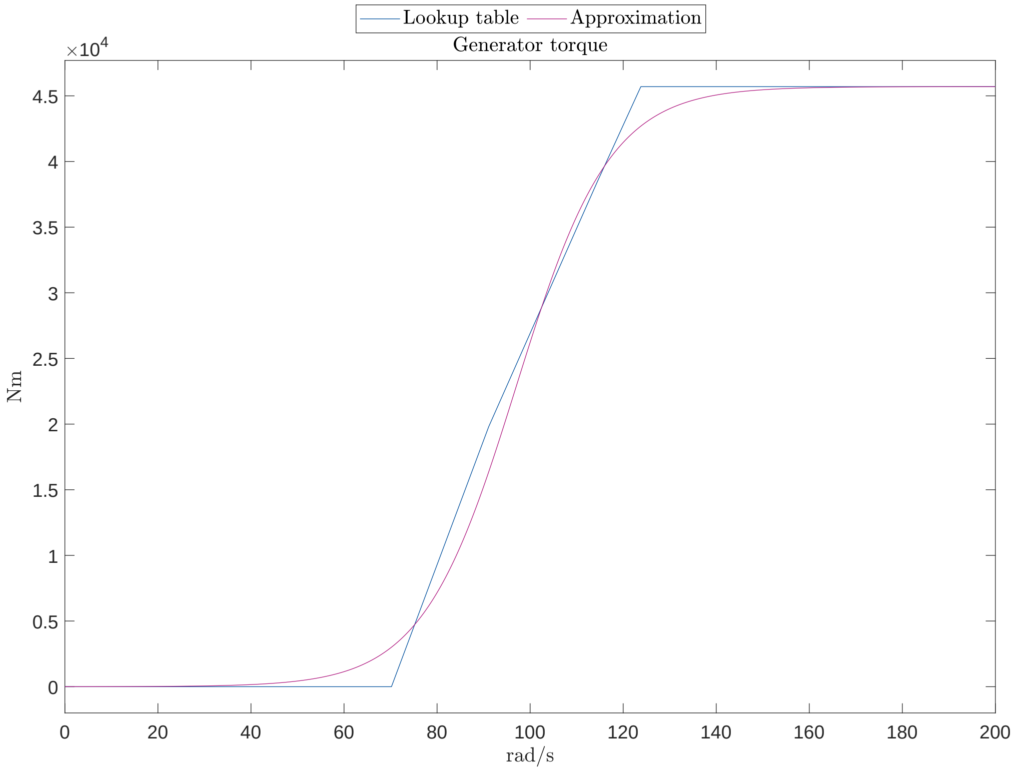

Figure 4.2: Generator torque lookup table and approximation of generator torque for a varying rotational speed

The approximation of the lookup table is given as a function in equation 4.1, where $M_{w_{gen_{max}}}$ is the maximum generator torque, $K_{w_{gen}}$ is a constant to adjust the curve steepness, and $\omega_{w_{gen_{mid}}}$ is the midpoint of the function's slope. The resulting approximation has an R-square value of 0.99, which means that the fit of the curve is quite good.

$$D_{w_{gen}} = \frac{M_{w_{gen_{max}}}}{1 + e^{-K_{w_{gen}}(\omega_{w_{gen}} - \omega_{w_{gen_{mid}}})}} \tag{4.1}$$

4.1.2 Turbine Lookup Table Approximation

The lookup table $C_{w_{tur}}$ is a function of the pitch β_w and tip speed ratio ϕ_w. The two inputs in different combinations give different values, meaning that the lookup table values shape a 3-dimensional figure. This fact implies that the continuous approximation of the lookup table is a plane wrapped in three dimensions. Unfortunately, finding a good approximation for a 3-dimensional figure is a lot harder than for a 2-dimentional one.

To approximate $C_{w_{tur}}$, a polynomial function is chosen. However, fitting the entire lookup table yields a high variance in the approximation around the operational area of the WTG. A reason for this is the lookup table's nonlinearities combined with a large span of table values. The entire span of values is about -210 to 0.6. After a thorough inspection of the lookup table and simulations of the WTG model at different operational modes, it is found that the operable lookup table values lay around -0.1 to 0.6. Every table value under -0.1 is therefore removed from the lookup table in order to obtain a relevant set of points to be curve fitted with high accuracy.

Another issue with the fitting is choosing the proper order of the polynomial to avoid underfitting or overfitting certain regions, which results in inaccurate fits. During tests of different orders, it is clear that a first-order fit of both inputs yields in underfitting, and combinations of fourth-order and fifth-order fits of the two inputs end in overfitting. This leaves the option of combining first, second, and third-order degrees of fit. Visually, it is hard to determine which one is the best fit, and the measurement of fit in the curve fitting tool does not eliminate the factor of overfitting. However, some of the polynomial combinations are eliminated due to obvious misshapes.

Figure 4.3 shows the result of the curve fitting of the operational area. The figure is primarily zoomed in on the z-axis, and the red dots represent a part of the excluded points. The black points are the points observed to be in the operational area, and the curve is fitted to intersect these points. The yellow curve is the 3-dimensional polynomial function fitted to the black points. The polynomial degree of the plane is 3 in β_w and 2 in ϕ_w.

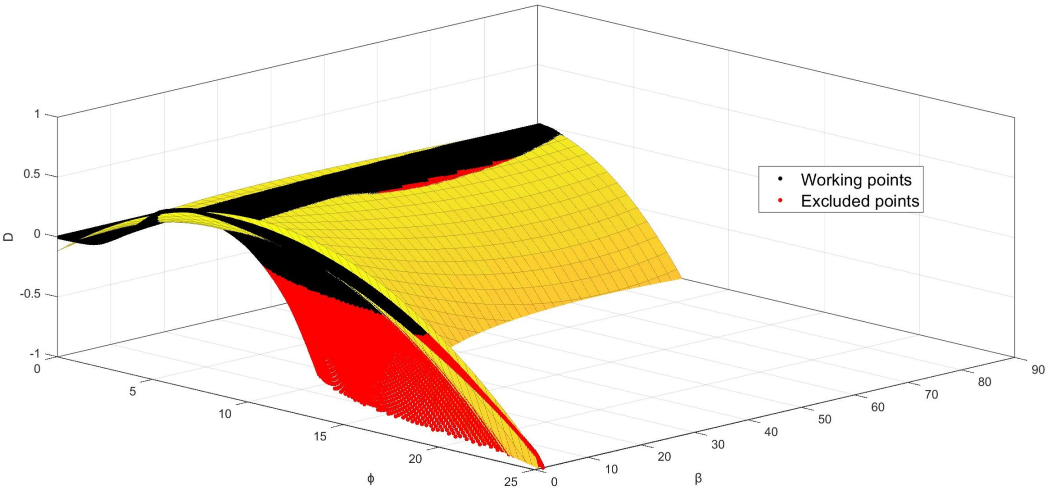

Figure 4.3: Curve fitted 3-dimensional plane for the turbine lookup table approximation

The combinations of degrees of the inputs in the polynomial are compared to the lookup table $C_{w_{tur}}$ at different wind speeds v_w to find the best fit. These wind speeds represent a sizeable operational range. A set interval of pitch values β_w from 0 to 30 degrees, which represents the nominal operational pitch range, is also used. The combination of different pitch values and wind speeds yields different values of ϕ_w, such that a larger specter of approximated table values is tested.

Average mean square error (AMSE), which is the average of the mean square errors (MSEs) for each wind speed, is used as a "goodness of fit" measurement where a small value is better than a large one. Table 4.1 shows the results of the test for different orders of the inputs with different winds.

Deg(β_w)	**Deg(ϕ_w)**	$v_w = 1$	$v_w = 6$	$v_w = 11$	$v_w = 16$	$v_w = 21$	**AMSE**
1	2	0.0107	0.0056	0.0016	0.0004	0.0011	0.0039
1	3	0.0058	0.0035	0.0013	0.0006	0.0012	0.0025
2	2	0.0107	0.0056	0.0016	0.0004	0.0011	0.0039
2	3	0.0045	0.0033	0.0037	0.0049	0.0051	0.0043
3	2	0.0050	0.0023	0.008	0.0007	0.0010	0.0020
3	3	0.0070	0.0061	0.0070	0.0085	0.0086	0.0074

Table 4.1: Test of polynomial approximations of the turbine lookup table

From looking at the results in table 4.1, it is observed that a β_w of degree 3 and a ϕ_w of degree 2 gives the least AMSE. This value tells that the average performance of this combination of polynomial order gives the best mean approximation of the lookup table. To ensure that the polynomial does not deviate too far from the lookup table at certain values, monitoring of the performance is also executed. The combination yielding the smallest AMSE also approximately gives the slightest maximum deviation. Therefore this polynomial combination is chosen, and it is expressed in equation 4.2, where p represents the coefficients of the polynomial. This polynomial fit is also the one shown in figure 4.3.

$$\begin{aligned} D_{w_{tur}} = p_{w_{00}} + p_{w_{10}}\phi_w + p_{w_{01}}\beta_w + p_{w_{20}}\phi_w^2 + p_{w_{11}}\phi_w\beta_w \\ +p_{w_{02}}\beta_w^2 + p_{w_{21}}\phi_w^2\beta_w + p_{w_{12}}\phi_w\beta_w^2 + p_{w_{03}}\beta_w^3 \end{aligned} \tag{4.2}$$

4.2 Prediction Model State-Space Formulation

In this section, two state-space formulations of the prediction model are formulated. First, in subsection 4.2.1 the original state-space formulation, where the inputs $\mathbf{u}$ are unchanged, is introduced. In subsection 4.2.2 the state-space formulation is augmented with dynamical properties of the inputs. The reasons for including the extra input dynamics are to smoothen the overall closed-loop system response and constrain the input dynamics. This augmentation reduces the physical stress in the HPS, yielding a lessened necessity for maintenance.

4.2.1 Original State-Space Formulation

To describe the dynamics of the HPS prediction model, the model equations from chapter 2 are rearranged and put into a nonlinear state-space form, meaning that the differential equations are of first-order and coupled [44]. Additionally, the lookup tables C are substituted with the approximated functions D form section 4.1.

The vectors belonging to the state-space model are given in equations 4.3a-4.3c, where $\mathbf{x}$ is the state vector, $\mathbf{u}$ is the input vector, and $\mathbf{p}$ is the parameter vector. The parameter vector is used to include the wind speed into the dynamics without having an explicit dynamical wind model. The matter of how $\mathbf{p}$ is treated in this thesis is a further subject in chapter 5. The differential equations representing the state-space is given with $\dot{\mathbf{x}}$ in equations 4.4a-4.4g.

$$\mathbf{x} = \begin{bmatrix} I_p & \omega_p & V_g & P_{g_l} & \omega_{w_{tur}} & M_{w_{gen}} & E_b \end{bmatrix}^\top \tag{4.3a}$$

$$\mathbf{u} = \begin{bmatrix} Q_p & \gamma_g & \beta_w \end{bmatrix}^\top \tag{4.3b}$$

$$\mathbf{p} = \begin{bmatrix} v_w \end{bmatrix} \tag{4.3c}$$

$$\begin{aligned}\dot{I}_p = H_{p_d} - (b_{p_0} + b_{p_1}\frac{Q_p - \mu_{Q_p}}{\sigma_{Q_p}} + b_{p_2}\frac{\omega_p Q_p - \mu_{\omega_p Q_p}}{\sigma_{\omega_p Q_p}} \\ + b_{p_3}\frac{\omega_p^2 - \mu_{\omega_p^2}}{\sigma_{\omega_p^2}} + b_{p_4}\frac{Q_p^2 - \mu_{Q_p^2}}{\sigma_{Q_p^2}} + \frac{Q_p^3 - \mu_{Q_p^3}}{\sigma_{Q_p^3}})\end{aligned} \tag{4.4a}$$

$$\begin{aligned}\dot{\omega}_p = K_{P_p}(H_{p_d} - (b_{p_0} + b_{p_1}\frac{Q_p - \mu_{Q_p}}{\sigma_{Q_p}} + b_{p_2}\frac{\omega_p Q_p - \mu_{\omega_p Q_p}}{\sigma_{\omega_p Q_p}} \\ + b_{p_3}\frac{\omega_p^2 - \mu_{\omega_p^2}}{\sigma_{\omega_p^2}} + b_{p_4}\frac{Q_p^2 - \mu_{Q_p^2}}{\sigma_{Q_p^2}} + \frac{Q_p^3 - \mu_{Q_p^3}}{\sigma_{Q_p^3}}) + K_{I_p} I_p\end{aligned} \tag{4.4b}$$

$$\dot{V}_g = \frac{\gamma_g - V_g}{\tau_{g_1}} \tag{4.4c}$$

$$\dot{P}_{g_l} = \frac{V_g P_{g_{max}} - P_{g_l}}{\tau_{g_2}} \tag{4.4d}$$

$$\dot{\omega}_{w_{tur}} = \frac{\frac{\begin{gathered}\frac{1}{2}v_w^3\rho_{air}A_w(p_{w_{00}} + p_{w_{10}}\frac{R_w\omega_{w_{tur}}}{v_w} \\ +p_{w_{01}}\beta_w + p_{w_{20}}(\frac{R_w\omega_{w_{tur}}}{v_w})^2 + p_{w_{11}}\frac{R_w\omega_{w_{tur}}}{v_w}\beta_w \\ +p_{w_{02}}\beta_w^2 + p_{w_{21}}(\frac{R_w\omega_{w_{tur}}}{v_w})^2\beta_w + p_{w_{12}}\frac{R_w\omega_{w_{tur}}}{v_w}\beta_w^2 + p_{w_{03}}\beta_w^3)\end{gathered}}{\omega_{w_{tur}}} - M_{w_{gen}}N_w}{I_{w_{tur}} + I_{w_{gen}}N_w^2} \tag{4.4e}$$

$$\dot{M}_{w_{gen}} = \frac{\frac{M_{w_{gen_{max}}}}{1+e^{-K_{w_{gen}}(\omega_{w_{tur}}N_w - \omega_{w_{gen_{mid}}})}} - M_{w_{gen}}}{\tau_w} \tag{4.4f}$$

$$\dot{E}_b = \frac{\begin{gathered}(a_{g_1}(\frac{P_{g_l}}{P_{g_{max}}})^2 + a_{g_2}\frac{P_{g_l}}{P_{g_{max}}} + a_{g_3})P_{g_l} \\ + \frac{M_{w_{gen}}\omega_{w_{tur}}N_w\eta_w}{1000} - (\frac{\omega_p}{\omega_{p_n}})^3(c_{p_0} + c_{p_1}\frac{(\frac{\omega_{p_n}}{\omega_p})Q_p - \mu_{Q_{p_n}}}{\sigma_{Q_{p_n}}})\end{gathered}}{\kappa} \tag{4.4g}$$

4.2.2 Augmented State-Space Formulation

An augmented state-space representation is formulated to account for the input dynamics. The previous inputs are transformed into states, and the new inputs are now the derivatives of these states. The new state and input vectors $\mathbf{x}_{aug}$ and $\mathbf{u}_{aug}$ are found in equations 4.5a and 4.5b. In addition, three new linear differential equations (4.6a-4.6c) are added to the state-space. In fact, this formulation also includes integral action into the system as long as the original inputs are not weighted [45]. Further, the augmented state-space formulation is used as the prediction model, and the original inputs are referred to as states whereas the input dynamics are referred to as inputs.

$$\mathbf{x}_{aug} = \begin{bmatrix} I_p & \omega_p & V_g & P_{gl} & \omega_{w_{tur}} & M_{w_{gen}} & E_b & Q_p & \gamma_g & \beta_w \end{bmatrix}^\top \tag{4.5a}$$

$$\mathbf{u}_{aug} = \begin{bmatrix} \Delta Q_p & \Delta\gamma_g & \Delta\beta_w \end{bmatrix}^\top \tag{4.5b}$$

$$\dot{Q}_p = \Delta Q_p \tag{4.6a}$$

$$\dot{\gamma}_g = \Delta\gamma_g \tag{4.6b}$$

$$\dot{\beta}_w = \Delta\beta_w \tag{4.6c}$$

4.3 Controller Constraints

The controller constraints are used to ensure that the HPS is controlled in such a way that its dynamics are valid with respect to the OCP. All of the constraints are inequality constraints and thus belonging in vector $\mathbf{h}$. The constraints are divided into state constraints and input constraints in subsections 4.3.1 and 4.3.2.

4.3.1 State Constraints

The state constraints for the NMPC are almost the same as for the HPS model in chapter 2. In the augmented state-space model, the constraints on the original inputs (for the original state-space model) are also state constraints. The constraints are summarized in equations 4.7a-4.7h.

The only constraint modification is on the flow rate Q_p, which initially has three regions (not allowable, allowable, and preferable). A choice is made for Q_p to be constrained in both the allowable and preferable region (as in equation 4.7f). In this way, the flow rate is ensured to be valid and not exceed values resulting in poor efficiency.

$$\omega_{p_{min}} \leq \omega_p \leq \omega_{p_{max}} \tag{4.7a}$$

$$P_{g_{l_{min}}} \leq P_{g_l} \leq P_{g_{l_{max}}} \tag{4.7b}$$

$$\omega_{w_{tur_{min}}} < \omega_{w_{tur}} \tag{4.7c}$$

$$\frac{P_{w_{min}}}{1000 N_w \eta_w} \leq \omega_{w_{tur}} M_{w_{gen}} \leq \frac{P_{w_{min}}}{1000 N_w \eta_w} \tag{4.7d}$$

$$E_{b_{min}} \leq E_b \leq E_{b_{max}} \tag{4.7e}$$

$$\sqrt{\frac{H_p - d_{p_0}}{d_{p_1}} \sigma_{Q^2_{p_{al}} + \mu_{Q^2_{p_{al}}}}} \leq Q_p \leq \sqrt{\frac{H_p - f_{p_0}}{f_{p_1}} \sigma_{Q^2_{p_{pu}} + \mu_{Q^2_{p_{pu}}}}} \tag{4.7f}$$

$$\gamma_{g_{min}} \leq \gamma_g \leq \gamma_{g_{max}} \tag{4.7g}$$

$$\beta_{w_{min}} \leq \beta_w \leq \beta_{w_{max}} \tag{4.7h}$$

4.3.2 Input Constraints

The input constraints for the augmented state-space (equations 4.8a-4.8c) are used to smoothen the reference tracking. However, it introduces dynamics that are not modeled explicitly. The chosen constraint values for the new inputs are found in table A.5.

$$\Delta Q_{p_{min}} \leq \Delta Q_p \leq \Delta Q_{p_{max}} \tag{4.8a}$$

$$\Delta \gamma_{g_{min}} \leq \Delta \gamma_g \leq \Delta \gamma_{g_{max}} \tag{4.8b}$$

$$\Delta \beta_{w_{min}} \leq \Delta \beta_w \leq \Delta \beta_{w_{max}} \tag{4.8c}$$

4.4 Objectives

The OCP is formulated as a minimization problem (equations 3.1). To weigh the importance of minimizing the different terms, the weights q and r are used to weigh the terms containing the states and inputs respectfully. These weights belong in the diagonal matrices $\mathbf{Q}$ and $\mathbf{R}$ (equation 3.13). The weights are further determined from tuning as described in section 4.5. Equations 4.9a and 4.9b represent the CV and MV parts of the tailored Lagrangian term in equation 4.9c, which is further used in the objective function.

$$\mathbf{L}_x = q_{Q_p}(Q_{p_d} - Q_p)^2 + q_{P_w}(P_{w_{max}}\delta_{P_w} - P_w)^2 + q_{\gamma_g}(\gamma_{g_{min}} - \gamma_g)^2 \tag{4.9a}$$

$$\mathbf{L}_u = r_{\Delta Q_p}\Delta Q_p^2 + r_{\Delta\gamma_g}\Delta\gamma_g^2 + r_{\Delta\beta_w}\Delta\beta_w^2 \tag{4.9b}$$

$$\mathbf{L} = \mathbf{L}_x + \mathbf{L}_u \tag{4.9c}$$

The type of MPC with an objective function which uses the Lagrangian term as in equation 4.9c, is called economic MPC [46]. The Lagrangian term defines the economic objectives directly (in this case maximizing P_w) instead of tracking each state to yield economic control. In this thesis, the term economic refers to using the least amount of fuel in the GTG, harvest the available wind power, while also running the pump at a desired level.

The first term, which contains the flow rate Q_p, targets to track the desired flow rate Q_{p_d}. The desired flow rate is assumed to be given externally, for example, from an individual optimization of the flow rate.

The next term, which involves the WTG power P_w, also has the goal of tracking a reference. This reference is the maximum power output $P_{w_{max}}$. The reference is used to utilize the maximum amount of renewable wind power available. The constant δ_{P_w} (> 1) is used to account for the low cost of the objective as P_w approaches its maximum value.

Further, the GTG throttle γ_g is desired to follow the reference $\gamma_{g_{min}}$ with the intent of minimizing the fuel usage, and by that, reduce GHG emission. The reference vector for the tracking objectives is expressed in equation 4.10.

$$\mathbf{r} = \begin{bmatrix} Q_{p_d} & P_{w_{max}} & \gamma_{g_{min}} \end{bmatrix}^\top \tag{4.10}$$

The last three terms in the Lagrangian term are weighted MVs (inputs). These terms are added to punish change in the inputs. The mentioned terms are less critical in this thesis since a model, and not a system, is the control objective. The tuning of these weights is therefore downgraded. For a real HPS however, the inputs might be set more expensive to use due to physical wear and tear.

To summarize, the objectives are to:

- Track a desired flow rate reference
- Maximize power production from the WTG
- Minimize the GTG fuel usage
- Decrease rapid movements in the system

4.5 Controller Tuning

This section concerns the tuning of the NMPC, and it is divided into two parts. In subsection 4.5.1 a guideline used for the tuning is described. The actual tuning is further a subject in subsection 4.5.2.

4.5.1 Tuning Guideline

The NMPC is firstly tuned in open-loop to get a picture of an optimal response. When the open-loop tuning is satisfied, the resulting tuning parameters are used in the initial tuning for the closed-loop control. The parameters are further tuned to respond to modeling imperfections and reflect the optimality in open-loop tuning.

The tuning of the NMPC is split into two categories. The first is the tuning of controller time periods, and the second is the tuning of objective weights. The time periods are the first to be tuned, and they are kept constant during the weight tuning. For the time period tuning, the theory described is taken from [47]. The weight tuning method builds on theory from [43].

Time Period Tuning

The first parameter to tune is the time-step Δt, which for a large value makes the controlled system more sensitive for errors and disturbances, and for a small value requires a large amount of computational power. Δt is after the guideline, set to be a factor between 0.1-0.25 of the desired closed-loop response T_d.

As Δt is set to a satisfying value, the prediction horizon T_{ph} is the next up for tuning. T_{ph} is desired to be of a value such that the controller can respond to possible constraint violations and, in addition, remain stable. A suggestion for an initial guess of T_{ph} is given by equation 4.11. The closed-loop response time is lower bounded by the HPS plant model, which also affects the choice of T_{ph}. A large prediction horizon results in a higher computational cost. Therefore, a method to keep T_{ph} at an acceptable level is to adjust the prediction horizon until the changes in the open-loop response are small.

$$T_{ph} = \frac{T_d}{\Delta t} \tag{4.11}$$

The final time period to tune is the control horizon T_{ch}, which can take on values between Δt and T_{ph}. To reduce computational time, T_{ch} should be set to a value significantly lower than T_{ph}.

Objective Weight Tuning

Before the objective weight tuning, the priority is to scale the objective function. This is to improve the performance of the optimization algorithm concerning its convergence tolerance settings. The weights of a scaled objective function are also scaled [48], making them more intuitive to tune with respect to each other. The objectives are divided by individual scales ψ. Note that scaling does not work for invariant methods, such as, for example, the pure Newton's method [49]. Throughout the objective weight tuning, the scaling factors are kept constant.

Some CVs can have opposite objectives, meaning that all objectives cannot be fulfilled at the same time. In this case, a priority of the importance of the objectives has to be made. A scale from low to high priority is then used for the weighting (the priority scale is based on [43]).

The MVs used to target objectives are set to nonzero values. It is suggested to set the MV weights to lower values than the average of the rest of the weights to avoid problems with the CV tracking. Since the NMPC prediction is inaccurate, the robustness can be increased by prioritizing MVs. However, this can turn out in an inadequate performance of the tracking.

4.5.2 Parameter Tuning

The tuning of the time periods is executed in the same manner as described in the guideline. Fast system response is desired, and an approximate of the fastest closed-loop response T_d obtainable is used. Because of limited computational resources, the time step Δt is set to a slightly larger value than initially desired. However, using this time step gives an adequate response. The prediction horizon T_{ph} is set to a value where the HPS plant model reaches a steady-state given an impulse response. The control horizon T_{ch} is set to 60% of the prediction horizon, as adding a more extended control horizon barely impacts the system response. Additionally, a noticeable amount of computational power is saved due to the reduced control horizon. The resulting values of the time periods are found in table B.2.

Different objective scales are tested to find the set of scales yielding the fastest algorithm convergence. The final set of weights granting the best performance is found in table B.3.

The weights in the objective function are set as constants to avoid excessive complexity. This choice results in a manageable tuning situation (with respect to this thesis), as opposed to the tuning of time-varying weights. The objective weights resulting from the tuning session are found in table B.4.

Objective Priorities

The objective weights are tuned in a recursive process (in both closed-loop and open-loop) to obtain a satisfying result for the objectives. The overall goal is to follow the reference Q_{p_d}, using minimal amounts of fossil fuel, and at the same time charge the battery with the use of renewable power when possible (as formulated in the Lagrangian term from equation 4.9c).

First off, the reference tracking of the flow rate is weighted at a high value. This high value is chosen due to the importance of operating the pump at the desired level and thereby obtaining the wanted flow rate.

A decision to make is how the power is distributed to the pump. There are three options to provide the pump power. The first is to use the energy stored in the battery, the second is to use the GTG, and the last option is to utilize the WTG. The preferred method is to use wind power directly. This method, however, depends on the available wind. If the wind is absent, the solution is to use the battery energy, which originates from stored wind power. At last, if there is no power available from the two mentioned sources, the GTG is used to provide the pump power.

The WTG power objective is weighted high, always to produce power at maximum capacity. If the power produced is above the power desired from the pump, the battery gets charged. The GTG throttle objective gets a medium weight as the throttle is not wanted to be used unnecessarily. A too high weight on the GTG throttle results in a significant deviation in the flow rate tracking if the battery is empty and the WTG power is low. Therefore, the weighting on the GTG throttle objective is not set to a high value.

It is also essential to eliminate unnecessary rapid dynamics in the inputs to prevent oscillations propagating in the system. Careful tuning of these weights is important due to the potential trouble of too slow closed-loop dynamics using large weights. All these weights are therefore set as low values.

4.6 Software and Implementation

The continuous time OCP emerging from the control design is formulated in equations 4.12a-4.12d. The different terms belonging in the objective function $\mathbf{J}$, transition function $\mathbf{f}$, and inequality constraint vector $\mathbf{h}$ are directly referred to their equations in this chapter.

$$\min_{\mathbf{x},\mathbf{u}} \mathbf{J}(\mathbf{x},\mathbf{u}) = \min_{\mathbf{x},\mathbf{u}}\Big(\int_0^{T_{ph}} 4.9a \; dt + \int_0^{T_{ch}} 4.9b \; dt\Big) \tag{4.12a}$$

$$\text{s.t.} \quad \mathbf{f} = \begin{bmatrix} 4.4a & 4.4b & 4.4c & 4.4d & 4.4f & 4.4e & 4.4g & 4.6a & 4.6b & 4.6c \end{bmatrix}^\top \tag{4.12b}$$

$$\mathbf{h} = \begin{bmatrix} 4.7a & 4.7b & 4.7c & 4.7d & 4.7e & 4.4e & 4.7f & 4.7g & 4.7h & 4.8a & 4.8b & 4.8c \end{bmatrix}^\top \leq \mathbf{0} \tag{4.12c}$$

$$\mathbf{x}(0) = \mathbf{x}_0 \tag{4.12d}$$

To implement the NMPC on a digital computer, the numerical methods as chosen in chapter 3 are further used. The optimization algorithm is implemented using CasADi, which is an "open-source tool for nonlinear optimization and algorithmic differentiation" [50]. CasADi is compatible with both Python and MATLAB. For this thesis, the resulting NMPC is implemented with CasADI in MATLAB/Simulink as the HPS plant model is implemented in the same software.

To formulate and solve the OCP defined using CasADI, direct multiple shooting, using RK4 is utilized together with the chosen nonlinear primal-dual optimizer (IPOPT). This optimizer requires a linear solver as a subroutine, and a solver called multifrontal massively parallel sparse direct solver (MUMPS) is chosen [51]. This solver is proven to perform well on sparse problems and is the preferred solver in this thesis. Figure 4.4 sums up the the chosen numerical methods for the NMPC design.

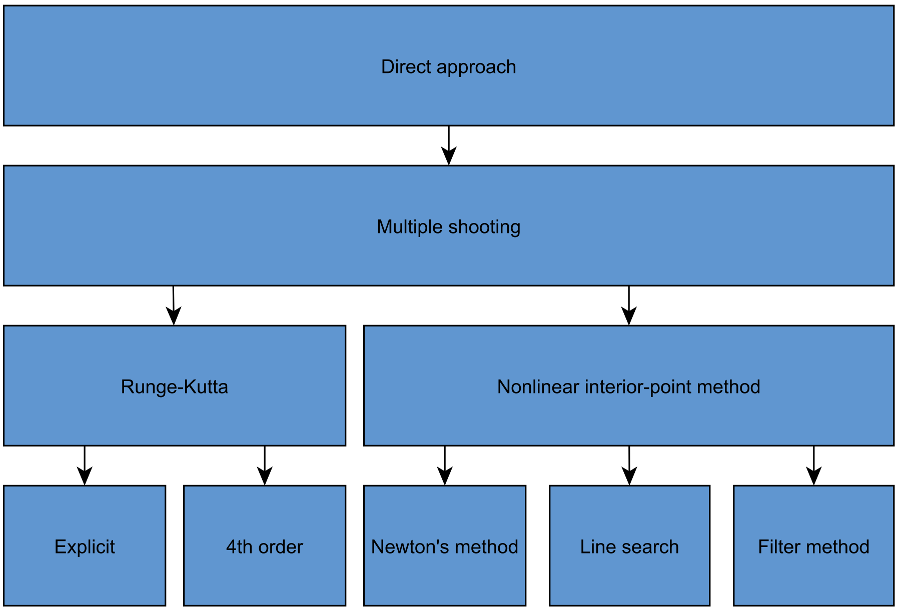

Figure 4.4: Numerical methods for the NMPC design

5 Simulations, Results, and Analysis

The NMPC is validated using the model from chapter 2 as a plant model. The NMPC and plant model are connected with a feedback connection as shown in figure 5.1. The aspects of interest in this thesis are to observe what happens with the controlled HPS plant model for different wind conditions, references, and inaccurate measurements. Firstly, in section 5.1 the setup of the simulations is described together with the values used in different simulation cases. Section 5.2 introduces scenarios with constant reference tracking where the wind speed is constant. In section 5.3 the wind and reference are time-varying. Lastly, section 5.4 investigates the robustness of the NMPC for noisy output feedback measurements.

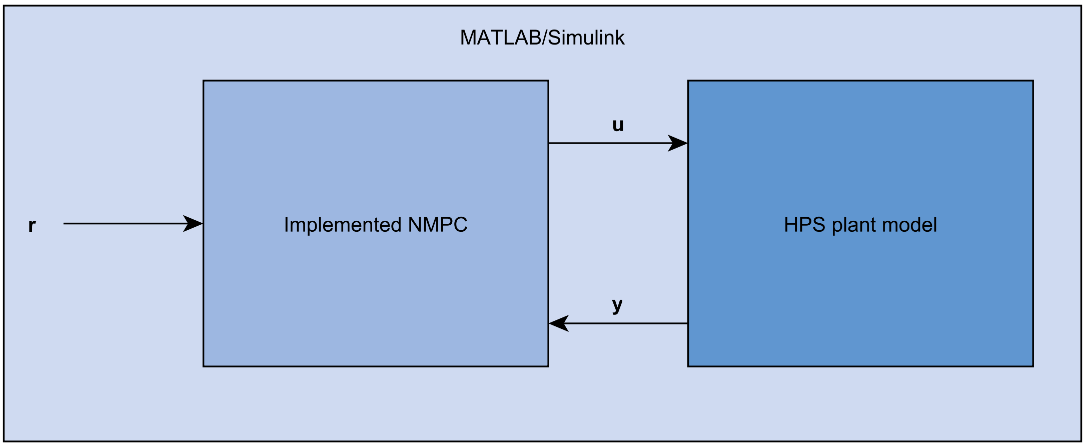

Figure 5.1: Feedback connection between the implemented NMPC and HPS plant model

5.1 Simulation Setup and Conditions

In this section, information about the simulation procedure, results, and analysis is found. Subsection 5.1.1 describes the software and hardware used for the simulations. In subsection 5.1.2 the focus of the analysis and the test cases are described. Further, the choices of simulation times are mentioned in subsection 5.1.3. The initial conditions used for the simulations are found in subsection 5.1.4. In the last subsection 5.1.5, the environmental conditions and reference values for the simulations are provided.

5.1.1 Hardware and Software

The digital computer used for simulations is a Microsoft Surface Book 2 with an integrated processor of the type: INTEL CORE i7-8650U and a graphics card of the type: NVIDIA GeForce GTX 1050. The software framework for the simulations is Simulink and MATLAB, where both the plant model and NMPC are implemented.

5.1.2 Analytic Focus and Test Cases

To keep the analysis narrow enough to go in depth, but broad enough to capture crucial overall system behaviors, some choices for the analysis are made beforehand. The HPS plant model and NMPC contains far too many variables to all be analyzed. The most important focus is on the objective variables and power flow in the plant model. Therefore these variables are chosen to be the main subjects for analysis. Additionally, the MVs are included in some of the analyses as they directly affect the system behavior. All the presented results are extracted directly from the output of the controlled HPS plant model in Simulink.

The test cases focus on testing the NMPC for distribution of power during a specter of wind, measurement, and reference conditions. Each of the individual test cases explicitly mentions the wind condition used. For all the simulations, the parameter $\mathbf{p}$ containing the wind speed v_w, is kept constant at the current wind speed value throughout the predictions. This implies that the wind model consists of a series of constant values equal to the present wind speed measurement.

The first case study in section 5.2 investigates the NMPC for constant wind speeds and a constant reference. This case study is executed in order to rule out system dynamics and analyze the steady-state power distribution. The wind speed is increased in four stages, where each stage of wind speed represents an individual case. All the feedback measurements are assumed to be perfect for these cases.

The following case study in section 5.3 explores varying winds and references. The goal of this study is to observe how well the NMPC handles uncertainties in the wind prediction and how it responds to a varying power demand. All of the feedback measurements are assumed to be perfect in this case study as well.

In reality, the measurements used for feedback are not perfect due to interaction with electrical equipment and other noise sources. Two cases of feedback measurement noise are tested in section 5.4 to investigate the robustness of the NMPC. The cases test two common noise forms, namely a random fluctuating noise (dynamic noise) and a constant biased noise (static noise) [52]. The wind speed is kept constant to isolate the effects of the noise.

Some extra simulations are performed to prove a number of statements in the different case studies. The values used for these extra simulations are found in table C.1.

5.1.3 Simulation Times

To obtain a sufficient resolution of the plant model output, the time step for the simulation is set to be 0.05 seconds. This choice of time step ensures a stable simulation of the plant model. The NMPC runs at a different time step Δt. A rate transition is applied to the feedback measurements to deal with the time step differences. In addition, the inputs are kept constant by the use of a zero-order hold (ZOH).

The simulation times are chosen according to the approximately slowest time for reaching the objectives. The resulting simulation times are 60 and 90 seconds. Longer simulation times are inefficient as the simulation of the NMPC is computationally expensive, and a steady-state is reached within the set simulation times (some of the cases do not reach a steady-state, but they obtain cyclic patterns).

5.1.4 Initial Conditions

The HPS plant model is initialized with some initial conditions for the states. These initial conditions are chosen so that they satisfy both the HPS plant model's and NMPC's constraints.

The initial flow rate for the pump Q_{p0} is set to be larger than its minimum constraint value to satisfy the other pump constraints. The initial value of the WTG rotational speed ω_{wtur_0} is also set to a significantly larger value than its minimum as the plant model is unstable for rotational speeds approaching the minimum constraint value. This choice of initial turbine rotational speed directly determines the initial WTG generator torque M_{wgen_0} as they are coupled.

The battery starts with an initial energy E_{b_0}. This initial condition is the only initial condition that changes in the different case studies. The reason for this is to show different attributes in the simulations. The initial condition used ($E_{b_{0_1}}$ or $E_{b_{0_2}}$) is mentioned in each section for the cases studies. The rest of the states are initialized from their minimum values. Table 5.1 shows the initial values of the states used for simulations.

Initial condition	Value	Unit	Symbol
Pump integration state	0	m s	I_{p0}
Pump rotational speed	0	rpm	ω_{p0}
Pump flow rate	650	$\mathrm{m^3\,s^{-1}}$	Q_{p0}
GTG fuel flow	0	pu	V_{g0}
GTG lossless power	0	kW	P_{gl_0}
GTG throttle	0	pu	γ_{g0}
WTG turbine rotational speed	1	$\mathrm{rad\,s^{-1}}$	ω_{wtur_0}
WTG generator torque	22850	N m	M_{ggen_0}
WTG turbine pitch	0	deg	β_{w0}
Battery energy 1	5	kW h	$E_{b_{0_1}}$
Battery energy 2	12	kW h	$E_{b_{0_2}}$

Table 5.1: Initial conditions for simulation cases

5.1.5 Environmental Conditions and Reference Values

For the simulation cases, some environmental conditions are chosen. These conditions are the desired pump head, wind speed, and measurement noise. The desired head of the pump uses a numerical value taken from [17]. Further, the selection of wind conditions and measurement noise are described in this subsection. The references for tracking are also determined here. All the numerical values for the variables mentioned in this subsection are found in table 5.2.

Geographical data is used to model the wind conditions. The winds are chosen from looking at typical wind data [53] in the northern sea. The stationary wind conditions used in section 5.2 (from Beauforts scale [54]) are a gentle breeze $v_{w_{gb}}$, fresh breeze $v_{w_{fb}}$, strong breeze $v_{w_{sb}}$, and gale $v_{w_{ga}}$. As the wind speed approaches storm, a standard procedure is to shut down the turbine to reduce physical stress, and potential damages on the WTG [55]. Stronger winds are therefore not investigated further in this thesis.

The varying wind $v_{w_{va}}$ used in section 5.3, is modeled as a sine function varying between a moderate breeze and a strong breeze. The variation is modeled to be fast enough to have a significant impact in the NMPC's prediction, such that the effects of an inaccurate wind prediction can be analyzed.

Concerning the reference values for the case studies, the only available change in reference value is for the desired flow rate. The flow rate is modeled as stationary ($Q_{p_{d_{st}}}$) or varying as a sine function ($Q_{p_{d_{va}}}$). The different sections mention which reference is used for the specific cases.

The measurement noise is given as a proportion of the latest measurement values $\mathbf{y}$. In this way, the proportion of noise is the same for all measurements. The dynamic noise vector $\mathbf{v}_{dy}$ is modeled with a uniformly distributed unit white noise $\mathbf{w}$, and the static noise vector $\mathbf{v}_{st}$ is modeled as a bias (this noise is static in steady-state). These measurement noises are only used in section 5.4.

Simulation variable	Value	Unit	Symbol
Desired pump head	1065	m	H_{p_d}
Desired stationary flow rate	800	$\mathrm{m^3\,s^{-1}}$	$Q_{p_{d_{st}}}$
Desired varying flow rate	$800 + 30\sin(0.1\pi t)$	$\mathrm{m^3\,s^{-1}}$	$Q_{p_{d_{va}}}$
Gentle breeze	4	$\mathrm{m\,s^{-1}}$	$v_{w_{gb}}$
Fresh breeze	9	$\mathrm{m\,s^{-1}}$	$v_{w_{fb}}$
Strong breeze	12	$\mathrm{m\,s^{-1}}$	$v_{w_{sb}}$
Gale	18	$\mathrm{m\,s^{-1}}$	$v_{w_{ga}}$
Varying wind	$9 + 2\sin(0.2\pi t)$	$\mathrm{m\,s^{-1}}$	$v_{w_{va}}$
Dynamic measurement noise vector	$0.01\mathbf{wy}$		$\mathbf{v}_{dy}$
Static measurement noise vector	$0.01\mathbf{y}$		$\mathbf{v}_{st}$

Table 5.2: Environmental conditions and reference values for simulation cases

5.2 Stationary Wind and Pump Flow Rate Reference

In this section, the NMPC is tested for different stationary wind speeds. Starting out with a gentle breeze (subsection 5.2.1), moving on to a fresh breeze (subsection 5.2.2), then a strong breeze (subsection 5.2.3), and lastly a gale (subsection 5.2.4). In this section the initial battery energy $E_{b_{0_1}}$ together with the constant flow rate reference $Q_{p_{d_{st}}}$ are used for all cases.

5.2.1 Gentle Breeze

For this simulation, the wind $v_{w_{ge}}$ is used and the results are shown in figure 5.2. The gentle breeze results in a low WTG power output due to the low potential energy in the gentle breeze. As the battery gets drawn for energy, the GTG gradually speeds up to produce the necessary power to supply the pump. The objective function formulation and objective weightings allow the battery and WTG to be the main suppliers of the pump power when there is enough battery charge or wind. In this case, the battery ends up empty, and the GTG handles most of the power production due to the lack of wind.

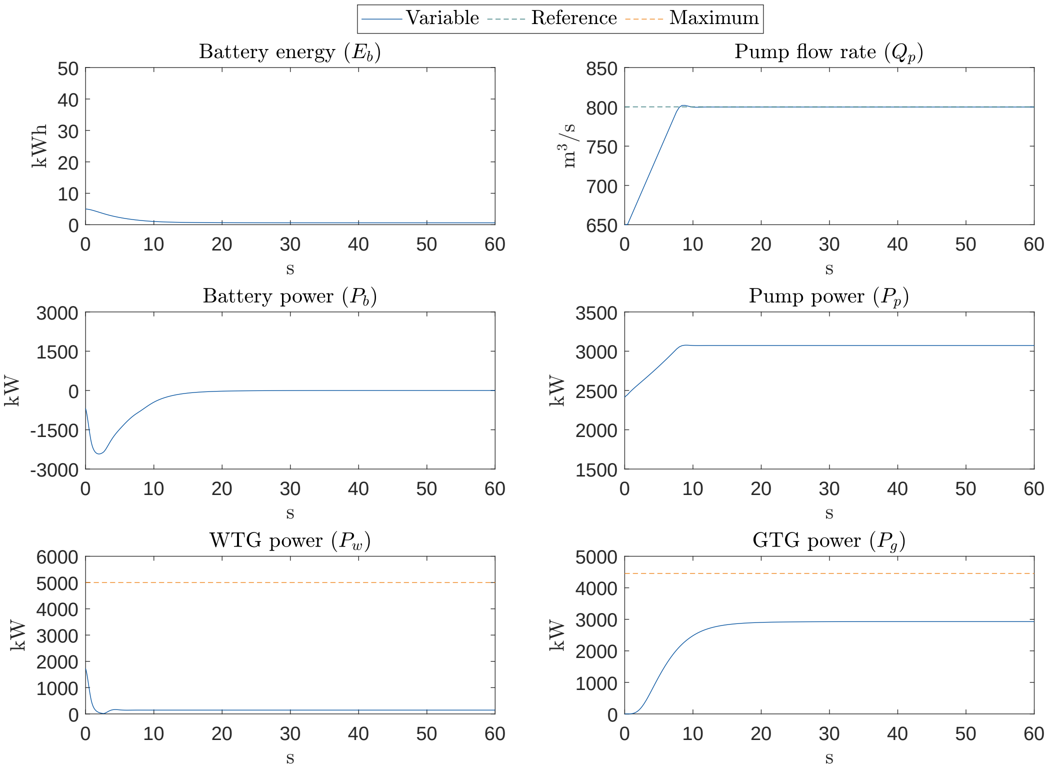

Figure 5.2: Measured battery energy, pump flow rate, and powers during a gentle breeze

Figure 5.2 shows that the flow rate converges to its reference. The barely noticeable difference in the desired and actual value of the pump flow rate is due to the proposed tuning. Controlling the flow rate to the reference is deemed the most important objective. Another objective that is also important is to minimize the GTG throttle. The proposed NMPC manages to reach a good trade-off between these two conflicting objectives.

A heavier weighting of the GTG throttle yields a larger steady-state offset in the flow rate tracking in addition to reduce the GTG power production. The minimization of the GTG throttle becomes more important with a heavier weighting, and thus the flow rate reference tracking becomes less prioritized. Modeling imperfections in the prediction model with respect to the plant model also impacts the steady-state reference tracking, but in this simulation case, the main offset comes from the objective weighting. To support these statements, figure C.1 presents an identical test case except for a significantly increased weighting on the GTG throttle.

5.2.2 Fresh Breeze

This subsection investigates the scenario where the wind speed corresponds to a fresh breeze, which is represented by $v_{w_{fb}}$. Figure 5.3 shows the plots resulting from the simulation. As expected, the power output from the WTG is drastically increased with the higher wind. This increase in power production results in less necessity for using the GTG to distribute power to the pump. The GTG provides power to the pump at a later time than in the previous case (in section 5.2.1) due to the WTG and battery managing the pump power distribution for an extended period.

An interesting observation from figure 5.3 is the small and long periodical oscillations in the GTG power. The prediction model imperfections are summed up in the battery prediction model, and when the battery energy approaches its lower constraint, the GTG quickly produces power to prevent a constraint violation. This phenomenon results in excessive power delivery to the battery. The battery energy together with the GTG power slowly drops, and the same incident occurs over again. The model imperfections are partly dependent on the wind speed as the WTG power prediction is used to predict the battery energy. The mentioned phenomenon is not present in the other simulation cases as the battery energy manages to stay further from its lower constraint (resulting from changes in the prediction and battery charging with different winds).

The reference tracking of the pump flow rate performs great in this simulation case as well. The steady-state deviation is lower compared to the last case (in section 5.2.1) due to a decreased use of the GTG. However, the oscillations in the GTG power affect the flow rate to an insignificant degree (noticeable by observing raw measurement data).

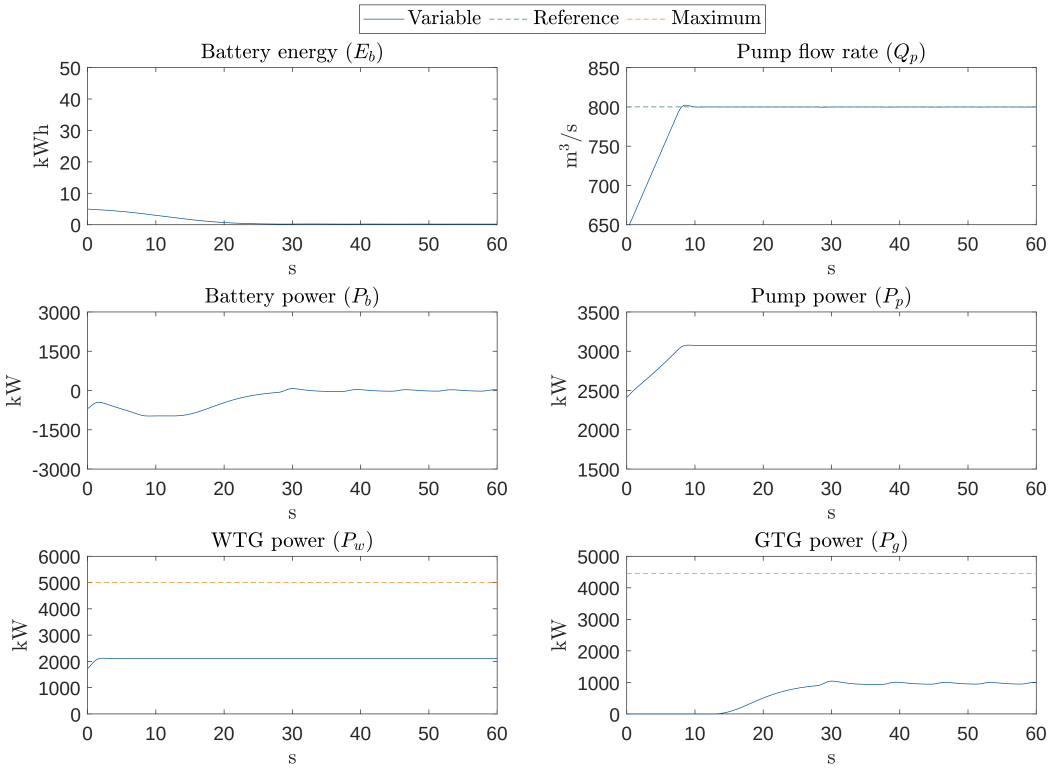

Figure 5.3: Measured battery energy, pump flow rate, and powers during a fresh breeze

5.2.3 Strong Breeze

This subsection investigates a case of a strong breeze, where the wind $v_{w_{sb}}$ is used. The results for this case can be seen in figure 5.4 which shows how the WTG uses its full potential power output while the GTG is barely used. The WTG single-handedly supplies the pump and charges the battery with excessive power.

The reference tracking of the flow rate is almost perfect as the GTG throttle obtains its minimum value. The need for a compromise between the GTG power production and flow rate is thus removed due to a sufficient amount of wind.

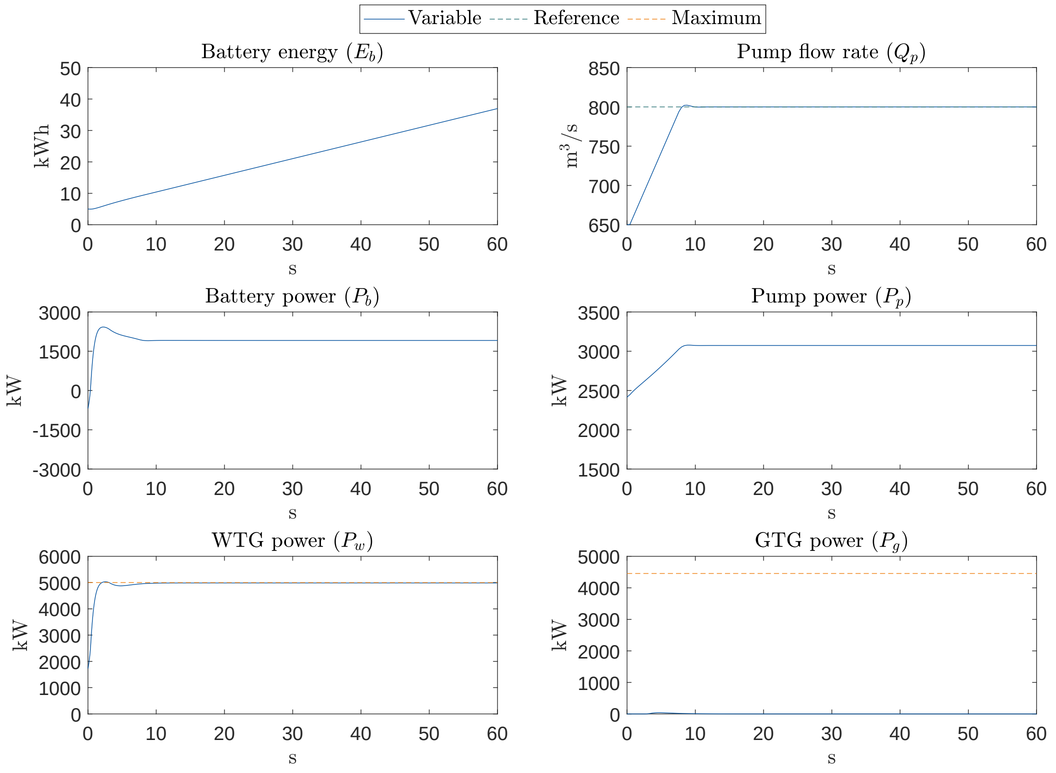

Figure 5.4: Measured battery energy, pump flow rate, and powers during a strong breeze

5.2.4 Gale

This subsection looks at a case where the wind is a gale $v_{w_{ga}}$. The results from this scenario can be found in figure 5.5 which shows that the WTG power quickly escalates to over the double amount of its maximum power constraint. After the large power peak, the WTG power oscillates around its maximum power constraint. The oscillatory behavior is due to two factors specifically. The first large peak of the WTG power comes from the fact that the pitch rate β_w is constrained, and the turbine blades cannot pitch fast enough to get a resulting lower power production (see figure 5.6). Figure C.2 shows a simulation where the initial pitch value is set to an increased value. It is found that the first large power peak is reduced drastically.

The smaller oscillations around the maximum WTG power are a result of significant differences in the prediction and plant model evolutions during high wind speeds (rapid dynamics). The difference decreases as the turbine speed approaches a steady-state (a steady-state is not reached in the case for this subsection). The prediction model (from chapter 4) uses the approximated function $D_{w_{tur}}$, which is continuous and evolves with the NMPC's time step. On the other hand, the plant model (from chapter 2) uses the lookup table $C_{w_{tur}}$ which is discontinuous (based on interpolation in the simulation) and evolves with the simulation time step. As a final result, the NMPC's predicted dynamics is too slow to comprehend the HPS plant model's dynamics during higher winds. Figure C.3 illustrates the difference in turbine speed for the two models during a gale with no change in the pitch.

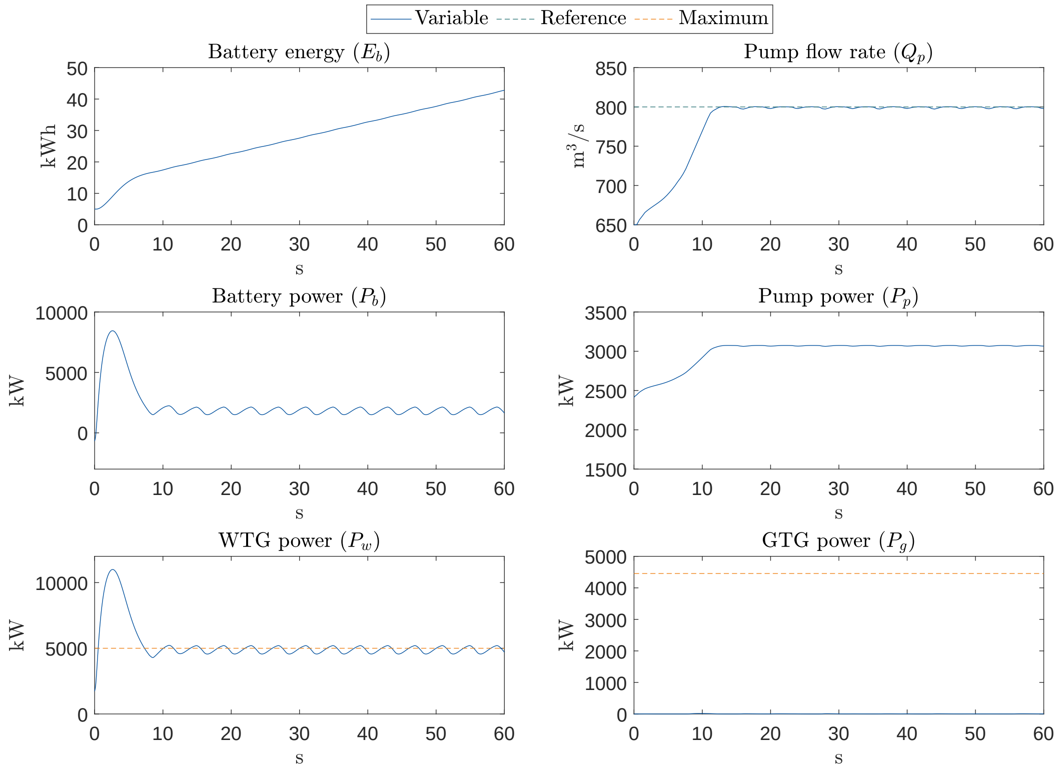

Figure 5.5: Measured battery energy, pump flow rate, and powers during a gale

A possible solution to remove the oscillations is to physically limit the power output of the WTG (for example, with the use of a braking system). Figure C.4 shows how the oscillations can be removed by using a saturation element in the plant model along with a larger initial pitch value.

Further analyzing figure 5.5, it can be observed that the oscillations are spreading throughout the different power components (except for the GTG due to the minimization of the throttle). This spreading comes from the common connection of the power components to the battery in the prediction model. The roots of the oscillations in the HPS plant model are the inputs that are governed by the inaccurate prediction (as seen in figure 5.6).

By ignoring the oscillations, at this wind speed, the steady-state reference tracking is quit accurate. The time for the flow rate to reach a steady-state is, however, a bit longer in this case as the power distribution in the system is disturbed by the WTG's behavior.

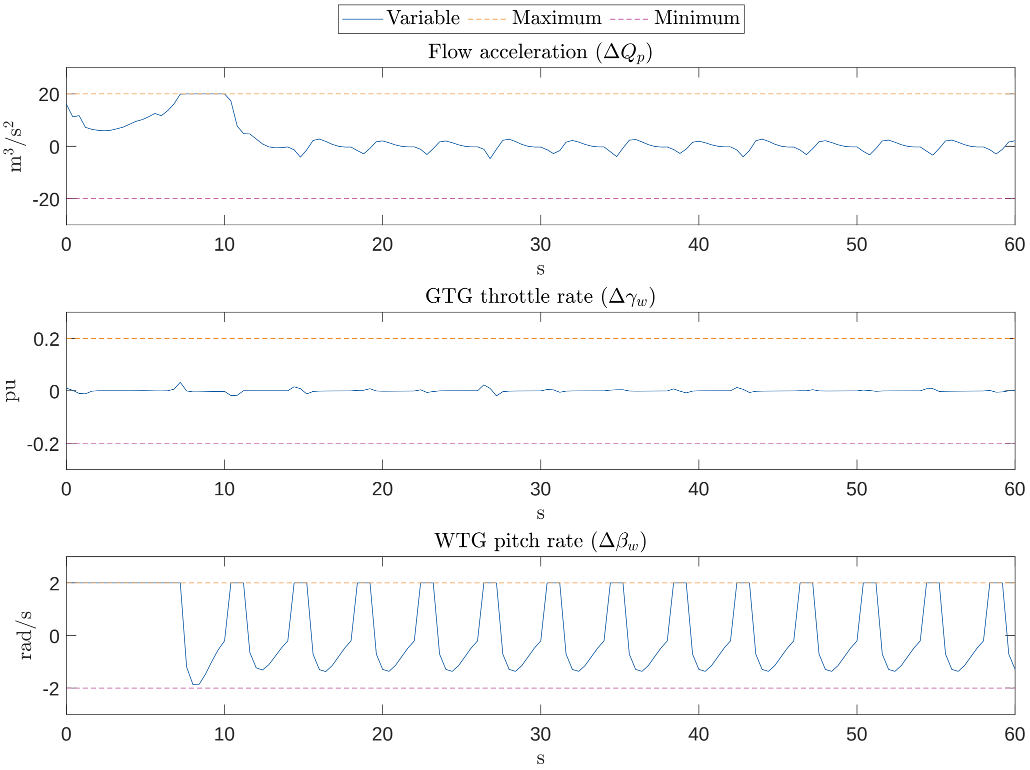

Figure 5.6: Inputs during a gale

5.3 Varying Wind and Pump Flow Rate Reference

This section investigates three scenarios that differ based on the wind speed and the reference. First, in subsection 5.3.1 a constant flow rate reference with a varying wind is used. Then a varying flow rate reference with a constant wind is tested in subsection 5.3.2. In the third case, in subsection 5.3.3, both the wind and flow rate reference vary to observe the total effects. For all the cases, the initial battery energy E_{b0_2} is used.

5.3.1 Varying Wind Speed and Constant Flow Rate Reference

For this simulation case, the varying wind v_{wva} is used together with the constant flow rate reference $Q_{p_{dst}}$. The results from the simulation of this case are shown in figure 5.7. Observing the WTG's power peaks and bottoms, the power delivery is about the expected values for the chosen wind, which means that the NMPC performs adequately despite its inaccurate wind prediction. As long as there is energy in the battery, the GTG remains at rest. A less wanted scenario occurs when the battery is approaching an empty state. The GTG power gradually begins to oscillate to compensate for the missing pump power. The overall power delivery is still quite good as the pump flow rate follows its reference accurately with only some insignificant oscillations (observed from measurement data).

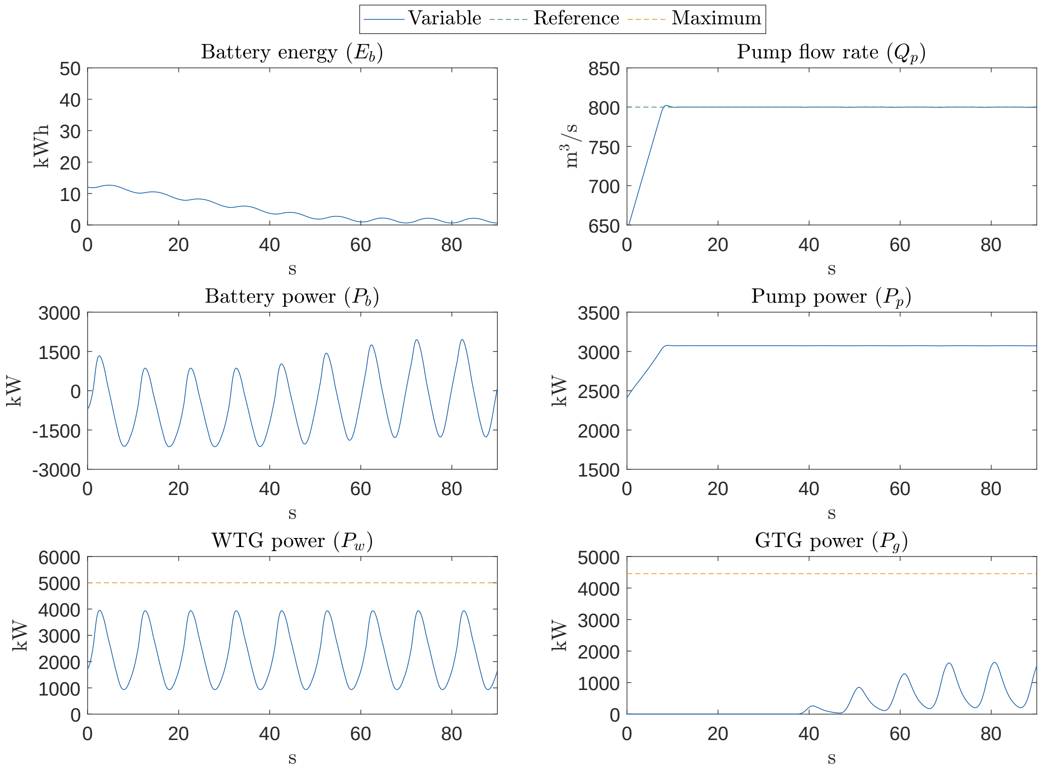

Figure 5.7: Measured battery energy, pump flow rate, and powers during a varying wind and constant flow rate reference

5.3.2 Constant Wind Speed and Varying Flow Rate Reference

The case in this subsection uses a fresh breeze $v_{w_{fb}}$ with the varying flow rate reference $Q_{p_{d_{va}}}$. Figure 5.8 shows that the NMPC manages to track the flow rate sufficiently after an initial converging phase. It is observed that the flow rate almost perfectly obtains the same oscillations as the reference after the convergence. Additionally, it is observed that the periodic flow rate reference tracking directly propagates to the pump power due to the flow rate's and pump power's sublinear relation.

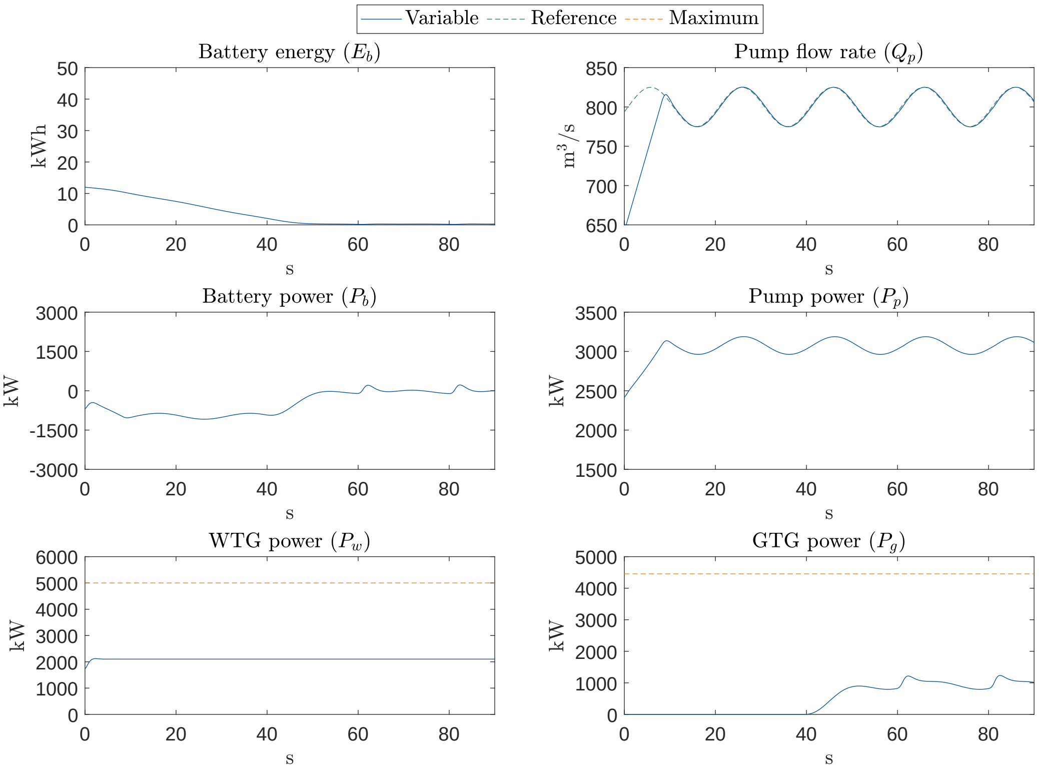

Figure 5.8: Measured battery energy, pump flow rate, and powers during a constant wind and varying flow rate reference

In this subsection, the effects of the model imperfections as described in the case in subsection 5.2.2 are amplified. As the power demand increases (and the battery approaches an empty state), the GTG is used to ensure enough power delivery to the pump. Since the power required by the pump is periodically varying, the power produced by the GTG is also periodical as the WTG is producing a constant power when the wind is constant. This periodical power demand, together with the model imperfections, creates the pattern as shown in the GTG power in figure 5.8.

5.3.3 Varying Wind Speed and Flow Rate Reference

This case investigates the scenario with a varying wind $v_{w_{va}}$ and flow rate reference $Q_{p_{d_{va}}}$. Figure 5.9 shows the results obtained from the simulation. The reference tracking of the flow rate is nearly identical to the previous case in subsection 5.3.2. This reference tracking performance implies that the NMPC manages to distribute the power adequately in the plant model.

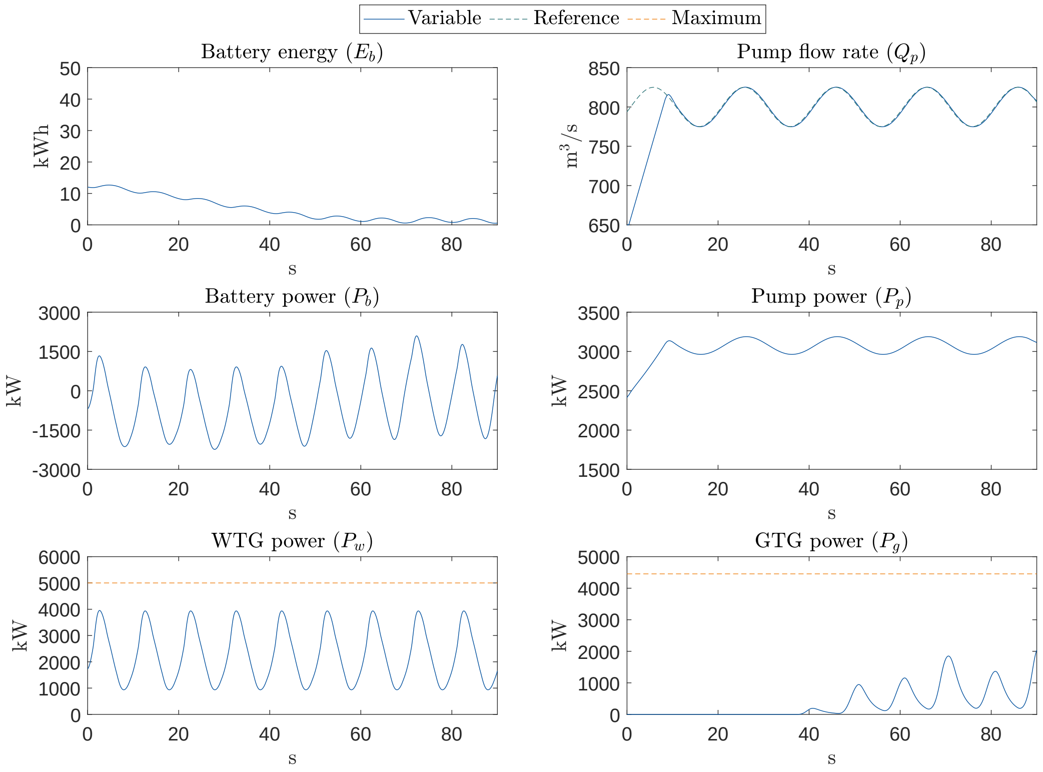

Figure 5.9: Measured battery energy, pump flow rate, and powers during a varying wind and flow rate reference

The GTG accounts for the varying wind and reference in this simulation. The flow rate reference and wind are not of the same frequency, and the GTG is therefore observed to be producing power in an asymmetrical pattern as shown in figure 5.9. A proportion of this pattern might also originate from model imperfections.

5.4 Feedback Measurement Noise Robustness

This section investigates the robustness properties of the proposed NMPC with respect to feedback measurement noise. Subsection 5.4.1 provides results for a dynamic noise (uniform white noise), and subsection 5.4.2 gives the results from using a static noise. The wind speed $v_{w_{fb}}$ is used in both cases, and the results are compared to the ones in subsection 5.2.2, where the wind is the same, but the measurements are noise-free. The initial battery energy $E_{b_{0_1}}$ is used in this section.

5.4.1 Dynamic Measurement Noise

The noise $\mathbf{v}_{dy}$ is used for this simulation, and the results are shown in figure 5.10. The pump flow rate uses the inaccurate measurement, resulting in an attempt to adjust to its predicted trajectory quickly. However, the noise is too quick, and the rapid change in the pump flow rate is not heavily punished. The pump flow rate response time is roughly the same as for the noise-free case, but the MSE for this case is about 5.1 % larger than for the noise-free case. The rapid change in flow rate is also directly reflected in the pump power. However, the power producing components (WTG and GTG) manages to distribute power without any noticeable side effects, despite the noisy measurements.

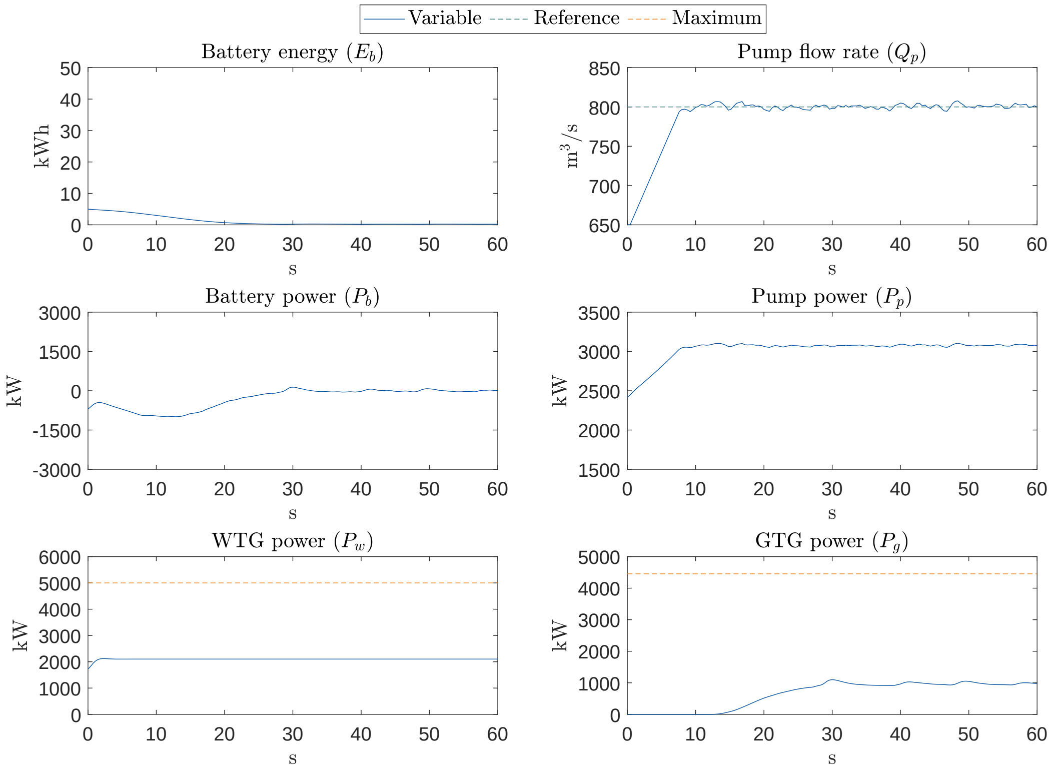

Figure 5.10: Measured battery energy, pump flow rate, and powers during a fresh breeze with dynamic noise in the feedback measurements

A practical method to smoothen out the oscillations due to the noisy measurements is to increase the weighting on the flow acceleration. Figure C.5 shows an identical simulation case, except for an increased flow acceleration weighting. As expected, the closed-loop response becomes noticeably slower with a high cost of changes in the flow rate, but the oscillations almost vanish.

5.4.2 Static Measurement Noise

This subsection investigates the case where the measurement noise is represented by the static noise $\mathbf{v}_{st}$. Figure 5.11 shows that the reference tracking for the pump flow rate is negatively shifted and obtains a larger steady-state error. The reason behind the steady-state error comes from the bias in the measured states. The actual states are lower than the NMPC interprets, resulting in a shift down. Apart from the bias, the power is being distributed well among the different components.

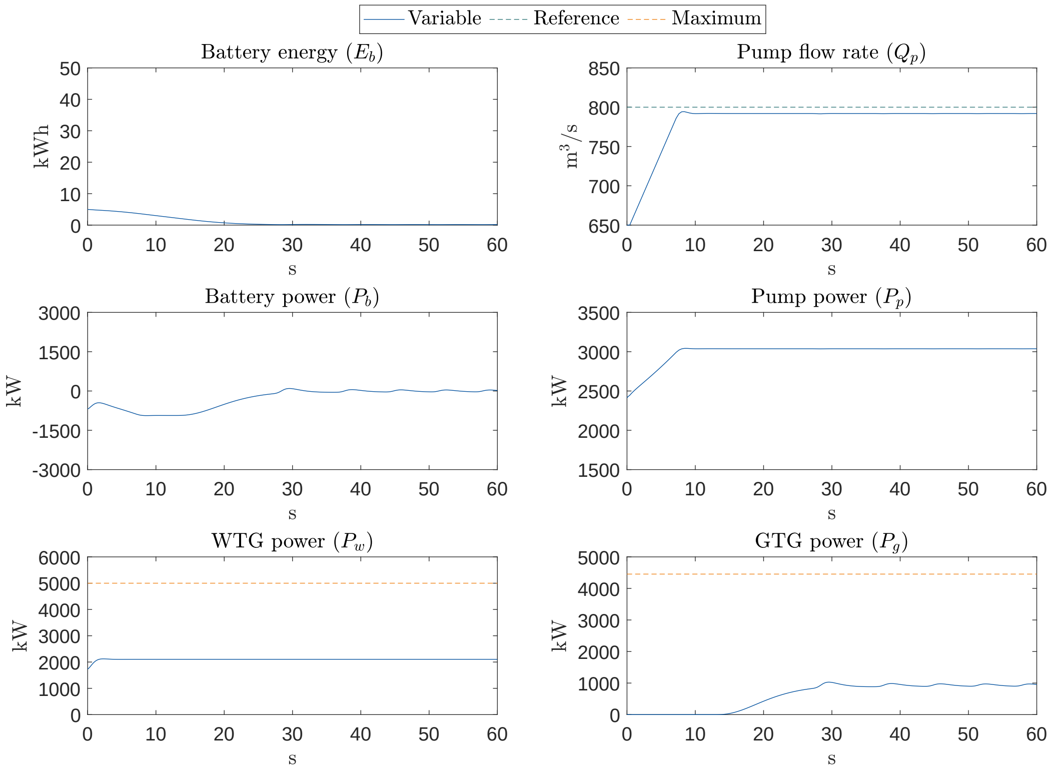

Figure 5.11: Measured battery energy, pump flow rate, and powers during a fresh breeze with static noise in the feedback measurements

If the NMPC interprets the states as lower values than the actual state values, which happens with a negative shifted static noise, the flow rate shift becomes positive. Figure C.6 shows the positive shift in the flow rate when using a negative static noise.

6 Discussion

There are in particular three subjects that need to be further discussed. The first subject in section 6.1 concerns itself with how well the NMPC performs based on the results from the case studies. The second subject of importance is the aspects of the NMPC design with respect to its complexity and model assumptions, which is discussed in section 6.2. Lastly, in section 6.3, requirements for computational power for implementing the NMPC are discussed.

6.1 Nonlinear Model Predictive Controller Performance

An important topic for discussion is the performance of the NMPC in the case studies. A good performance measure is to use the goals set for the NMPC. The goals for the NMPC are, as previously stated, to utilize the potential wind energy, distribute power to satisfy objectives, and handle disturbances. The NMPC performance in this thesis is evaluated from the control of a plant model and not an actual plant. The performance is therefore interpreted as optimistic. Subsection 6.1.1 discuss how well the power is distributed concerning wind energy utilization and reference tracking. In subsection 6.1.2 the NMPC robustness with respect to external disturbances (noise in the feedback measurements) is discussed.

6.1.1 Power Distribution and Reference Tracking

In all of the simulation cases, the WTG delivers sufficient amounts of renewable wind power with respect to its potential (compared to an adjusted approximation of the maximum WTG power output from [17]). The GTG is only used at instances where there is an insufficient amount of power from the WTG or battery. The battery is almost exclusively charged by the WTG, yielding a nearly emission-free use of the battery for pump power supply. The stated results imply that the goal of utilizing the available wind energy can be considered met satisfactorily.

As the wind is varying, the predictions from the NMPC becomes more inaccurate, resulting in reduced utilization of the wind energy. The reason for this is the wind model used in the NMPC, which is based on an assumption of a constant wind. In reality, the wind is varying in a complex manner, and the constant wind prediction model used in the NMPC might not be sufficient. An alternative approach to increase the wind model accuracy is to predict the variations in the wind by using a stochastic model predictive control (SMPC). This control method is further described in subsection 7.2.1.

The power is in most cases distributed across the power components without sizable rapid changes. However, a significant problem with severe constraint violations occurs as the WTG is exposed to larger winds, and the initial pitch value is at its minimum. A part of the problem can be solved by starting the WTG with a lower initial pitch value, which in reality, is feasible. The smaller oscillations are, on the other hand, a bit of a challenge. These oscillations can be removed with the use of a physical saturation in the HPS. This approach, however, is doubtfully a feasible way of handling the problem in reality. Instead, the problem should be fixed in the NMPC. A way of handling the oscillation might be to use a disturbance estimator in the control scheme. The use of a disturbance estimator is further described in subsection 7.2.2.

If the pump power requirement is larger than the power from the battery and WTG, the GTG power begins to oscillate in some of the cases. These oscillations come from the working of the NMPC. That is, either from the prediction model imperfections or the objective function design. The modeling imperfections can also be reduced with the use of a disturbance estimator. The oscillations resulting from the objective function need another approach to be reduced. The NMPC has a short prediction horizon concerning energy storage and usage. An alternative way of controlling the GTG is to use it at optimal efficiency for some periods and turn it off for other periods (charging the battery and use the battery power for the power peaks). A larger prediction horizon is then needed in order to predict the battery charging. This solution also requires a reformulation of the OCP, which is further proposed in subsection 7.2.3. By using this approach, the oscillations in GTG power can be reduced, yielding less wear and tear on the GTG components, in addition to a reduction in working on poor efficiencies. However, the GTG oscillations are not a significant issue if they do not occur often, and they are not a problem at all when wind power is available (stored in the battery or delivered directly from the WTG).

In all of the cases, the pump flow rate follows the reference reasonably well. The modeling imperfections for the pump model only originate from the difference in prediction and plant model simulation methods and are therefore barely noticeable. As the power distribution to the pump works well, it follows that the reference tracking also is quite accurate. However, when the power distribution to the pump is insufficient, it is reflected directly in the flow rate as there is not enough available power to maintain the desired flow rate. A higher power production from the GTG results in a larger deviation in the flow rate reference tracking. This effect is, however, insignificant as it has a small impact on the overall reference tracking performance.

An attribute to consider implementing for the controlled HPS is for it to hold backup energy stored in the battery for emergencies. A potential method for adding this attribute is to lower constraint the battery energy to a desired backup energy value (add a hard constraint) in the NMPC. This constraint can then be removed if there is use for the extra energy. The NMPC response with adding backup energy do not change compared to the response in this thesis, as the only difference is a shift in lower battery energy. Another way of adding this attribute is to add a soft constraint by including a battery energy term in the objective function. A high weighting of this term makes it hard to use excessive energy and charge the battery to a energy over the reference value. On the other hand, a low weighting makes it hard to hold on a minimum desired energy. Therefore, this energy term requires a variable weighting (gain scheduling) to allow flexibility.

6.1.2 External Disturbances

In some of the simulations, the feedback measurements to the NMPC from the HPS plant model are affected by noise. A subject to discuss is how realistic this noise is and how the noise affects the controlled HPS. In reality, the feedback measurement noise depends on the source of the noise and the method of measurement transferring. In this thesis, the noise is modeled as a proportion of the measurement values. This behavior is great for testing due to the same magnitude of disturbances in each feedback signal, but it does not likely appear in reality. If the noises in the measurements originate from a common source, all the measurements are roughly affected with the same magnitude of noise. A way of dealing with this is to scale the feedback measurement signals before sending them to reduce the noise impact. Other techniques also exist for the reduction of noise in cables, dependent on the cause of the noise [52]. If the noise cannot be directly removed, a disturbance estimator can also be used to obtain more accurate measurements. Using techniques to reduce the noise reduces the requirement for the NMPC to handle noisy feedback measurements.

By observing the HPS plant model's response to feedback measurements affected by dynamic noise, it is clear to see that the most affected variable is the pump flow rate. The reason for this significant affection is the flow rate's quick dynamic, as the pump flow rate is modeled as an integration of the flow acceleration input. Furthermore, the flow acceleration constraints are set relatively large, and a rapid dynamic is not heavily punished (relatively low weighting on the objective term). As the flow acceleration is higher weighted, the effect of the dynamic noise is mostly removed in exchange for a slower dynamic flow rate response. The powers produced/consumed by the components have a slower dynamic and are therefore harder to change quickly, yielding more robustness for dynamic noise.

The mean of the dynamic noise is zero, and the pump power is approximately linear for small changes in flow rate. This means that the net value of the change in pump power is approximately zero. The battery energy is the integrated sum of powers in the system; the battery, therefore, smoothens out the noisy pump power. This effect of an approximately unchanged net supply to the pump and the smoothing of pump power stops the small rapid pump power oscillations from spreading in the HPS. The final result is that the NMPC handles the overall power distribution well but suffers from deviations in the flow rate reference tracking for dynamic noises.

In the case of static noise, the flow rate is shifted while otherwise remaining the same as for the case with no noise. The result of this is a shift in power distribution, where the GTG produces less or more power dependent on the sign of the static noise while the WTG still produces the same amount of power. The reason for the change in GTG power is that less power is needed for the pump at a lower flow rate, and more power is needed for a higher flow rate. The overall response to static noise is a solid power distribution but a significant deviation in flow rate reference tracking. However, a heavier weighting on the flow acceleration input reduces the flow rate reference tracking deviation and yields sufficient reference tracking.

6.2 Control Design Complexity and Model Assumptions

In the NMPC's prediction model, a number of simplifications and assumptions are made with respect to a real HPS. The MPC's performance is dependent on the accuracy of the prediction model, and the most significant model assumptions are therefore discussed in this section. The purpose of this thesis is not to make a NMPC to be directly applied to a real HPS, but rather to investigate the potential of MPC in offshore HPSs. The main focus of this discussion, however, is how the control design should be concerned with the assumptions for the NMPC in a potential realistic implementation.

All of the electrical dynamics are removed from the components in the HPS model. With these simplifications, the NMPC is designed regardless of the behavior of the electrical dynamics in the HPS. This simplification is not significant if the electrical properties in the HPS can be controlled decoupled from the power distribution. A way of integrating the effects of an electrical grid (electrical dynamics) into the control scheme is further examined in subsection 7.2.4.

The pump model is based on a real pump used in offshore oil and gas applications. The simplifications for this model are the removal of dynamics and the missing options of turning off the pump. However, some dynamics are introduced through a PI controller in this thesis. If this PI controller is tuned in the right way to resemble the pump dynamic, this pump model might be sufficient to predict the behavior of a real pump of the same type. The problem of not being able to turn off the pump is something that should be considered as the pump is not desired to be running all the time. This is further a subject in subsection 7.2.3.

The GTG model is based on a second-order model with two time constants. This model is great for simulation purposes, but it is very likely to come short when dealing with predictions of the behavior of a real GTG. If it is to be used in a real setting, the time constants should at least be found and adjusted as the time constants in this thesis do not belong to a real GTG. The efficiency function, however, should work great if it is modeled with a curve fitting tool to resemble the real GTG's efficiency.

When it comes to the WTG model, this model is based on a real wind turbine. In this thesis, the WTG model has been modified a bit. The wind is assumed to be perpendicular to the turbine. In reality, the wind changes its direction, and the turbine should be controlled in order to face the wind. This implies that the turbine should rotate about the tower and that such a model should be added to the prediction model. Another modification is the removal of dynamics in the shaft and gearing. The effect of this might not be necessary for a prediction model as its impact is limited for the WTG prediction. Lastly, the torque control of the electrical generator is removed. The NMPC can probably benefit from adding this trait back in, but it is dependent on the generator type for the real WTG. A realistic efficiency for the WTG should also be added to the model.

The battery model is a simple integrator, and it models the main workings of a real battery. The simplifications for this model are the absence of chemical and electrical properties. The battery model in this thesis can deliver a large amount of power, only dependent on the stored energy. A real battery is limited in its power delivery/charge by cable sizes and chemical reaction times. For a realistic implementation, the NMPC should add constraints on the battery power based on data from the cables and batteries used in the HPS. Additionally, an efficiency for the battery should be found and added.

The augmentation of the state-space model used for the predictions in the NMPC introduces some input dynamics. The values for the constraints on the input dynamics do not come from real components. These values should also be found from the components in the specific HPS where the NMPC is to be implemented.

6.3 Computational Resources for Implementation

This section discusses the computational resources needed for the NMPC implementation. As discussed in the previous section, the design of the NMPC is not ready for direct implementation. The current design of the NMPC can, however, give an estimate of the computational resources needed for the implementation of a finalized NMPC.

In the way the current setup and tuning of the NMPC are executed, using the same computer as for the simulations is feasible for a real implementation of the controller. To calculate the optimal control inputs for the prediction horizon takes about 0.1 seconds on average with a deviation of about $\pm\ 0.05$ seconds. The NMPC performs these calculations every 0.4 seconds, meaning that there is a reasonable safety margin in computational time. That being said, for such a nonlinear system as the HPS, the NMPC might encounter regions where the solution is hard to find. This can result in a longer computational time.

To increase the safety margins for computational time, the time step of the NMPC can be increased. A larger time step for the NMPC however, might result in a decrease in the controller accuracy. Another way to take on this issue is to tune the tolerance and iteration limits of the NMPC and thereby ensure a shorter computational time. This scheme can, on the other hand, end up giving suboptimal solutions. The key is to find a trade-off between computations afforded and the quality of the NMPC solutions. If economically efficient, the best solution is to buy more computational power.

A solution for obtaining better results in many cases (decrease the effects of model inaccuracies) is to decrease the NMPC time step. A correction by the feedback measurements is then executed oftener, yielding a more accurate control. This, however, requires more computational power but might be considered in some situations. In this thesis, decreasing the time step is not preferred as the computational resources are limited. In a real implementation of the NMPC, the model imperfections are larger, but more computational power is most likely also available. The time step setting should therefore be reconsidered in the case of a real implementation.

7 Conclusion and Further Work

This section firstly provides the conclusion for this thesis in subsection 7.1. Multiple proposals for topics regarding further work are included in subsection 7.2.

7.1 Conclusion

The outcomes from this thesis are a prototype NMPC for control of an offshore HPS plant model, a finalized HPS plant model, and a series of case studies to analyze the potential of the NMPC. The NMPC is specifically designed to control the power distribution in the HPS in addition to control the flow rate of the pump used in offshore operations.

First, a mathematical model of an offshore HPS, which consists of a pump, a GTG, a WTG, and a battery is finalized. The lookup tables in the turbine part of the WTG model are then curve fitted in order to approximate the lookup tables as continuous functions. With these continuous functions, a state-space representation of the HPS model is formulated and augmented with inputs dynamic in order to be used in the NMPC's prediction model. The constraints for the NMPC are also formulated. In order for the NMPC to meet the control goals in this thesis, a tailored objective function is derived. The NMPC is further implemented on a digital computer with the use of numerical methods before it is tuned to its desired response partly using a tuning guideline.

By feedback connecting the implemented NMPC to the implemented HPS plant model, a simulation environment is established in MATLAB and Simulink. Case studies are then carried out by simulating the controlled HPS model under several realistic conditions. The HPS powers, battery energy, and pump flow rate are measured to be analyzed with respect to the objectives.

The results from the case studies show that the NMPC is able to utilize considerable amounts of wind power to power the pump and charge the battery during significant wind speeds. Two noticeable behaviors resulting in unwanted control scenarios at specific wind conditions are; the WTG constraint violations during large winds and the GTG power oscillations for some wind conditions. The oscillations in the GTG are, however, mostly insignificant, but the WTG constraint violations should be fixed with, for example, disturbance estimation. Generally, the power distribution in the HPS still works well in all of the simulation cases regardless of the power oscillations. When it comes to feedback measurement noise, the pump flow rate reference tracking is quite sensitive. The tracking, however, works properly for noise-free feedback measurements. Additionally, a higher flow acceleration weighting eliminates the problem with deviation in the flow rate reference tracking for noisy measurements in exchange for a slower flow rate dynamic.

In this thesis, the NMPC is used to show the potential of MPC in offshore HPSs. For a future implementation of a NMPC on a real offshore HPS, the control design should be tailored to the real components with their respective parameter values. The computational resources required for implementing a NMPC in a HPS is estimated to be relatively low as a regular computer can run the current NMPC in real-time. From the obtained results in this thesis, it certainly looks like MPC has a future in offshore HPSs.

7.2 Further Work

Regarding further work, there are especially five topics that are worth investigating further. First off, a proposition for further work in subsection 7.2.1 is to use SMPC to reduce uncertainties in the power production. To decrease the effects of model imperfections, introducing a disturbance estimator is possible, as further described in subsection 7.2.2. By reformulating the current OCP to a MIP there is a potential for creating a more effective control scheme as explained in subsection 7.2.3. A proposition for a method of expanding the NMPC to include electrodynamics is found in subsection 7.2.4. Lastly, in subsection 7.2.5, a method for estimating unobservable states in a real HPS is described.

7.2.1 Stochastic Model Predictive Control

The current way of controlling the HPS using the NMPC is deterministic, meaning that the controller does not account for the uncertainties in the wind (even though the controller is robust to a certain degree of inaccurate wind information). In practice, wind predictions can be based on probabilistic models in order to approximate perfect wind information. This approximation can, for example, be accomplished with the use of SMPC. Two approaches for using SMPC can be found in [56].

7.2.2 Disturbance Estimation

As seen from the results in chapter 5, model inaccuracies can result in significant disturbances. A common way of ensuring constant offset-free reference tracking is with integral action. Integral action can, however, only handle constant disturbances. As a side note, the integral action resulting from the state-space augmentation in this thesis does not work properly as the reference tracking objectives in the objective function cancel out the effect. For time-varying disturbances, it is common to use a disturbance estimator. This disturbance estimator estimates the combined effects of model inaccuracies and external disturbances. The estimates are further used in the MPC to account for the estimated disturbances. There are multiple ways of implementing the disturbance estimation, and more information can be found in [57].

7.2.3 Mixed Integer Program Formulation

A more efficient power control scheme can be obtained by using a mixed integer formulation. However, the reformulation is at the cost of computational power, as nonconvex MINLPs generally are the hardest OCPs to solve. It is, on the other hand, an interesting field for exploration. To solve the occurring MINLP, an algorithm type such as the spatial Branch-and-Bound (sBB) can be used [58].

The pump is limited to be in an area where it is constantly running. This might not always be desired due to operational periods, available water for pumping, or optimal energy usage. A proposition to solve this problem is to model the pump using integers, allowing the pump to be turned off. The OCP is then formulated as a MINLP. As a result, the pump can take on the continuous values in its original operational area or take on discrete values, corresponding to the pump not running. The GTG can also benefit from the same type of formulation due to the possibility of eliminating low-efficiency modes and power oscillations.

7.2.4 Electrodynamic Extension

If the NMPC in this thesis cannot be decoupled from the control of electrodynamics in the HPS, an extension of the NMPC is called for. An introduction of an electrical grid model, either connected to the mainland or locally at the offshore platform, can be produced. Additionally, the existing HPS model components need to obtain electrodynamic attributes to be connected with the electrical grid model.

The extended HPS model can get quite complex with added electrodynamics. To balance the electrical power system, control of frequencies is vital. Some NMPC solutions for frequency control in uncertain power systems have already been developed (see [59] for more information). An option for further work is to combine model based frequency control with the NMPC developed in this thesis.

7.2.5 Moving Horizon Estimation

The pump integral state I_p, GTG fuel flow state V_g, and GTG lossless power state P_{g_l} are not actual quantities in a real HPS, and they must therefore be estimated. A method for estimating such unobservable states is moving horizon estimation. This method can estimate the states online with the use of the past measurements in a moving time window, and it is based on an optimization problem similarly structured as a OCP. Further information about this estimation strategy can be found in [32].

Bibliography

[1] The Norwegian Government. *The Norwegian Economy – Key Facts*. Tech. rep. 2013.

[2] T. Nguyen et al. *Exergetic assessment of energy systems on North Sea oil and gas platforms*. 2013.

[3] P. Jansohn et al. *Modern Gas Turbine Systems: High Efficiency, Low Emission, Fuel Flexible*. 1st ed. Woodhead Publishing, 2013. ISBN: 978-1845697280.

[4] S. J. Davis et al. *Future CO2 Emissions and Climate Change from Existing Energy Infrastructure*. 2010.

[5] OECD. *Effective Carbon Rates on Energy*. Tech. rep. 2016.

[6] United Nations. *Paris Agreement*. 2015.

[7] W. He et al. *The Potential of Integrating Wind Power with Offshore Oil and Gas Platforms*. 2010.

[8] I. Legorburu et al. "Multi-use maritime platforms - North Sea oil and offshore wind: Opportunity and risk". In: *Ocean & Coastal Management* 160 (2018), pp. 75–85.

[9] J. Lofthouse et al. *RELIABILITY OF RENEWABLE ENERGY: WIND*. 2015.

[10] B. Ge et al. "Energy storage system-based power control for grid-connected wind power farm". In: *International Journal of Electrical Power & Energy Systems* 44 (2013), pp. 115–122.

[11] M. Arnold and G. Andersson. *Model Predictive Control of Energy Storage including Uncertain Forecasts*. 2011.

[12] B. Foss and T. A. N. Heirung. *Merging Optimization and Control*. Norwegian University of Science and Technology, 2016. ISBN: 978-82-7842-201-4.

[13] W. H. Lio et al. "A review on applications of model predictive control to wind turbines ". In: *UKACC International Conference on Control (CONTROL)*. 2014. ISBN: 978-1-4799-5011-9.

[14] R. Tang et al. "Optimal power flow dispatching of maritime hybrid energy system using model predictive control ". In: *Energy Procedia* 158 (2019), pp. 6183–6188.

[15] SINTEF. *LowEmission*. Accessed: 05.04.2021. URL: https://www.sintef.no/projectweb/lowemission/.

[16] Equinor. *Quote - wind energy*. Accessed: 05.04.2021. URL: https://www.equinor.com/en/what-we-do/wind.html.

[17] T. S. Solberg. "Modeling and Simulation of Energy Flow in Offshore Gas and Oil Production using Renewable Energy". Specialization project. Norwegian University of Science and Technology, 2020.

[18] P. Jakobsen et al. "Electrical power system challenges during the expansion of offshore oil & gas facilities". In: *PCIC Europe Petroleum and Chemical Industry Conference Europe - Electrical and Instrumentation Applications*. IEEE, 2012. ISBN: 978-3-9523333-9-6.

[19] O. Ivo and L. Imsland. "Analysis of Optimal Control Strategies for Efficient Operation of a Produced Water Reinjection Facility for Mature Fields". In: *ADCHEM 11TH IFAC Symposium on Advanced Control of Chemical Processes*. 2021.

[20] J. F. Gülich. *Centrifugal Pumps*. 2nd ed. Springer, 2010. ISBN: 978-3-642-12824-0.

[21] A. K. Coker. *Ludwig's Applied Process Design for Chemical and Petrochemical Plants*. 4th ed. Vol. 1. Gulf Professional Publishing, 2007. ISBN: 9780750677660.

[22] P. J. Lefebvre and W. P. Barker. "Centrifugal Pump Performance During Transient Operation". In: *Fluids Engineering*. Vol. 117. 1995, pp. 123–128.

[23] P. Breeze. *Gas-Turbine Power Generation*. 1st ed. Academic Press, 2016. ISBN: 9780128040553.

[24] M. Nagpal et al. "Experience with testing and modeling of gas turbines". In: *IEEE Winter Meeting Power Engineering Society*. IEEE, 2001.

[25] MathWorks. *Curve Fitting*. Accessed: 02.02.2021. URL: https://www.mathworks.com/help/curvefit/curvefitting-app.html.

[26] R. H. Kehlhofer et al. *Combined-Cycle Gas Steam Turbine Power Plants*. 2nd ed. Pennwell Books, 1999. ISBN: 978-0878147366.

[27] S. Barth et al. *Wind Power Generation and Wind Turbine Design*. Ed. by W. Tong. WIT Press, 2010. ISBN: 978-1-84564-205-1.

[28] J. D. Grunnet et al. *Aeolus Toolbox for Dynamics Wind Farm Model, Simulation and Control*. 2010.

[29] Aeolus. *SimWindFarm Toolbox*. URL: http://www.ict-aeolus.eu/SimWindFarm/turbine.html.

[30] R. M. Dell and D. A. J. Rand. *Understanding Batteries*. Royal Society of Chemistry, 2001. ISBN: 978-1-84755-222-8.

[31] J. Mclaren. *Batteries 101 Series: How to Talk About Batteries and Power-To-Energy Ratios*. Accessed: 10.11.2020. 2016. URL: https://www.nrel.gov/state-local-tribal/blog/posts/batteries-101-series-how-to-talk-about-batteries-and-power-to-energy-ratios.html.

[32] S. Gros and M. Diehl. *Numerical Optimal Control*. 2020.

[33] J. Nocedal and S. J. Wright. *Numerical Optimization*. 2nd ed. Springer, 2006. ISBN: 978-0-387-40065-5.

[34] S. P. Boyd and L. Vandenberghe. *Convex Optimization*. 1st ed. Cambridge University Press, 2004. ISBN: 978-0-521-83378-3.

[35] L. Imsland. "TTK16 Introduction - Constrained Optimization". Lecture notes. 2020.

[36] L. Grüne. *Numerical methods for nonlinear optimal control problems*. 2013.

[37] S. Gros. "Numerical Optimal Control". Lecture notes. 2017.

[38] S. Gros. “Modelling and Simulation”. Additional lecture notes. 2020.

[39] A. Wächter and T. L. Biegler. “On the implementation of an interior-point filter line-search algorithm for large-scale nonlinear programming”. In: *Mathematical Programming* 106 (2005), pp. 25–57.

[40] T-V. Vu et al. “A Model Predictive Control Approach for Fuel Economy Improvement of a Series Hydraulic Hybrid Vehicle”. In: *Energies* 7 (2014).

[41] ABB. *Model predictive control technology demystified*. Accessed: 15.03.2021. URL: https://new.abb.com/control-systems/features/model-predictive-control-mpc.

[42] M. Nikolaou. “Model predictive controllers: A critical synthesis of theory and industrial needs”. In: *Advances in Chemical Engineering*. 1st ed. Vol. 26. Academic Press, 2001, pp. 131–204. ISBN: 9780120085262.

[43] MathWorks. *Tune Weights*. Accessed: 13.04.2021. URL: https://se.mathworks.com/help/mpc/ug/tuning-weights.html.

[44] H. K. Khalil. *Nonlinear Systems*. 3rd ed. Prentice Hall PTR, 2001. ISBN: 978-0130673893.

[45] D. Di Ruscio. “Model Predictive Control with Integral Action: A simple MPC algorithm”. In: *Modeling, Identification and Control* 34 (2013), pp. 119–129.

[46] T. Tran et al. “Economic Model Predictive Control - A Review ”. In: *The 31st International Symposium on Automation and Robotics in Construction and Mining*. 2014.

[47] MathWorks. *Choose Sample Time and Horizons*. Accessed: 13.04.2021. URL: https://se.mathworks.com/help/mpc/ug/choosing-sample-time-and-horizons.html.

[48] P. E. Gill and W. H. Wright. *Practical Optimization*. ACADEMIC PRESS LIMITED, 1981. ISBN: 978-0122839528.

[49] K. T. Hoang. “Towards a Degradation-Conscious Control Strategy for Polymer Electrolyte Membrane Fuel Cells in Automotive Applications”. MA thesis. Norwegian University of Science and Technology, 2020.

[50] CasADi. *CasADi home page*. Accessed: 26.04.2021. URL: https://web.casadi.org/.

[51] MUMPS. *MUMPS home page*. Accessed: 26.04.2021. URL: http://mumps.enseeiht.fr/index.php?page=home.

[52] M. C. Mathiesen. “Instrumentation and Data Networks”. Lecture notes. 2016.

[53] Vind Nå. *Wind data*. Accessed: 28.04.2021. URL: https://xn--vindn-qra.no/.

[54] Met Office. *National Meteorological Library and Archive Fact sheet 6 – The Beaufort Scale*. 2010.

[55] V. Petrovi and C. L. Bottasso. “Wind turbine optimal control during storms”. In: *Journal of Physics* 524 (2014).

[56] A. Mesbah. “Stochastic Model Predictive Control”. In: *IEEE CONTROL SYSTEMS MAGAZINE* 36 (2016), pp. 30–44.

[57] Y. Yan et al. “Nonlinear-disturbance-observer-enhanced MPC for motion control systems with multiple disturbances”. In: *IET Control Theory and Applications* (2019), pp. 63–72.

[58] L. Liberti et al. "A good recipe for solving MINLPs". In: *Matheuristics*. 2009, pp. 231–244.

[59] A. M. Ersdal et al. "Model Predictive Control for Power System Frequency Control Taking into Account Imbalance Uncertainty". In: *IFAC Proceedings Volumes*. Vol. 47. The International Federation of Automatic Control, 2014, pp. 981–986.

Acronyms

AMSE Average Mean Square Error 38

BVP Boundary Value Problem 22

CO_2 Carbon Dioxide 1

CV Controlled Variable 33, 34, 43, 45

DAE Differential Algebraic Equation 17, 27

DP Dynamical Programming 22

GHG Greenhouse Gases 1, 2, 43

GTG Gas Turbine Generator xi, xiii, 1, 5, 6, 10, 11, 14, 18, 43, 44, 46, 53–55, 57, 58, 60–62, 65–68, 71, 73, 81, 84

HJB Hamilton-Jacobi-Bellman 22

HPS Hybrid Power System xi, xiii, 1–6, 14–18, 20–22, 26, 31, 35, 39, 41, 43–45, 47, 49–51, 56, 57, 66–69, 71–73

IP Integer Program 21

IP Interior-Point 28–31

IPOPT Interior Point Optimizer 30, 47

KF Kalman Filter 31

KKT Karush–Kuhn–Tucker 28–30

LP Linear Program 21

MHE Moving Horizon Estimator 31

MINLP Mixed Integer Nonlinear Program 36, 73

MIP Mixed Integer Program 21, 72

MISO Multiple-Input Singel-Output 9

MPC Model Predictive Control 1–5, 17, 18, 31, 33–35, 43, 68, 72

MSE Mean Square Error 38, 62

MUMPS MUltifrontal Massively Parallel Sparse direct Solver 47

MV Manipulation Variable 33, 34, 43, 45, 50

NLP Nonlinear Program 21, 22, 24, 26, 28, 29, 31, 36

NMPC Nonlinear Model Predictive Control xi, xiii, 17, 33, 35, 41, 44, 45, 47, 49–54, 56, 58–61, 63, 65–69, 71–73, 83

OCP Optimal Control Problem xi, 17, 19–22, 25, 26, 31–33, 36, 41, 43, 46, 47, 66, 72, 73

ODE Ordinary Differential Equation 17, 19, 22, 24, 26, 27

PDE Partial Differential Equation 17, 22

PI Proportional-Integral xi, xiii, 1, 6, 9, 10, 68, 82

Qη Efficiency-Flow-Rate 6, 9

QH Head-Flow-Rate 6, 7, 9

QP Quadratic Program 21, 31

QP Power-Flow-Rate 6, 8

RK Runge-Kutta 26, 27

RK1 Runge-Kutta of first order 27

RK4 Runge-Kutta of fourth order 27, 47

sBB spatial Branch-and-Bound 73

SISO Single-Input Singel-Output 9

SMPC Stochastic Model Predictive Control 65, 72

SoC State of Charge 6, 14

SQP Sequential Quadratic Programming 28, 29, 31

WTG Wind Turbine Generator xii, xiii, 1, 2, 5, 12–14, 18, 36, 37, 43, 44, 46, 51–58, 60, 62, 65–68, 71, 81, 82, 85

ZOH Zero-Order Hold 51

Appendix

A Model Parameters

Parameter	Value	Unit	Symbol
Time constants	0.5	s	τ_{g_1}
	0.5	s	τ_{g_2}
Efficiency coefficients	-0.5714		a_{g_1}
	1.286		a_{g_2}
	0.2757		a_{g_3}
Power constraints	0	kW	$P_{g_{l_{min}}}$
	4500	kW	$P_{g_{l_{max}}}$
Throttle constraints	0	pu	$\gamma_{g_{min}}$
	1	pu	$\gamma_{g_{max}}$

Table A.1: GTG parameters

Parameter	Value	Unit	Symbol
Rotor disk area	12468.98	m^2	A_w
Blade radius	63	m	R_w
Gear ratio	97		N_w
Inertia of turbine	35444067	$\mathrm{kg\,m}^2$	$I_{w_{tur}}$
Inertia of generator	534.116	$\mathrm{kg\,m}^2$	$I_{w_{gen}}$
Generator time constant	0.5	s	τ_w
Efficiency	0.78	s	η_w
Power constraints	0	kW	$P_{w_{min}}$
	5000	kW	$P_{w_{max}}$
Rotational speed constraint	0	$\mathrm{rad\,s}^{-1}$	$\omega_{w_{tur_{min}}}$
Pitch constraints	0	deg	$\beta_{w_{min}}$
	90	deg	$\beta_{w_{max}}$

Table A.2: WTG parameters

Parameter	Value	Unit	Symbol
Unit conversion factor	3600	s	κ
Energy capacity constraints	0 5000	kW h kW h	$E_{b_{min}}$ $E_{b_{min}}$

Table A.3: Battery parameters

Parameter	Value	Unit	Symbol
Maximum generator torque	45700	N m	$M_{w_{gen_{max}}}$
Steepness constant	0.099		$K_{w_{gen}}$
Rotational speed lookup table middle value	97	rad s^{-1}	$\omega_{w_{gen_{mid}}}$
Torque lookup table coefficients	-0.118600000 0.128900000 0.009222000 -0.006314000 -0.005206000 -0.000159800 -0.000102600 0.000040100 0.000000806		$p_{w_{00}}$ $p_{w_{10}}$ $p_{w_{01}}$ $p_{w_{20}}$ $p_{w_{11}}$ $p_{w_{02}}$ $p_{w_{21}}$ $p_{w_{12}}$ $p_{w_{03}}$

Table A.4: WTG lookup table approximation parameters

Constraint	Value	Unit	Symbol
Flow acceleration constraints	-20 20	m^3 s^{-2} m^3 s^{-2}	$\Delta Q_{p_{min}}$ $\Delta Q_{p_{max}}$
Throttle rate constraints	-0.2 0.2	pu s^{-1} pu s^{-1}	$\Delta\gamma_{w_{min}}$ $\Delta\gamma_{w_{max}}$
Pitch rate constraints	-2 2	deg s^{-1} deg s^{-1}	$\Delta\beta_{w_{min}}$ $\Delta\beta_{w_{max}}$

Table A.5: Input constraints for augmented state-space

B Control Parameters

Parameter	Value	Unit	Symbol
Proportional gain	1		K_{P_p}
Integral gain	4		K_{I_p}

Table B.1: PI controller parameters

Time period	Value	Symbol
Prediction horizon	10	T_{ph}
Control horizon	6	T_{ch}
Desired closed-loop time constant	1.6	T_d
Time step	0.4	Δt

Table B.2: NMPC time periods

Objective scale factor	Value	Symbol
Flow rate	5	ψ_{Q_p}
WTG power	500	ψ_{P_w}
WTG maximum power	1.01	δ_{P_w}
GTG throttle	0.1	ψ_{γ_g}
Flow acceleration	2	$\psi_{\Delta Q_p}$
Throttle rate	0.02	$\psi_{\Delta \gamma_g}$
Pitch rate	0.2	$\psi_{\Delta \beta_w}$

Table B.3: NMPC objective scaling factors

Objective weight	Value	Symbol
Flow rate	20.9	q_{Q_p}
WTG power	24.5	q_{P_w}
GTG throttle	2.5	q_{γ_g}
Flow acceleration	2.1	$r_{\Delta Q_p}$
Throttle rate	1.2	$r_{\Delta \gamma_g}$
Pitch rate	1.4	$r_{\Delta \beta_w}$

Table B.4: NMPC objective weights

C Extra Simulation Plots and Values

Simulation parameter	Value	Symbol
New GTG throttle weight	100	$q_{\gamma_{g_{new}}}$
New initial pitch value	20	$\beta_{w0_{new}}$
Pitch value for turbine dynamic test	2.5	$\beta_{w_{new}}$
WTG power saturation	5000	$P_{w_{sat}}$
New flow acceleration weight	200	$r_{Q_{p_{new}}}$
New (negative) static noise	$-0.01\mathbf{y}$	$\mathbf{v}_{st_{new}}$

Table C.1: Extended simulation case values

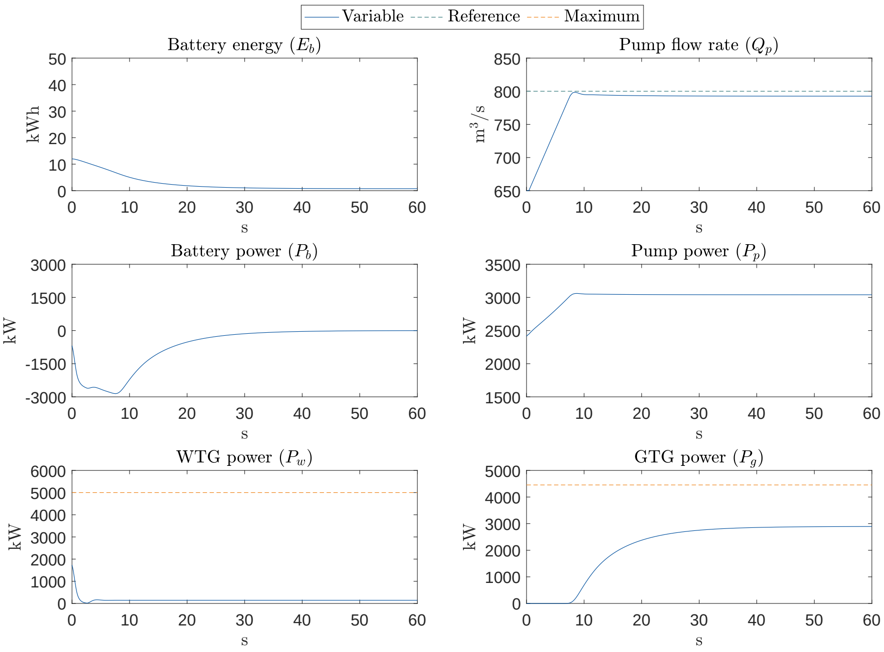

Figure C.1: Measured battery energy, pump flow rate, and powers during a gentle breeze with a high GTG throttle weighting

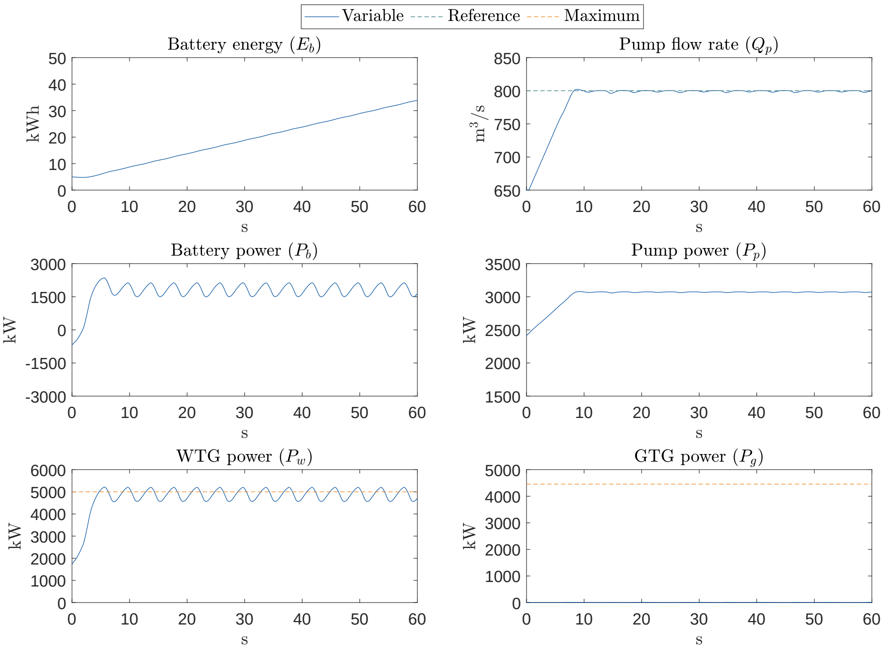

Figure C.2: Measured battery energy, pump flow rate, and powers during a gale with an adjusted initial pitch

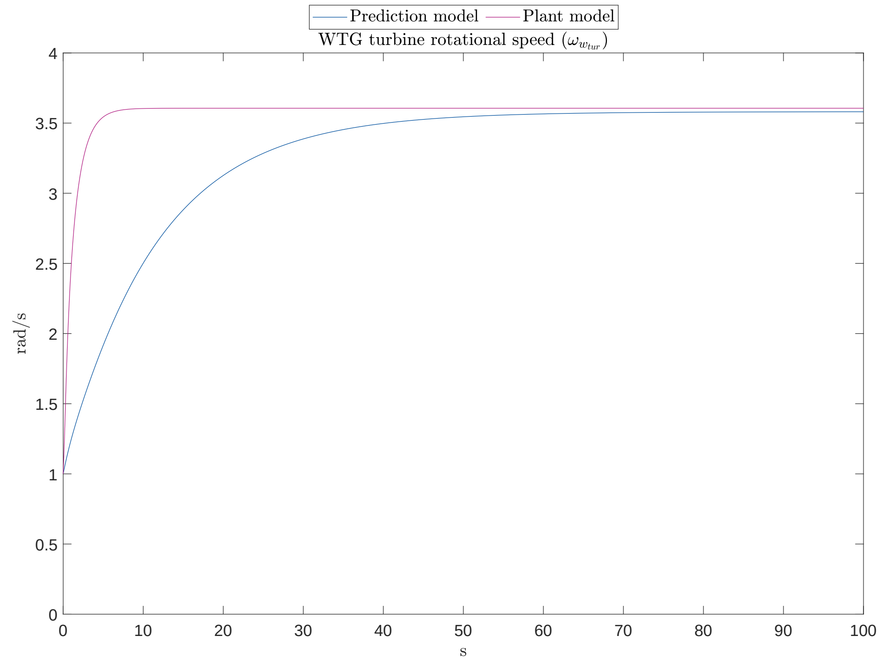

Figure C.3: Rotational speed of the wind turbine; comparing the plant and prediction model

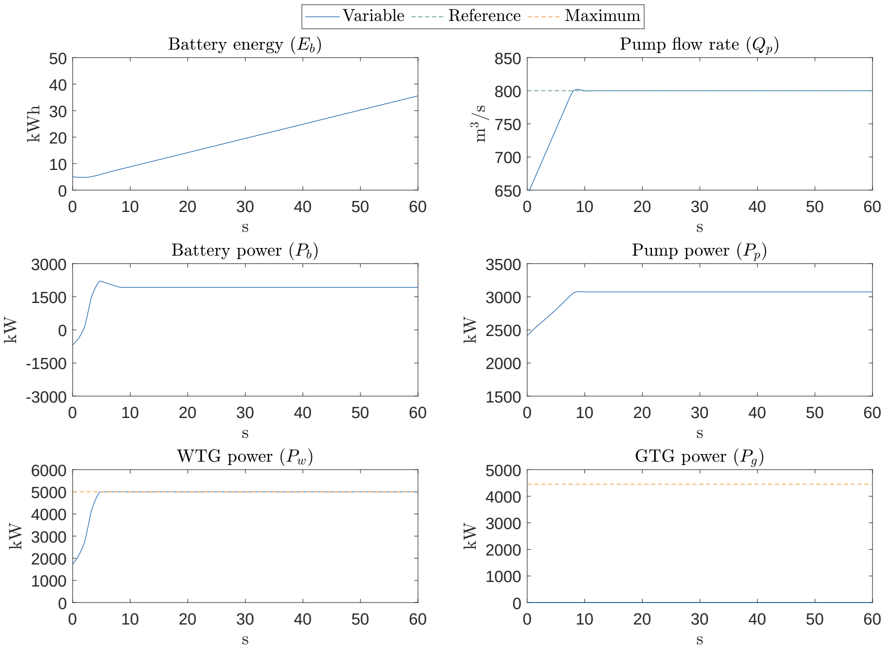

Figure C.4: Measured battery energy, pump flow rate, and powers during a gale with an adjusted initial pitch and physical WTG power saturation

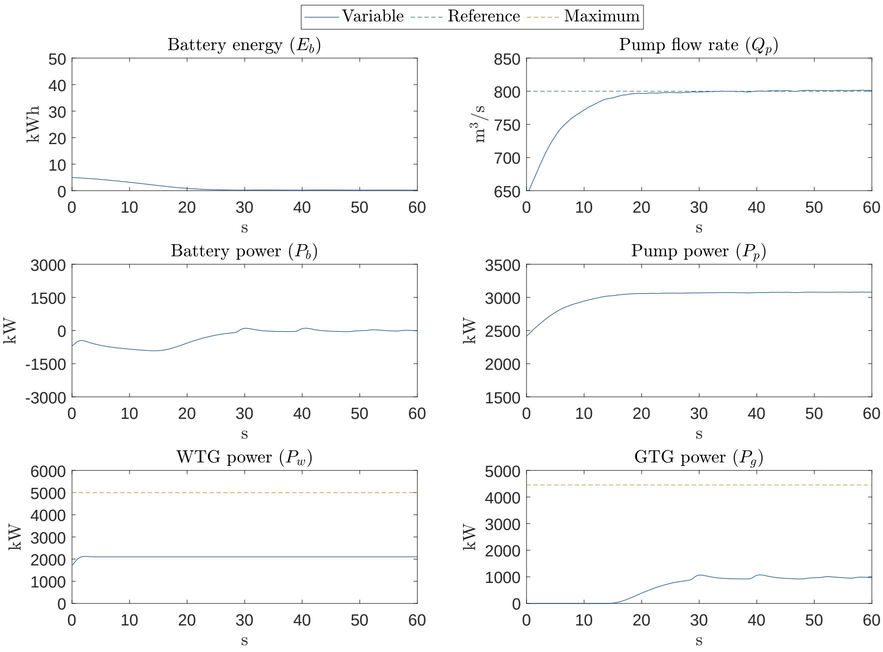

Figure C.5: Measured battery energy, pump flow rate, and powers during a fresh breeze with a high flow acceleration weighting and dynamic noise in the feedback measurements

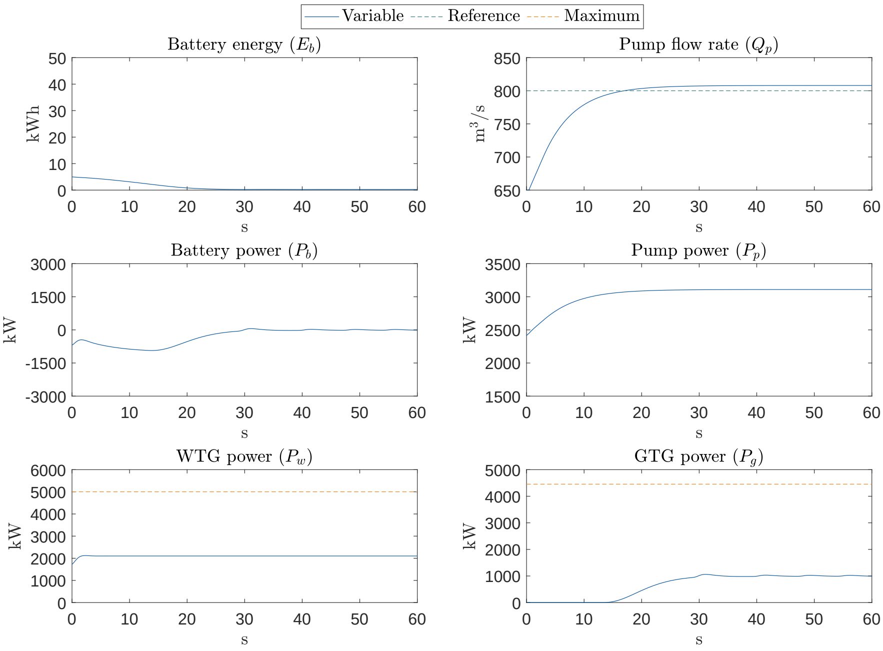

Figure C.6: Measured battery energy, pump flow rate, and powers during a fresh breeze with a negative static noise in the feedback measurements

NTNU
Norwegian University of
Science and Technology